

12-1998

## Uncertainty in recharge from subsidence craters at Frenchman Flat, Nevada Test Site: Impacts of initial and boundary conditions and media properties

David Matthew Ely  
*University of Nevada, Las Vegas*

Follow this and additional works at: <https://digitalscholarship.unlv.edu/thesesdissertations>



Part of the [Geology Commons](#), and the [Hydrology Commons](#)

---

### Repository Citation

Ely, David Matthew, "Uncertainty in recharge from subsidence craters at Frenchman Flat, Nevada Test Site: Impacts of initial and boundary conditions and media properties" (1998). *UNLV Theses, Dissertations, Professional Papers, and Capstones*. 1414.  
<http://dx.doi.org/10.34917/3339065>

This Thesis is protected by copyright and/or related rights. It has been brought to you by Digital Scholarship@UNLV with permission from the rights-holder(s). You are free to use this Thesis in any way that is permitted by the copyright and related rights legislation that applies to your use. For other uses you need to obtain permission from the rights-holder(s) directly, unless additional rights are indicated by a Creative Commons license in the record and/or on the work itself.

This Thesis has been accepted for inclusion in UNLV Theses, Dissertations, Professional Papers, and Capstones by an authorized administrator of Digital Scholarship@UNLV. For more information, please contact [digitalscholarship@unlv.edu](mailto:digitalscholarship@unlv.edu).

UNCERTAINTY IN RECHARGE FROM SUBSIDENCE CRATERS  
AT FRENCHMAN FLAT, NEVADA TEST SITE: IMPACTS  
OF INITIAL AND BOUNDARY CONDITIONS  
AND MEDIA PROPERTIES

by

David Matthew Ely

Bachelor of Science  
University of South Carolina  
1990

A thesis submitted in partial fulfillment  
of the requirements for the degree of

**Master of Science**

**in**

**Geoscience**

**Department of Geoscience  
University of Nevada, Las Vegas  
December 1998**

## ABSTRACT

### **Uncertainty in Recharge Potential from Subsidence Craters at Frenchman Flat, Nevada Test Site: Impacts of Initial and Boundary Conditions and Media Properties**

by

David Matthew Ely

Dr. Glenn V. Wilson, Examination Committee Chair  
Professor, Water Resources Center  
Desert Research Institute

The Nevada Test Site has over 400 subsidence craters formed by the collapse of overlying rock following underground nuclear tests. Under natural conditions, infiltration and recharge would not be considered likely due to infrequent precipitation events and extreme evapotranspiration. Crater U5a in Frenchman Flat was chosen for study because it intercepts significantly more drainage than surrounding craters.

Vadose zone modeling was conducted to test the sensitivity of water movement to boundary and initial conditions. The effects of ponding depth was negligible but depth of wetting front movement was highly dependent on the lateral extent of the ponds. The model was insensitive to the initial conditions tested due to the extreme dryness of the soil.

Field and laboratory observations provide evidence for a 63,000 m<sup>3</sup> pond occurring on the initial crater surface. Model results predict such a wetting front

reaching the water table in 30 years. Sediment deposited by this large pond, however, provides an effective barrier to future infiltration and recharge.



**Thesis Approval**  
The Graduate College  
University of Nevada, Las Vegas

November 19 \_\_\_\_\_, 19 98

The Thesis prepared by

David Matthew Ely

**Entitled**

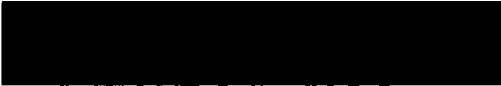
Uncertainty in Recharge from Subsidence Craters at

Frenchman Flat, Nevada Test Site: Impacts of Initial

and Boundary Conditions and Media Properties

is approved in partial fulfillment of the requirements for the degree of

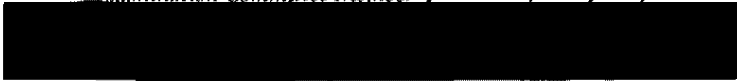
Master of Science



*Examination Committee Chair*



*Examination Committee Member*



*Examination Committee Member*



*Graduate College Faculty Representative*

*Dean of the Graduate College*

## TABLE OF CONTENTS

ABSTRACT.....	iii
LIST OF FIGURES.....	vii
LIST OF TABLES.....	ix
ACKNOWLEDGEMENTS.....	x
CHAPTER 1 LITERATURE REVIEW.....	1
Recharge in Arid Environments.....	1
Recharge at the Nevada Test Site.....	3
Phenomenology of Craters.....	6
Hydrologic Impacts of Craters.....	9
Impact of Playa on Recharge Potential at Crater U5a.....	14
Objective.....	17
CHAPTER 2 MATERIALS AND METHODS.....	27
Geologic Setting.....	27
Hydrogeologic Setting.....	28
Nevada Test Site.....	28
Frenchman Flat and Crater U5a.....	30
Theoretical Methods.....	33
Flow Equations.....	33
Water Retention Function.....	35
Unsaturated Hydraulic Conductivity.....	36
Experimental Methods.....	39
Water Retention.....	39
Saturated Hydraulic Conductivity.....	41
Unsaturated Hydraulic Conductivity.....	41
Particle Size Analysis.....	42
Subsurface Characterization.....	43
Water Harvest.....	44
Numerical Methods.....	45
HYDRUS-2D.....	45
Sensitivity Analysis I and II.....	46

CHAPTER 3 RESULTS AND DISCUSSION.....	56
Introduction.....	56
Sensitivity Analysis I.....	57
Sensitivity Analysis II.....	59
Particle Size Analysis along Surface Transect.....	62
Particle Size Analysis with Depth.....	62
Saturated and Unsaturated Hydraulic Conductivity.....	65
Water Retention Characteristics.....	67
van Genuchten Parameters.....	68
Final Modeling Scenarios.....	70
Method of Final Modeling Scenario.....	71
Results of Final Modeling Scenario.....	75
Conclusions of the Final Modeling Scenario.....	80
CHAPTER 4 SUMMARY.....	108
REFERENCES.....	114
APPENDIX A.....	122
APPENDIX B.....	124
APPENDIX C.....	144
VITA.....	148

## LIST OF FIGURES

Figure 1.	Location map of Crater U5a at the Nevada Test Site.....	18
Figure 2.	Generalized mechanical effects as a result of underground nuclear weapons testing.....	19
Figure 3.	Topographic map depicting the initial topography of crater U5a and the location of wells U5a-N1 and U5a-N2.....	20
Figure 4.	Topographic survey of crater U5a completed in 1996.....	21
Figure 5.	Simulated water content profile in the U3bh Collapse Zone following redistribution with a homogeneous profile.....	22
Figure 6.	Simulated water content profile in the U3bh Collapse Zone following redistribution with a layered profile.....	23
Figure 7.	Picture of crater U5a showing erosional gullies, vegetation, and surface playa, and sediment line.....	24
Figure 8.	Summary of field and laboratory procedures for sampling sites along transect of crater U5a.....	50
Figure 9.	Diagram of the boundary conditions for Sensitivity Analysis I illustrating the top B.C. of pond depth and lateral extent variation.....	51
Figure 10.	Diagram illustrating the initial conditions for Sensitivity Analysis II in which the pressure head was in equilibrium with the bottom water table (WT) or set to a constant head of -200 m (NWT).....	52
Figure 11.	Schematic of three soil types used in Sensitivity Analysis I and II.....	53
Figure 12.	HYDRUS-2D modeling results for SA I showing depth of infiltration after 2 ponding events for 30 and 90 cm head at two lateral extents.....	81
Figure 13.	HYDRUS-2D modeling results for SA I showing the depth of water movement into the 40 m deep domain after two ponding events for 5, 12, 15, and 20 m lateral extent of ponds.....	82
Figure 14.	HYDRUS-2D modeling results for SA II indicating the initial conditions tested at two selected time periods.....	83
Figure 15.	Maximum depth of water movement for 33 years of simulations...	84
Figure 16.	Unsaturated hydraulic conductivity for loamy sand and silty clay...	85
Figure 17.	Water retention measurements and van Genuchten model for three representative soil types.....	86
Figure 18.	Particle size analysis profiles at transect locations along crater bottom.....	87
Figure 19.	Picture of surface playa within crater U5a.....	88
Figure 20.	Particle size analysis profiles at transect locations 30, 70, and 120.....	89
Figure 21.	Simplified cross-section of crater U5a based upon analysis of the drilling samples.....	90

Figure 22.	Potential evapotranspiration calculated with the Penman combination equation from micro-meteorological data for Area 5.....	91
Figure 23.	Diagrams showing the mesh and domain for the final modeling scenarios.....	92
Figure 24.	Domain and geometry depicting sediment layering.....	93
Figure 25.	Modeling results showing water movement to the bottom of the 200 m deep domain following infiltration of 63,000 m <sup>3</sup> ponding event.....	94
Figure 26.	Modeling results of water content (m <sup>3</sup> /m <sup>3</sup> ) versus depth (m) from the center of the playa region following infiltration of 63,000 m <sup>3</sup> ponding event.....	95
Figure 27.	Water content measurements with a neutron moisture meter during the spring and summer of 1996 for U5a-N1.....	96
Figure 28.	Observation regions for examination of inflow/outflow.....	97
Figure 29.	HYDRUS-2D modeling results showing water content distribution in the multi-layered sediment in the crater at the end of four time steps.....	98

## LIST OF TABLES

Table 1.	Means and standard deviations for physical and hydraulic properties of Area 3 RWMS characterization samples listed by location category.....	25
Table 2.	Hydraulic parameters from Area 5 Performance Assessment.....	26
Table 3.	Ponding event characteristics.....	54
Table 4.	HYDRUS-2D soil properties used for SA I and II.....	55
Table 5.	Combined time (in days) for infiltration of two pond events for SA I.....	99
Table 6.	Maximum depth (in meters) of water movement for SA I.....	99
Table 7.	Particle size analysis along crater transect.....	100
Table 8.	Particle size analysis for depth (m) at transect locations 30, 70, 120, and 150 for very fine sand, fine sand, medium sand, coarse sand, and very coarse sand.....	101
Table 9.	Hydraulic conductivities for sampling stations.....	102
Table 10.	Soil properties determined by the RETC code.....	103
Table 11.	Hydraulic properties for soil types used in the final modeling scenario.....	104
Table 12.	Summary of large pond infiltration/drainage simulation.....	105
Table 13.	Summary of layered profile infiltration/drainage simulation.....	106
Table 14.	Total inflow/outflow of water for six infiltration/drainage events.....	107

## ACKNOWLEDGEMENTS

Financial support for this study was provided by the Nevada Risk Assessment/Management Program (NRAMP), U.S. DOE Grant #DEFG 01 96 EW 56093, through the Harry Reid Center for Environmental Studies. This study relied heavily upon the data acquired from Hokett and Gillespie (1996), funded by the U.S. DOE UGTA Program.

I would like to express immense appreciation to my examining committee members, Dr. Glenn Wilson, Dr. Donald Baepler, Dr. Richard French, and Dr. David Weide, for the guidance and scientific expertise that were instrumental to this study. My very special gratitude goes to Dr. Glenn Wilson, who not only served as an advisor and major source of knowledge, but also as a source of encouragement, humor, and friendship. You taught me the importance of sound science, as well as the importance of ethics and moral principles.

I would also like to thank the scientists and professionals at the Desert Research Institute, the Harry Reid Center for Environmental Studies, and the Department of Geoscience. Special notes of appreciation go to Tod Johnson, for first approaching me with the idea for this thesis topic; Sam Hokett, for innumerable hours of patient instruction, explanations, and exchange of ideas; Brian Ogan, Shane Magner, and Michele Lamb, for their assistance in the laboratory and in the field; and Cheryl

Radeloff, for never failing to provide me with a healthy dose of distraction and joculariry.

I would like to thank my father, mother, and sister for their emotional (and financial) support throughout this entire Graduate School ordeal. You believed in me when I doubted my own abilities. To all my friends who feigned endless interest in my thesis-related ramblings, I owe you all a special debt of gratitude. And to Espresso Roma for all the free refills.

Finally, I would like to thank Branda Waggoner. You remained a constant in my life when everything else seemed to be in upheaval. You sat with me on Saturday mornings and watched my computer iterate. Lured by the promise of a night on the town, you stood in the lab and weighed dirt with me. You kept me fed and kept me laughing. But most importantly, you agreed to marry me.

## CHAPTER 1

### LITERATURE REVIEW

#### **Recharge in Arid Environments**

Recharge, the rate at which water is replenished in an aquifer, is generally one of the most difficult components of the hydrologic budget to quantify (Stephens and Knowlton, 1986). An increased interest in the hydrologic processes of arid region infiltration and recharge has been caused by the need for safe disposal sites for hazardous and radioactive waste (Tyler et al., 1996). Groundwater resources of many semiarid and arid basins in the western United States are limited and need to be carefully developed to avoid loss of their use over the long term (Dettinger, 1989). An understanding of the recharge mechanisms involved can assist in such a determination.

An area is considered arid if it receives less than 250 mm of average annual rainfall. In such a dry environment, surface and near surface processes regulate the amount of precipitation that can penetrate beyond the deep root zones of native desert vegetation. The extensive root system consumes almost all precipitation and transmits losses as transpiration. Although mountain regions may facilitate recharge, soilwater storage capacity, transpiration, solar radiation, temperature, and wind generally negate

any net gain into the vadose zone of the alluvial fans. As a result local recharge rates are very low, but generally very constant in the alluvial fans (Allison et al., 1994).

Allison et al. (1994) report on the many approaches to estimating recharge fluxes. Indirect physical methods can include empirical expressions, soil water balance, zero-flux plane method, or numerical estimation of water fluxes. Direct physical methods include lysimeters and natural or applied tracers.

The simplest of the methods is the empirical expression of the type

$$R = k_1(P - k_2) \quad (1)$$

where  $P$  is precipitation and  $k_1$  and  $k_2$  are constants. This method is used mainly in areas where annual recharge is fairly high ( $> 50$  mm/yr).

Soil water balance can be represented, in the absence of surface runoff, by

$$R = P - E_a + S \quad (2)$$

where  $E_a$  is actual evapotranspiration and  $S$  is the change in soil water storage.

However this method is not likely to be successful in an arid or semiarid region because of long periods of less than potential evapotranspiration, when errors in  $E_a$  are greatest and  $P$  and  $E_a$  are nearly equal (Gee and Hillel, 1988).

The zero-flux plane method relies on locating a plane of zero hydraulic gradient in the soil profile. Recharge is then obtained by summation of the changes in water content below the plane. Allison et al. (1994) further state that this method fails during periods of high infiltration when the hydraulic gradient becomes positive throughout the profile. This period is when recharge will most likely be the greatest.

Sophocleous and Perry (1985) and Stephens and Knowlton (1986) attempted to use unsaturated zone hydraulic conductivities to solve Darcy's Law

$$q = K(\theta) \frac{\Delta H_t}{\Delta z} \quad (3)$$

where  $\Delta H_t$  is the total head gradient and  $K(\theta)$  is the unsaturated hydraulic conductivity.

The water flux,  $q$ , calculated below the root zone, is assumed to be equal to groundwater recharge,  $R$ . Stephens and Knowlton (1986) found that annual recharge fluxes were highly dependent upon how they computed mean hydraulic conductivity, resulting in fluxes that varied by more than a factor of five.

Gee et al. (1992, 1993) successfully used lysimeters as a means of direct, physical estimation of recharge at arid sites. They fail, however, to capture the spatial variability produced by changes in flow pathways.

Natural tracers ( $^3\text{H}$ ,  $^{14}\text{C}$ ,  $^{36}\text{Cl}$ ,  $^{15}\text{N}$ ,  $^{18}\text{O}$ ,  $^2\text{H}$ ,  $^{13}\text{C}$ , and  $\text{Cl}$ ) and applied tracers ( $^{18}\text{O}$ ,  $^3\text{H}$ ,  $^2\text{H}$ , and  $\text{Br}$ ) have been very successful in estimating recharge in arid environments (Tyler et al., 1996). This method provides results that incorporate actual flow domains by integrating spatial and temporal variability to provide a record of historical recharge fluxes. However, this method assumes a uniform wetting front, i.e. No preferential flowpaths, and assumptions regarding the paleoenvironment.

### **Recharge at the Nevada Test Site**

The Nevada Test Site (NTS) lies within the northern edge of the Mojave Desert, 105 km northwest of Las Vegas, occupying an area of 3500 km<sup>2</sup> (Figure 1). The present climate at the study area is extremely arid, with an annual precipitation of 124

mm/yr for 30 years of record (French, 1986). Precipitation in this physiographic province of the western United States is categorized in two distinctly different periods. Winter rainfall is driven by cyclonic frontal systems carrying moisture from the Pacific Ocean off the western coast of the United States. Summer storms are convective thunderstorms originating in the Gulf of California. Although summer storms are of far greater intensity, storms tend to be more localized and of shorter duration. In contrast, winter systems are more spatially uniform, low intensity and longer duration, and account for 75% of the annual rainfall.

Evaporation in the basins of the NTS occurs only at potential rates following significant precipitation events (Bechtel Nevada, 1998d). Shouse et al. (1982) found evaporation from the soil in such an arid environment to occur in two stages. Stage 1: Immediately following a precipitation event, evaporation from wet soil conditions is controlled by meteorological conditions. Stage 2: As the soil dries, movement of water to the surface is lower than the evaporative demand as soil properties govern the rate of moisture loss.

Soil-water flux in the Southern Great Basin was studied by Tyler et al. (1996) to examine the appropriateness of locating Radioactive Waste Management Sites (RWMS) at the Nevada Test Site. To study both current recharge and paleorecharge mechanisms, Tyler et al. (1996) examined ten boreholes (seven shallow series and three deep series) drilled to the water table (approximately 230 to 270 m below land surface) to characterize the thick vadose zone of Frenchman Flat (NTS Area 5). Stable chloride and  $^{36}\text{Cl}$  indicated that soil waters deep in the unsaturated profile range in age from approximately 20,000 to 120,000 years. Secondary chloride bulges were evidence of

and Figure 6) are substantially different. The homogeneous profile redistributed water to a depth of 80 m below U3bh in about 100 years (0.8 m/yr). This result was in contrast to the measured water content. For the layered profile, effectively no downward movement of the wetting front occurred. Bechtel Nevada (1998d) stated that for the layered soil profile, successfully eliminating water flux at the surface would limit water movement at depth. The depth of the zone of increased water content, however, could be increased if current engineering structures for the prevention of runoff and ponding events degrade.

A concern that excess moisture in waste containers could have a significant impact on the Area 5 Performance Assessment (Shott et al., 1997) with respect to water movement and radionuclide transport prompted a study (Crowe et al., 1998) of soil water flow. Two scenarios of soil water flow were conducted: redistribution of moisture based on ambient conditions and a flooding scenario. In each, the waste column was assumed to be either 25, 50, 75, or 100 percent saturated and the waste was assigned identical hydraulic properties as the surrounding media. Those hydraulic properties were derived from the Area 5 PA summarized in Table 2.

The base case scenario simulated infiltration, redistribution, bare-soil evaporation, and precipitation for a 50 year period. All meteorological data incorporated actual measurements from Area 5 RWMS. Results show that some moisture from the initially saturated areas moves to zones of lesser water content, both above and below. After 50 years, the wetting front traveled to depths ranging from 14 m for the 25 % wet waste to 33 m for the 100 % wet waste. After 30 years, the wetting front velocity decreased to 2 cm/year for the 25 % wet waste to 10 cm/year m for the

material providing a fast mechanism for deep water movement and the fine-textured playa material serving as storage. As a conservative approach, Hokett and French (1998) simulated ponding events as a 0.3 m head that extended just 2 m beyond the edge of a 10 m wide playa. They also assumed an initial condition of uniform matric head of -10 m throughout the profile. Simulations suggest that such a mechanism would infiltrate a 0.3 m pond in less than a day and drainage to a depth of 129 m could occur within a 32 years.

### **Objective**

The objectives of this study were (1) to evaluate uncertainty in the crater recharge estimates of Hokett and French (1998) due to boundary conditions and initial conditions and (2) to determine the effects of media properties on recharge estimates. Regions of possible recharge were distinguished by morphological descriptions and patterns in landscape dependent infiltration were determined in order to more accurately model recharge. This research will also assist in the study of risk assessment at the Nevada Test Site by incorporating ponding events, based on historic precipitation records, coupled with detailed vadose zone characteristics to predict potential recharge by craters.

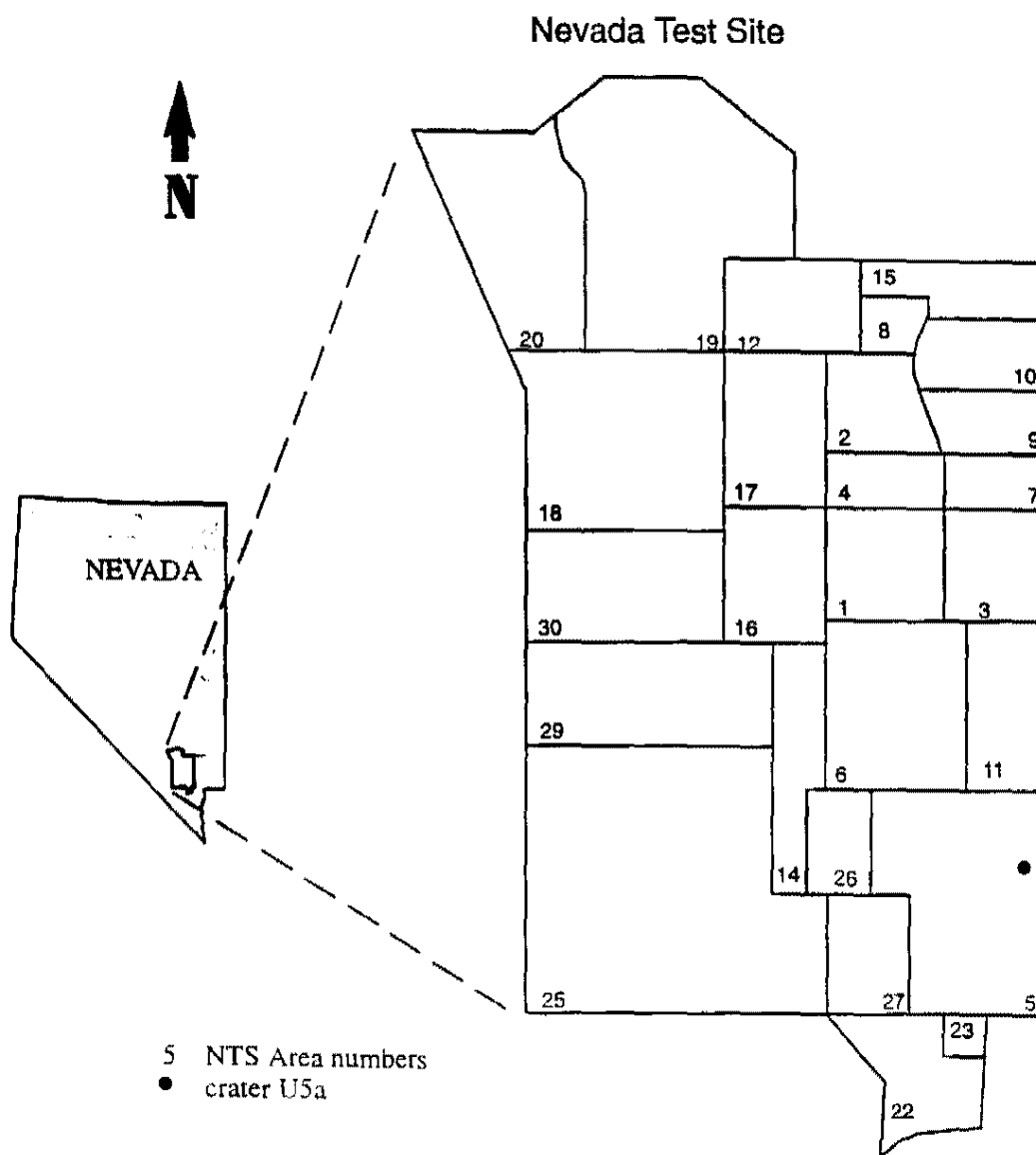
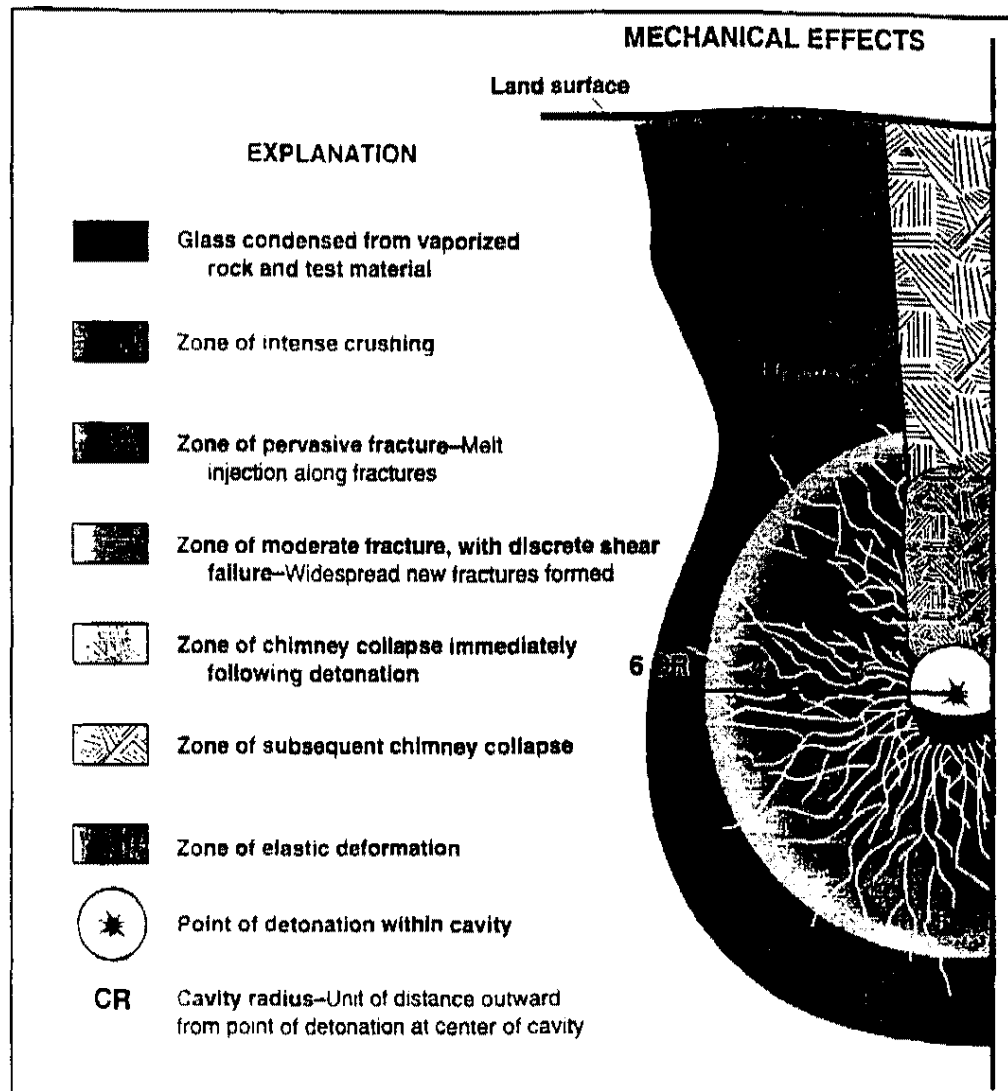
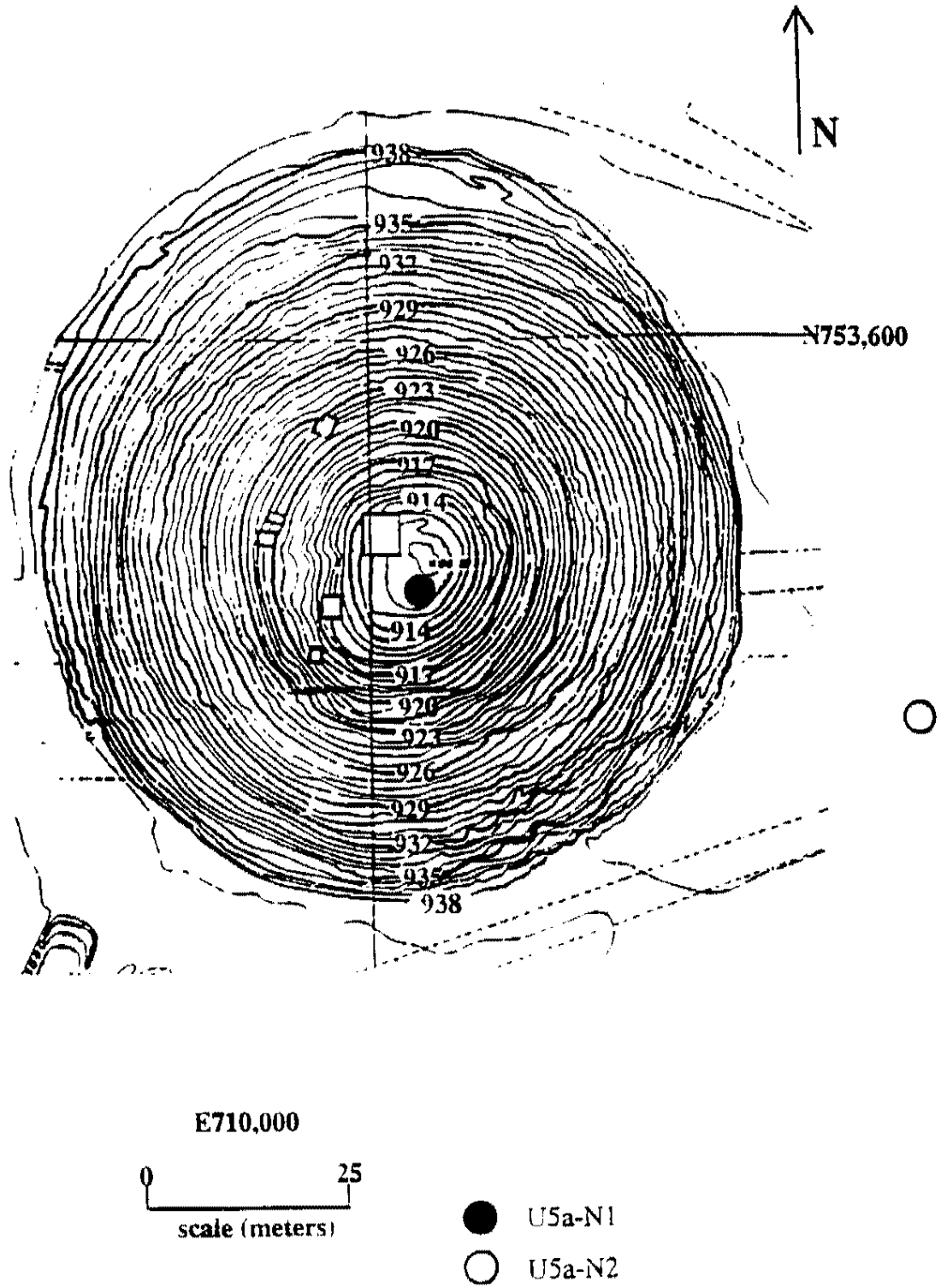


Figure 1. Location map of crater U5a at the Nevada Site (From Hokett and Gillespie, 1996).



**Figure 2.** Generalized mechanical effects as a result of underground nuclear weapons testing (From Lacziniak et al., 1996).



**Figure 3.** Topographic map depicting the initial topography of crater U5a and the location of wells U5a-N1 and U5a-N2 (From Hokett and Gillespie, 1996).

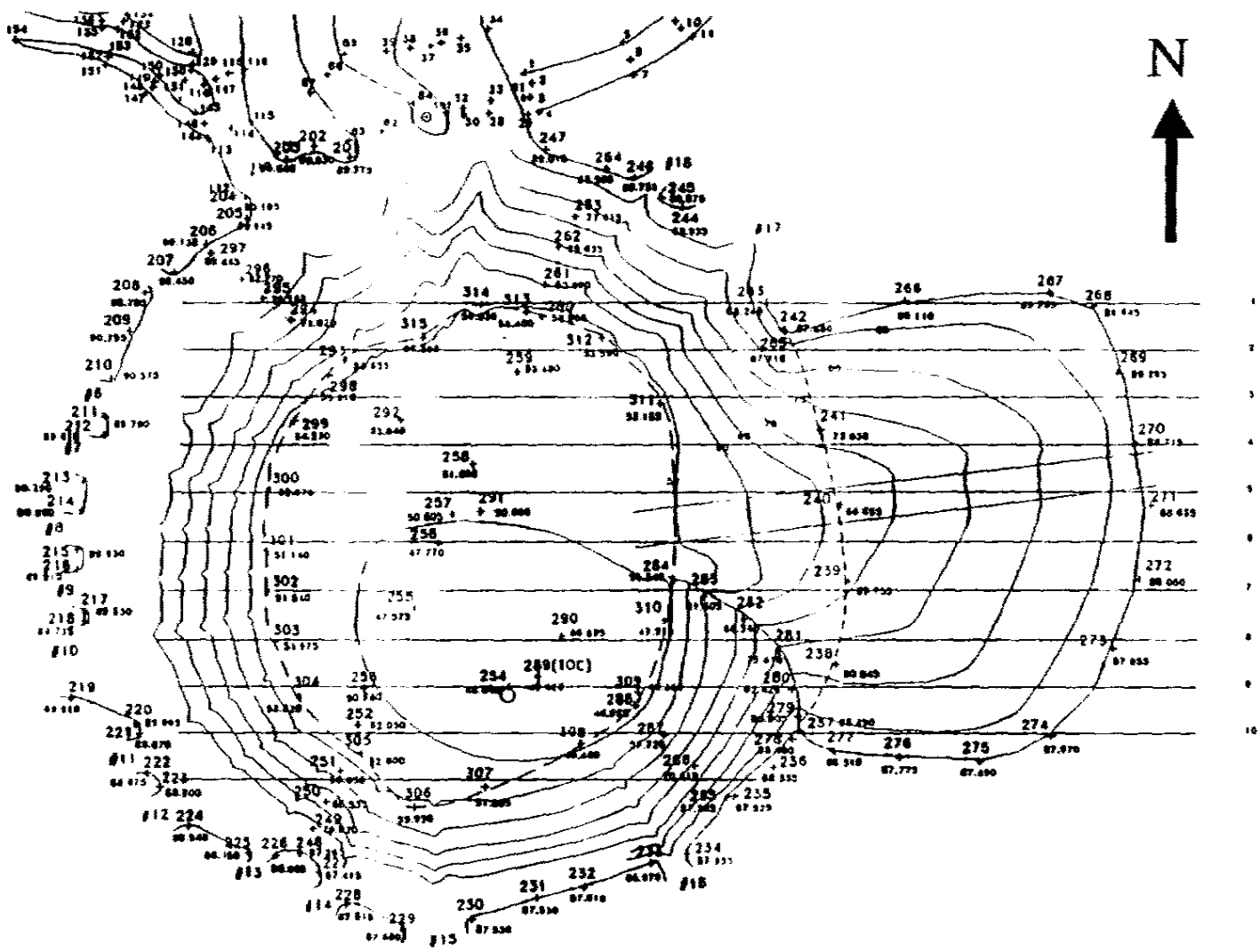
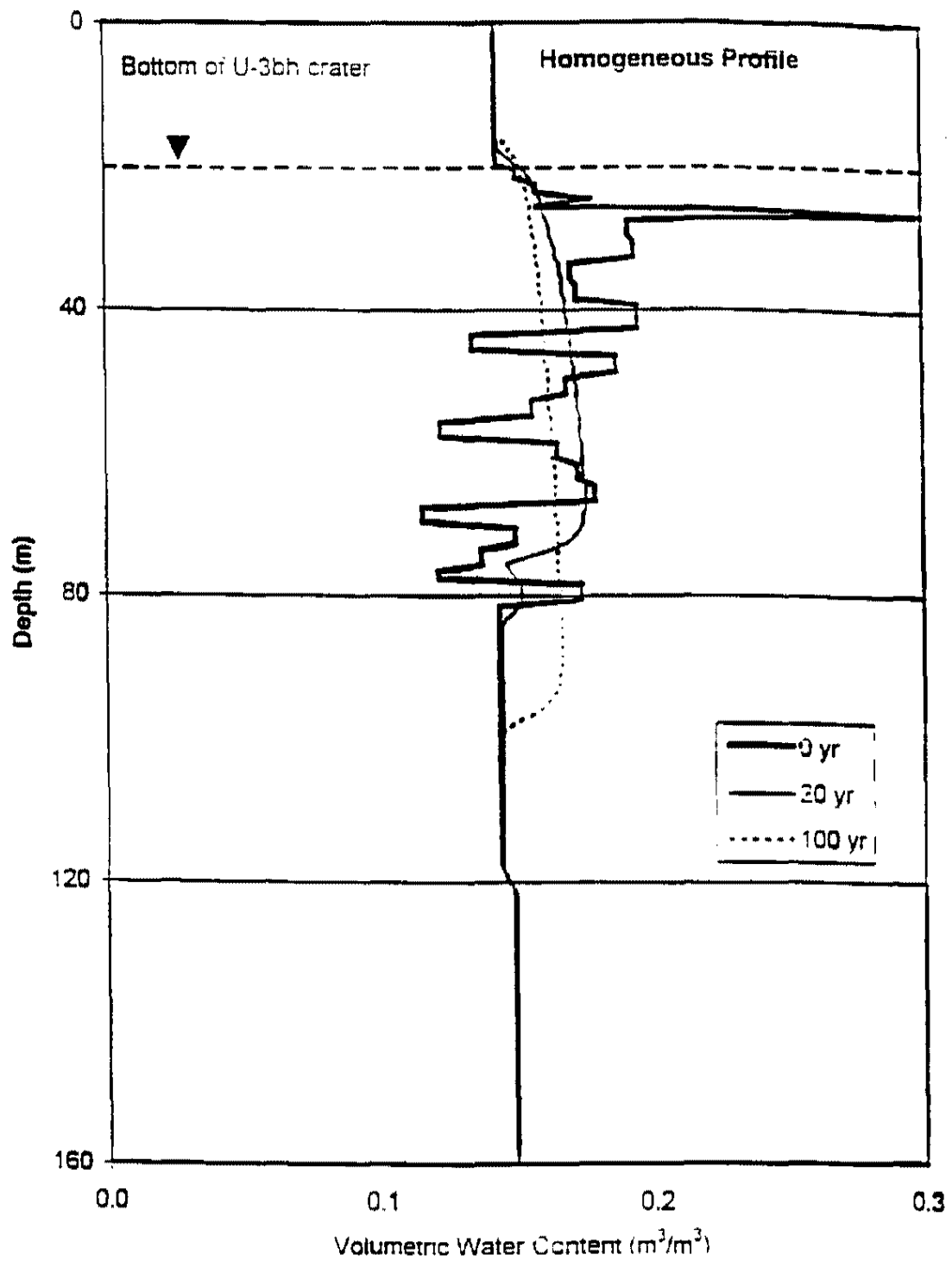
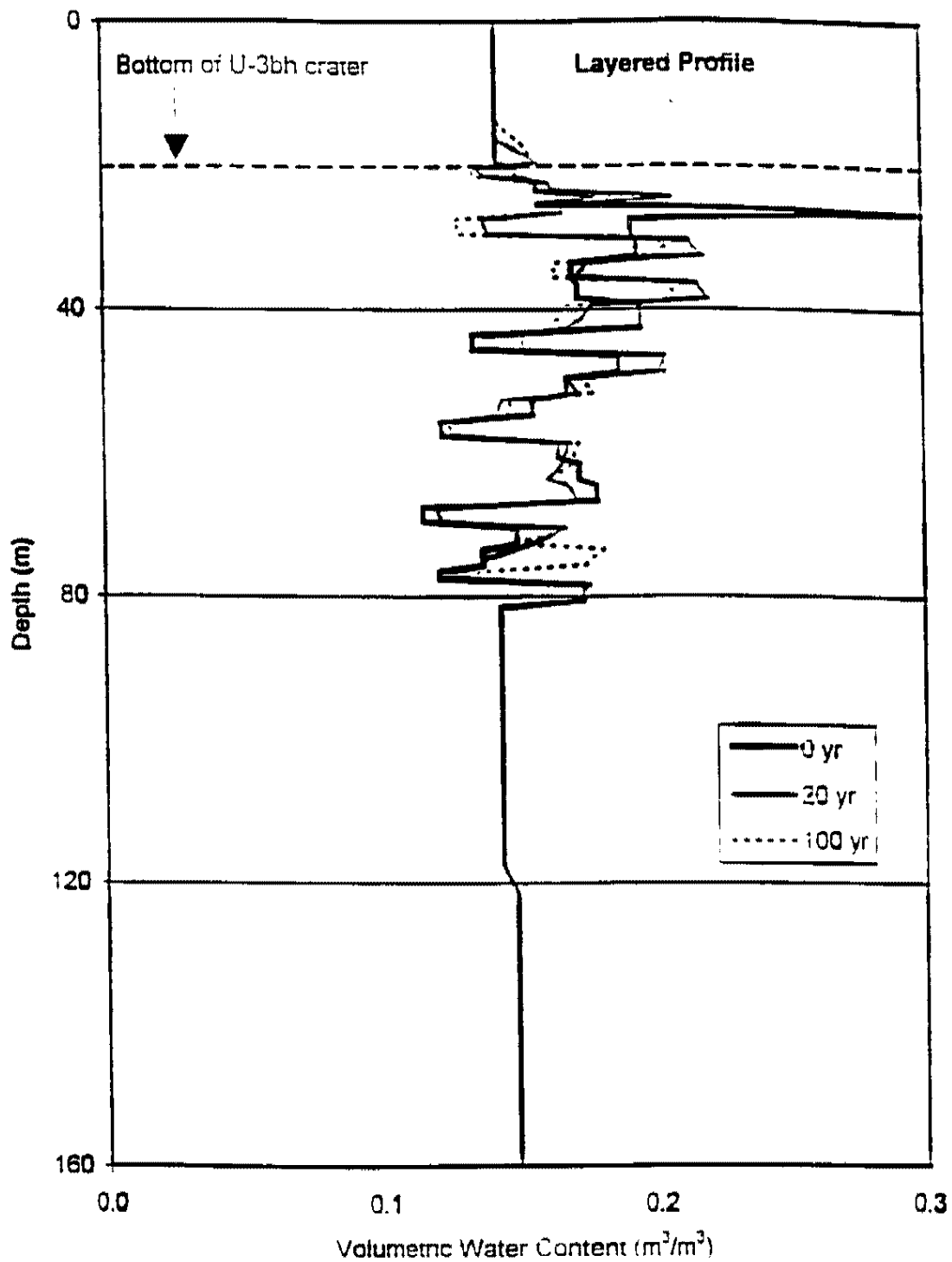


Figure 4. Topographic survey of crater U5a completed in 1996.



**Figure 5.** Simulated water content profile in the U3bh Collapse Zone following redistribution with a homogeneous profile (From Bechtel Nevada, 1998d).



**Figure 6.** Simulated water content profile in the U3bh Collapse Zone following redistribution with a layered profile (From Bechtel Nevada, 1998d).



**Figure 7.** Picture of crater U5a showing erosional gullies, vegetation, surface playa (foreground), and high water sediment line. View NNE.

**Table 1.** Means and standard deviations for physical and hydraulic properties of Area 3 RWMS characterization samples listed by location category (From Bechtel Nevada, 1998d).

Property	Undisturbed		Shallow CZ		Mid-CZ		Combined	
	Mean	SD	Mean	SD	Mean	SD	Mean	SD
Particle Density [ $\text{Mg m}^{-3}$ ]	2.49	0.0815	2.44	0.0646	2.41	0.0876	2.4	0.0863
Bulk Density [ $\text{Mg m}^{-3}$ ]	1.5	0.154	1.49	0.114	1.55	0.15	1.52	0.137
Porosity [ $\text{m}^3 \text{m}^{-3}$ ]	0.382	0.0632	0.387	0.0466	0.364	0.0618	0.373	0.0581
Sand Fraction [wt %]	83.8	8	81	7.6	80.1	8.9	80.6	8.5
Silt Fraction [wt %]	7.3	4.2	10.2	7.3	10.3	6.8	10.1	6.8
Clay Fraction [wt %]	8.9	4.3	8.5	2.6	9.7	4.4	9.3	4
ln Saturated Conductivity [ $\ln (\text{m s}^{-1})$ ]	-11.4	1.45	-11.2	1.6	-12.1	1.74	-11.7	1.68
van Genuchten Parameters								
ln alpha [ $\ln(\text{cm}^{-1})$ ]	-3.34	1.37	-4.42	0.89	-4.42	1.06	-4.18	1.18
n	1.49	0.368	1.74	0.274	1.74	0.337	1.68	0.344
residual water content [ $\text{m}^3 \text{m}^{-3}$ ]	0.067	0.057	0.132	0.033	0.135	0.041	0.12	0.052

**Table 2.** Hydraulic parameters from Area 5 Performance Assessment (Shott et al., 1997).

<b>Parameter Description</b>	<b>Value for Simulation</b>
Saturated hydraulic conductivity	0.6390 $\text{m d}^{-1}$
van Genuchten n parameter	1.9 $\text{m}^{-1}$
van Genuchten alpha parameter	1.831
Residual water content	0.075 $\text{m}^3\text{m}^{-3}$
Saturated water content	0.361 $\text{m}^3\text{m}^{-3}$

## CHAPTER 2

### MATERIALS AND METHODS

#### **Geologic Setting**

The local geology of the Nevada Test Site may be considered representative of Frenchman Flat. Frenchman Flat occupies the southeast portion of the Nevada Test Site in Nye County, Nevada. To the north Frenchman Flat is bounded by Yucca Flat, to the south by Mercury Valley, to the east by Indian Spring Valley, and to the west by Jackass Flat. Much of our knowledge of the geology of the Nevada Test Site can be attributed to the work of Winograd and Thordarson (1975). The NTS contains Tertiary volcanic rocks and Quaternary alluvial fill deposited unconformably on the deformed clastic and carbonate rocks of the Late Precambrian and Paleozoic western North American passive margin. Up to 3000 m of Precambrian to Middle Cambrian quartzite and siltstone are overlain by 4500 m of Middle Cambrian through Upper Devonian limestone and dolomite. The Eleana Formation, 2400 m of Devonian and Mississippian quartzite, siltstone, argillite, and conglomerate, is exposed in the northwest corner of Frenchman Flat. Pennsylvanian and Permian limestone constitutes the upper 1200 m of Paleozoic strata. No record of Mesozoic rock is locally present at Frenchman Flat.

The region was affected by three episodes of deformation. The first occurred

during Paleozoic time and is locally represented by the Eleana Formation. The second took place during Mesozoic time and resulted in the folding and thrust faulting of Precambrian and Paleozoic rocks. The third occurred during the Cenozoic and produced the normal block faults responsible for modern Basin and Range topography.

During Cenozoic time, 2600 m of volcanic and sedimentary rocks were deposited in the deep basins produced by Basin and Range faulting. The Tertiary volcanic rocks primarily are ash-flow and air-fall tuff. The associated sedimentary rocks are conglomerates, tuffaceous sandstone, siltstone, calcareous lacustrine tuff, claystone, and freshwater limestone. Quaternary detrital sequences are largely alluvial deposits and typically less than 610 m in thickness.

The same stratigraphic sequence occurs locally at crater U5a. Thickness of the Cenozoic alluvium is estimated between 500 m to 350 m, underlain by 550 m of interbedded Tertiary ash-flow and air-fall tuff. Paleozoic carbonates extend beneath the tuffs to the Precambrian basement rocks. Structural features near crater U5a include the Cane Spring and Rock Valley fault zones, the Frenchman flexure, and the Scarp Canyon lineament. Nearest to crater U5a is the Cane Spring fault zone, a northeast trending left lateral strike-slip fault located approximately 6.4 km to the west-northwest.

### **Hydrogeologic Setting**

#### **Nevada Test Site**

The lithology of the NTS can be divided into valley-fill alluvium, clastics, tuffs, and carbonates (Shott et al., 1997). In general, the saturated portion of the alluvium, welded tuffs, and carbonates store and transmit enough water to be considered aquifers.

The bedded tuffs and clastics form aquitards. Winograd and Thordarson (1975) identified nine hydrostratigraphic units (5 aquifers and 4 aquitards) at the NTS, although these do not occur at all locations. In stratigraphic order, these units are the valley-fill aquifer, lava flow aquifer, welded tuff aquifer, lava flow aquitard, bedded tuff aquitard, upper carbonate aquifer, upper clastic aquitard, lower carbonate aquifer, and lower clastic aquitard.

The Nevada Test Site lies within the most arid part of Nevada. Average annual precipitation ranges from 8 cm to 25 cm, depending on elevation. Principle recharge occurs in the higher elevations of the mountains. Infiltration at the recharge sites is vertical through the carbonate bedrock and then flows horizontally into the alluvial valley-fill (Domenico et al., 1964). Discharge occurs through evapotranspiration and through springs. Potential evapotranspiration rates of 150 to 200 cm a year in the basins greatly exceed precipitation and create a vadose zone often over 350 m thick. Most of the larger springs in the area issue from carbonate rocks or from basin-fill overlying or adjacent to carbonate rocks (Burbey and Prudic, 1991).

The principle reservoir used for water supply at the Nevada Test Site is the Tertiary and Quaternary valley-fill aquifer. It comprises alluvial fan, fluvial, lakebed, and mudflow deposits. The alluvial deposits include a range of grain sizes from clay to gravel and can be unconsolidated within a basin (Anderson, 1995). The upper alluvium is Paleozoic detritus and Tertiary rocks; deeper alluvium is predominantly tuffaceous. Maximum thickness is 730 m but the saturated thickness is only a fraction of that.

### Frenchman Flat and Crater U5a

Frenchman Flat is surrounded on all sides by mountains and therefore drains internally. The alluvial valley-fill aquifer is saturated beneath an area of 70 km<sup>2</sup>. Winograd and Thordarson (1975) examined three possibilities for water movement out of the basin from this valley-fill aquifer: (1) lateral flow through the Tertiary aquitards, (2) downward movement through the tuff aquitard into the carbonate aquifer, or (3) lateral flow through the aquitard then downward movement into the carbonate aquifer. They stated that the strongest case could be made for downward movement to the carbonates. This belief is based on no gradient existing between Frenchman Flat and Yucca Flat and a small range (3 m) between the lowest water levels in the Cenozoic rocks for Frenchman Flat, Yucca Flat, and Jackass Flat. In any event, the lower carbonate aquifer rises above Frenchman Flat on all sides so groundwater movement will eventually flow into the carbonate aquifer.

Average annual rainfall at the Well 5B precipitation gage 2700 m southwest of crater U5a, is only 12.4 cm. This extremely arid environment has no perennial streams or standing bodies of water. Surface water flow occurs only infrequently and channels are rarely deeper than 1 m. Schmeltzer et al. (1993) established that crater U5a is located on the Barren Wash alluvial fan (alluvial fan area = 14.5 km<sup>2</sup>) with the entire Barren Wash watershed measuring 210 km<sup>2</sup>. The upstream watershed is likely to contribute flows to the crater very infrequently (French, 1997).

The “Wishbone” event that formed Crater U5a was detonated at a working point depth of 174.9 m below land surface. The static water table was estimated to be 206 m below land surface. Some estimation of cavity size must be made to determine the

bulking factor and the position of the nuclear melt debris and radionuclides relative to the static water level. In turn, these attributes are directly related to geologic media and device yield. Drill logs for the emplacement hole record alluvium throughout the profile down to the water table. The actual yield of the weapons test, however, is classified. The "Wishbone" event is officially listed as < 20 kilotons. Such a large range produces enormous differences in possible cavity radii. The "Wishbone" event was buried at a fairly shallow depth, 174.9 meters. Minimum depth of burial for any test was normally 183 meters but the proximity of the water table at 206 meters may have forced a slightly shallower burial. The scaled depth of burial (SDOB) was calculated by the simple formula:

$$\text{SDOB (ft)} = 350(\text{kt}^{1/3}) \quad (\text{Germain and Kahn, 1968}) \quad (4)$$

Many tests in the 1960's used a less conservative  $\text{SDOB} = 300(\text{kt}^{1/3})$ . In 1990, "Baneberry" vented large amounts of gases to the atmosphere causing concern that a deeper SDOB was warranted. Post-Baneberry, the SDOB became  $400(\text{kt}^{1/3})$ .

Knowing the depth of burial of the detonation that formed crater U5a helps to confine the likely maximum yield. Some venting did occur with this event which may indicate slight under burial for the given weapon yield. The reported range of yields for "Wishbone" is < 20 kt, simplified equations show that the actual yield was most likely significantly less. The range can be conservatively constrained to 3 to 7 kt.

From the device yield estimation, a further extrapolation may be made to estimate the size of the cavity produced from the vaporization of the surrounding rock and soil. Olsen (1993) gives the formula for approximating the length of the cavity radius:

$$R_c = \frac{CW^{1/3}}{(\rho h)^{1/4}} \quad (5)$$

where C is a constant, nominally 70.2, W is the yield in kilotons,  $\rho$  is the overburden density in  $\text{Mg/m}^3$ , and h is the depth of burial in meters. This approximation of the radius has 1-sigma error bars of about 10%. Using the estimated range of yields and an overburden pressure  $\rho$  of  $2.0 \text{ g/cm}^3$  (Olsen, 1993), cavity radius can be approximated in the range of 17 to 23 m. This estimate places the working point within 2 cavity radii of the water table, possibly allowing the introduction of some radionuclides directly.

All rubble chimneys exhibit a bulking factor *beta*, not the compaction of rock that may be intuitive. This bulking has been thought to possibly provide a preferential pathway for infiltrating water. A common formula for estimating the bulking porosity, *beta*, is given by:

$$\text{beta} = \frac{(\text{top of the cavity to the ground surface}) - (\text{bottom of cavity to bottom of crater})}{\text{bottom of cavity to bottom of crater}}$$

This simple equation approximates *beta* at 5% to 12%. The formula for the bulking factor is uncomplicated but results fit well with those observed in the field.

A topographic survey of crater U5a was conducted in 1996 by Bechtel Nevada Corporation showing a depth of 12.8 m, representing 14.6 m of infilling over the last 30 years. Hokett and Gillespie (1996) conducted particle size analysis on 30 samples from crater U5a (Borehole U5a-N1) and 6 samples from an undisturbed area adjacent to the crater (Borehole U5a-N2). The soil texture in the top three meters of the playa is clay loam to loam. The remainder of the borehole (<2 mm fraction) was comprised of loamy sand, sandy loams, and sand. The finer textured soils are the result of deposition during ponding events. Samples from the undisturbed borehole outside the crater were

all sandy loam or loamy sand.

The bottom of crater U5a is dominated by *Tamarix ramosissima* (saltcedar), a naturalized shrub with a reputed high evapotranspiration (ET) rate. Sala et al. (1996) reported that the key biological characteristics that have allowed its spread include (1) production of massive amounts of small, easily dispersed seeds over long periods of time (Warren and Turner, 1975), (2) ability to germinate and survive in highly saline soils (Brotherson and Winkle, 1986; Shafroth et al., 1995), (3) the ability of seedlings to tolerate both desiccation and inundation, (4) active vegetative reproduction, and (5) the facultative phreatophytic nature of mature individuals (Busch et al., 1992). The presence of these plants are further evidence of the periodic flooding and subsequent infiltration of ponding events.

Smith et al. (1996) found that in dense stands of *T. ramosissima* with high leaf area index, ET can dramatically exceed net radiation (and thus predicted  $ET_0$ ) under conditions of moist soils and high water table. These conditions are only partially met in the wintertime, when antecedent moisture content is higher, or directly following ponding events. This situation occurs primarily in the winter months (October - April) when cooler temperatures provide naturally reduced ET. During the summer months (May - September) hydraulic resistance for transport of water to leaf canopy, causes ET to be significantly lower than net radiation.

## **Theoretical Methods**

### **Flow Equations**

Darcy's law (1856) was originally established for flow of water through a

saturated, homogeneous soil but was later extended to include non-steady state, unsaturated flow as:

$$q = \frac{Q}{At} = -K(h) \frac{\partial h}{\partial z} \quad (6)$$

where  $q$  is the flux density ( $LT^{-1}$ ), i.e., the volume of water,  $Q$  ( $L^3$ ), passing through a cross sectional area,  $A$  ( $L^2$ ), per unit time,  $t$  ( $T$ ). The hydraulic head,  $H$  ( $L$ ), is the sum of the gravitational head,  $z$  ( $L$ ), and pressure head,  $h$  ( $L$ ). The latter term attains positive values below and negative values above the water table. The hydraulic conductivity  $K$ , ( $LT^{-1}$ ), represents the ability of a soil to conduct water and is considered to be constant under saturated conditions. In variably saturated flow, however, it is a function of matric (i.e. negative pressure) head. As the matric head varies throughout the soil, so too will the water content and hydraulic conductivity. The hydraulic conductivity, being the slope of the flux versus hydraulic gradient line, varies with the average negative pressure.

Darcy's law can be combined with the continuity equation:

$$\frac{\partial \theta}{\partial t} = -\nabla q \quad (7)$$

where  $-\nabla q$  is the divergence of the flux, i.e., the difference between inflow and outflow at a given point. The left hand side of this equation can be written as

$$\frac{\partial \theta}{\partial t} = \frac{\partial \theta}{\partial h} \frac{\partial h}{\partial t} = C(\theta) \frac{\partial h}{\partial t} \quad (8)$$

where  $C(\theta)$ , the slope of the water retention curve, is referred to as the specific water capacity.

Combining the continuity equation with the Darcy equation, results in the

Richards' equation (1931) for one-dimensional, non-steady state flow of water in the vertical direction:

$$C(\theta) \frac{\partial h}{\partial t} = \frac{\partial}{\partial z} \left[ K(h) \frac{\partial h}{\partial z} + K(h) \right] \quad (9)$$

### Water Retention Function

The water retention function can be defined as the relationship between the soil water content and the matric pressure head. Matric pressure head for unsaturated soils are negative and will be referred to in units of depth of water. A soil's ability to retain soil water under different matric heads gives much information as to how the soil will regulate infiltration *in situ*. The water retention function is primarily controlled by two soil characteristics: the texture or particle-size distribution, and the structure or pore-size distribution due to arrangement of the particles into units called aggregates (Salter and Williams, 1965; Reeve et al., 1973; Sharma and Uehara, 1968). Secondary structures contained in the soil can dramatically affect the water retention function. Organic matter can produce preferred pathways for water flow and alter retention due to its hydrophilic nature. Desiccation cracks create large macro-structures that can act as a conduit for soil water movement. Also the presence of shrink/swell clays affect the amount of water retained at a given pressure head (Bolt, 1956; El-Swaify and Henderson, 1967; Thomas and Moodie, 1962; Warkentin et al., 1957).

The water retention curve may be measured in the laboratory under conditions of drying an initially saturated soil sample to the residual water content, or measured for the wetting curve, beginning at the residual water content and increasing the matric

head (less negative) to saturation. Hysteresis explains the difference between the wetting and drying curves. This principle states that a given pressure head for a wetting soil is less than that for a drying soil (Topp, 1969; Haines, 1930; Pavlakis and Barden, 1972). This study will only utilize the drainage curve.

### Unsaturated Hydraulic Conductivity

Reliable estimates of unsaturated hydraulic conductivity,  $K(h)$ , are especially difficult to obtain, partly because of its extensive variability in the field, and partly because measuring this parameter is time-consuming and expensive (van Genuchten, 1978). It is for this reason that investigators began using models to calculate  $K(h)$  from water retention data. Early attempts, including the Millington-Quirk method (Millington and Quirk, 1964), produced acceptable results but were difficult to apply in actual field conditions. Brooks and Corey (1964) and Jeppson (1974) used closed-form analytical expressions based on the Burdine theory (Burdine, 1953) to estimate  $K(h)$ . The Brooks-Corey method can be described reasonably well with the following equation:

$$\Theta = \left( \frac{h}{h_a} \right)^{-\lambda} \quad (10)$$

where  $h_a$  is the air entry value and  $\lambda$  is a soil characteristic parameter. It produces fairly accurate predictions but a discontinuity exists in the slope of the water retention curve and unsaturated hydraulic conductivity curve at the air-entry value,  $h_a$ .

A model utilizing a simple integral formula for unsaturated hydraulic conductivity was developed by Mualem (1976) allowing one to derive a closed-form

analytical expression from the water retention curve:

$$K_r = \frac{K(h)}{K_s} = \Theta^{1/2} \left[ \frac{\int_0^\Theta \frac{1}{h(x)} dx}{\int_0^1 \frac{1}{h(x)} dx} \right]^2 \quad (11)$$

where  $h$  is the matric head and  $\Theta$  is the dimensionless parameter representing the effective moisture content:

$$\Theta = \frac{\theta - \theta_r}{\theta_s - \theta_r} \quad (12)$$

where  $\theta_r$  and  $\theta_s$  are the saturated and residual water contents, respectively.

van Genuchten (1978) incorporated the theories of Burdine and Mualem to generate a  $\Theta$  model. The van Genuchten closed-form analytical expression contains three fitting parameters obtained from a non-linear least-square curve-fitting computer model of the water retention curve. The dimensionless effective moisture content is related to the pressure head by the following:

$$\Theta = \left[ \frac{1}{1 + (\alpha h)^n} \right]^m \quad (13)$$

where  $\alpha$ ,  $m$ , and  $n$  are fitted parameters.

Most available techniques for measuring soil hydraulic properties (conductivity and retention) can neither distinguish between the different flow domains (macro-, meso-, or micro-) and their relative contribution to flow (Luxmoore et al., 1990) nor be used to determine the between-domain exchange terms during variably saturated flow (Mohanty et al., 1997). Tension infiltrometers can determine a hydraulic conductivity at a given tension, and this  $K(h)$  value can be matched with a known  $K_{SAT}$  value,

shifting the entire  $K(h)$  curve to this matching point.

Smettem and Kirby (1990) and Smettem et al. (1991) proposed a method for modeling  $K$  and  $\theta$  as a function of head for a macropore-matrix system. They used the van Genuchten (1978, 1980) model to determine the closed form analytical solutions for  $\theta(h)$  and  $K(\theta)$ . Structured soils may contain macropores, mesopores, and micropores, with flow through each region dictated by the physical attributes of the soil. Wilson et al. (1992) developed techniques for modeling  $\theta(h)$  and  $K(h)$  in multiple porosity systems using van Genuchten  $\theta(h)$  and  $K(h)$  models for the meso- and micropore regions. It was initially assumed that a linear relationship exists for  $\theta(h)$  and  $K(\theta)$  between saturation and near saturation ( $h = -10$  cm), i.e. macropore region. However, this assumption failed to reach convergence when used in the three-dimensional multi-region flow model MURF (Gwo, 1991, unpublished data). It is essential that the  $\theta(h)$  relationship remain continuous throughout the range of  $h$  values to prevent convergence problems in flow modeling. To accomplish this, Wilson et al. (1992) maintained the pressure head untransformed and obtained continuity between regions by selectively fixing and fitting the saturated and residual water content values to a nonlinear model called a Fermi function. Utilizing this approach, continuity was achieved and excellent agreement between measured and predicted values was reached, although the derivative of the  $\theta(h)$  and  $K(\theta)$  functions were occasionally not continuous at the junction points between regions.

Mohanty et al. (1997) used *in situ* and laboratory measurements to develop piecewise-continuous soil water retention and hydraulic conductivity functions using

small increments in  $h$  to describe preferential flow. In contrast to the Wilson et al. (1992) approach of using numerous piecewise-continuous functions joined at different junction points, Mohanty et al. (1997) invoked a hybrid sum-junction approach using two or more piecewise-continuous functions based on the different conducting pore regions. They set the  $K_{SAT}$  as a floating parameter based on measured hydraulic conductivities at the junction point between capillary and non-capillary driven flow. Similar to the approach of Wilson et al. (1992), Mohanty et al. (1997) extrapolated  $K$  values from the mesopore range to the macropore range using a non-linear equation. The authors reported that this new bimodal soil water retention and hydraulic conductivity functions performed well in describing the observed conditions at their field site.

## **Experimental Methods**

### **Water Retention**

The hanging water column and pressure plate methods were used for water retention analysis as outlined in Klute (1986). Two undisturbed soil cores were taken from each station along a transect across the crater bottom (Figure 8) and one undisturbed soil core from each of the three stations adjacent to the crater. The undisturbed cores allowed the soil structure to be preserved. The soil core cells had an inside diameter of 5.3 cm and a height of 6 cm. The soil core samples were saturated in a 0.005 M  $CaSO_4$  deaerated solution with 0.1% phenol. Saturation of the samples was accomplished slowly and incrementally from the bottom up to limit the entrapment of air. 350 ml Pyrex brand 80 mm fine-fritted disk Buchner funnels saturated in 0.005 M

CaSO<sub>4</sub> deaerated solution were used for the hanging water column measurements. Water retention at selected matric heads were obtained by lowering the water-filled tubing to the prescribed level below the semi-permeable membrane and allowing at least one day for equilibration. Matric heads of -15 cm, -50 cm, -100 cm, -150 cm, and -200 cm were completed and the soil sample was weighed after each. Due to practical height restraints involved in the hanging water column method, -200 cm was the limit of the system.

Mid-range (-500 to -3000 cm) water retention values were accomplished with the laboratory pressure chamber method outlined in Klute (1986). The soil core samples were placed on a fully saturated 3-bar ceramic pressure plate and pressures of -500 cm, -750 cm, and -1000 cm were applied. The samples were weighed after allowing a minimum of 2 days equilibration. Disturbed soil samples placed in rubber rings were moistened in 0.005 M CaSO<sub>4</sub> deaerated solution with 0.1% phenol and placed on a 5-bar ceramic pressure plate. Pressures of -1000 cm and -3000 cm were applied for a minimum of 2 days equilibration. The soil cores and disturbed soil samples were then oven-dried at 105° C for 2 days and weighed.

Bulk density  $\rho_B$  was determined by oven-drying a core sample of a known volume  $V_{CORE}$  and recording the mass  $M_{DRY}$ .

$$\rho_B = \frac{M_{DRY}}{V_{CORE}} \quad (14)$$

Volumetric water content,  $\theta_V$ , was calculated from the core samples at various pressures,  $M_i$

$$\theta_v = \frac{\rho_B \left( \frac{M_i - M_{DRY}}{M_{DRY}} \right)}{\rho_w} \quad (15)$$

The RETC code (van Genuchten, 1980), a non-linear least-squares curve-fitting program, calculated  $\alpha$  and  $n$  parameters from the volumetric water content and the associated pressure head with the assumption that  $m = 1 - 1/n$ .

#### Saturated Hydraulic Conductivity

Single ring infiltrometer measurements were conducted at each station along the transect (Figure 8) and at the three stations adjacent to the crater. This method of point infiltration was chosen to simulate the conditions of pond seepage. A metal ring (diameter = 24.7 cm) was driven into the ground 10 cm and a predetermined volume of water was applied to the soil. Two hoses, one for water application and one for air, were run into a 50 liter carboy with rubber stopper to create a Mariotte device for head control. By securing the air hose at a given height within the metal ring, a constant head of 4 cm was maintained on the soil. Lateral spreading was not considered a concern so an outer ring was not utilized. Intake measurements were recorded until a steady-state condition was observed.

#### Unsaturated Hydraulic Conductivity

The tension infiltrometer (also known as disc permeameter) is a field method to measure unsaturated hydraulic conductivity,  $K(h)$ . The procedures for confined tension infiltrometer techniques are described in Wilson and Luxmoore (1988). Tension infiltration was measured immediately following the constant head ring infiltrometer

procedure at each station along the crater transect and at the three stations adjacent to the crater. Within the ring, the soil surface was cleared of any debris or organic matter and covered with a thin layer of wet fine sand. This action ensures a proper “seal” around the disk of the instrument and eliminates air entry. The tension infiltrometer allowed water to be infiltrated into the soil surface under a constant matric head of -15 cm. The outflow of water from the device was recorded until a steady-state infiltration rate was achieved. For confined infiltration, the steady-state infiltration rate equals the hydraulic conductivity for the prescribed matric head. Upon completion, a soil sample was collected and oven-dried at 105° C to determine water content,  $\theta$ .

#### Particle Size Analysis

Particle size analysis of bulk samples was accomplished using the hydrometer and dry sieve methods as described by Gee and Bauder (1986). Loose soil samples were collected from 16 sites along the transect (Figure 8). In addition, 3 sites adjacent to the crater were sampled. From each sampling site, 40 to 50 g of air-dried soil were weighed into a 600 mL beaker. 250 mL of distilled water and 100 mL of sodium-hexametaphosphate (HMP) solution (50 g/L) were added to the beaker and allowed to soak overnight. The HMP solution neutralizes the charge on small soil grains, thus prohibiting the attraction of the grains from each other. The HMP treated soil sample was transferred to an electric blender and mixed for 5 minutes. Distilled water was then added to bring the volume to 1 L. For calibration purposes, a 1-L sedimentation cylinder contained 100 mL of HMP solution and 900 mL of distilled water. The calibration value of this blank solution was used to correct for fluid viscosity and soil

solution concentration. Time was allowed for both sedimentation cylinders to thermally equilibrate and the temperature was recorded. The cylinders were stoppered and end-over-end shaking was performed for 1 minute. One drop of amyl alcohol was added to eradicate surface foam. A standard hydrometer, ASTM no. 152 H, was slowly lowered into suspension and readings were recorded after 30 s, 1, 3, 10, 30, 90, 120, and 1440 minutes, removing and rinsing the hydrometer after each reading.

Upon completion of all hydrometer measurements, the sedimentation cylinders were poured through a 63  $\mu\text{m}$  sieve, the remaining sediment in the sieve being very fine sand to gravel. This sieved material was placed in a pan and oven-dried at 105° C. The dried sand and gravel grains were weighed and then sieved through a stack of seven sieves (63  $\mu\text{m}$ , 125  $\mu\text{m}$ , 250  $\mu\text{m}$ , 500  $\mu\text{m}$ , 850  $\mu\text{m}$ , 1180  $\mu\text{m}$ , 1180  $\mu\text{m}$ , and 2360  $\mu\text{m}$ ). The stack of sieves was placed in an automatic sieve shaker for 5 minutes. Each sieve was then weighed and a soil fraction mass was calculated.

Results of the hydrometer and dry sieve procedures yield a mass fraction % for gravel, sand, silt, and clay. The gravel mass of each sample was disregarded and the remaining sand, silt, and clay percentages were used to classify the soil, using the USDA soil classification triangle.

### Subsurface Characterization

To more accurately and completely characterize the subsurface, a series of sites along the transect were augered using a Gidding's probe. Due to the hardness of the fine-grained layers encountered, continuous core samples were not recovered. Eight locations spaced approximately 10 m apart (Figure 8), were drilled to a depth of 6 m

and the cuttings bagged and logged. The soil texture was estimated by the feel technique on all samples by Dr. G. V. Wilson, a Certified Professional Soil Scientist. In the laboratory, hydrometer and dry sieve techniques were used to determine particle size distributions on selected samples. To separate the fine grained sands from the silts, hydrometer measurements were recorded at 0.25, 0.5, 3, 15, 45, 120, and 1440 minutes and sieve screen diameters of 2.0, 0.707, 0.425, 0.250, 0.150, and 0.090 mm were used.

### Water Harvest

The quantity of water that may be captured by the subsidence crater was estimated by French (1997) using the Soil Conservation Service (SCS) curve number approach. By definition, the curve number is

$$CN = \frac{1000}{S + 100} \quad (16)$$

where CN = SCS curve number and S = maximum retention. Assuming that the initial abstraction of precipitation is 20% of the maximum retention, the relationship between the depths of precipitation (P) and runoff (Q) is

$$Q = \frac{\left( P - \frac{200}{CN} - 2 \right)^2}{P + \frac{800}{CN} - 8} \quad (17)$$

French (1997) stated that although other methods for estimating direct runoff are available, relative to the quantity and quality of data available, the curve number approach is reasonable. French (1997) used the precipitation data for the Well 5B station, located 2700 m southwest of crater U5a. The average annual depth of precipitation was 12.4 cm. French originally intended to study two flow capture

scenarios: (1) capture of the entire flow from the small watershed (approximately 0.65 km<sup>2</sup>) and (2) sheetflow capture from the Barren Wash Alluvial fan watershed (210 km<sup>2</sup>) on which the crater is located. Because of the ratios of the watershed areas and the U5a diameter to the alluvial fan contour passing through it, the larger flow capture area was considered unnecessary.

To properly represent soil conditions, Antecedent Moisture Condition II (AMC-II) curve number of 77 was used for the winter months (October - April) and AMC-I curve number of 59 was used for the summer months (May - September). Table 3 shows the results of a 32 year simulation period using the 0.65 km<sup>2</sup> capture area. Following crater formation in 1965, 14 ponding events were modeled with 14 corresponding drainage periods.

## **Numerical Methods**

### **HYDRUS-2D**

HYDRUS-2D, developed by Simunek et al. (1996), is a Microsoft Windows based model for analysis of water flow and solute transport in variably saturated media. It includes the SWMS\_2D finite element model for simulating two-dimensional water and solute movement in the variably saturated media. HYDRUS-2D numerically solves the Richards' equation for saturated-unsaturated water flow. The flow region may consist of heterogeneous, anisotropic soils and irregular flow domains. A catalog of soil hydraulic properties, based on soil texture, is included in the program. Flow can be modeled in the vertical plane, horizontal plane or in a three-dimensional region by simulating radial symmetry about a vertical axis. Boundary conditions can be

prescribed as heads, fluxes, atmospheric, or free drainage. Initial conditions can be made constant throughout the flow domain, varied heterogeneously, or set in equilibrium with a bottom value. Data preprocessing, involving specification of the flow domain and construction of an unstructured finite element mesh, is accomplished with the mesh generation program MESHGEN-2D by PC-Progress, based on Delauney triangulation. Post-processing is also accomplished within the HYDRUS-2D model, with output graphics in 2D isolines or color spectra.

Three separate modeling scenarios were conducted to assess the uncertainty in the approaches taken by Hokett and French (1998) by determining the effects of (1) areal extent and depths of ponds (boundary conditions) and (2) initial matric head conditions. The goal of the final scenario was to modify the conceptual model and flow domain (i.e. boundary conditions, initial conditions and media properties) to provide a “best” estimate of recharge based upon the new site characterization data. This final modeling scenario incorporates hydraulic properties determined from field and laboratory investigations, as well as surface runoff and subsequent ponding events as evidenced by physical attributes of the crater morphology.

#### Sensitivity Analysis I and II

Sensitivity Analysis I (SA I) examined the effects of varying the top boundary conditions on the depth of water movement in an unsaturated soil. The geometry and domain were held constant throughout the sensitivity analysis. The dimensions modeled were 40 m x 40 m, with no flow boundaries along the vertical sides and free drainage along the bottom boundary (Figure 9). Two separate boundary conditions,

depth of pond and areal extent of pond were applied to a series of ponding events and subsequent drainage event. Pond depths were set at 30 cm and 90 cm and areal extents at 5 m, 12 m, 15 m, and 20 m and allowed to infiltrate until the prescribed volume of water was infiltrated. Following pond infiltration, an evapotranspiration boundary condition was applied until the next pond event. The ET was set uniform with time at 0.008 m/d after Hokett and Gillespie (1998). The pond was simulated with a constant pressure head at the desired depth and horizontal extent along the upper boundary, with the remaining surface set as a no flow condition. The first pond volume equaled 271 m<sup>3</sup>, followed by 990 days of drainage and evapotranspiration, followed by a second pond of volume 419 m<sup>3</sup>. Initial condition (matric head) was set at -100 m.

Sensitivity Analysis II (SA II) used flow domain geometry, properties and boundary conditions consistent with Hokett and Gillespie (1998) to examine the effects of varying initial conditions on the depth of water movement beneath the crater. The three scenarios modeled to compare and contrast with the initial matric head of -10 m by Hokett and Gillespie were (1) initial matric head of -10 m throughout the domain, (2) initial matric head of -200 m throughout the domain, and (3) initial matric head set at equilibrium with the water table at the bottom boundary, resulting in a linear function with height above the water table. The initial and boundary conditions for Sensitivity Analysis II are represented in Figure 10. The dimensions modeled more closely represented the actual crater and rubble chimney assuming axial symmetry with a 60 m wide by 200 m deep domain. The great depth of the underlying water table produced extremely dry conditions when set to equilibrium with the bottom boundary condition. The entire 33 years of predicted surface runoff, ponding events, and drainage

events were used to adequately capture the difference between the two modeling environments.

MESHGEN-2D generated a mesh of 2574 nodes, 4987 triangles, and 7560 line segments for the smaller domain of Sensitivity Analysis I and 2959 nodes, 5677 triangles, and 8635 line segments for the larger domain of Sensitivity Analysis II. Finer discretizations were used near the soil surface to handle the region of distinct differences in fluxes and pressure gradients. For SA I, maximum vertical discretization was 2.2 m near the bottom boundary and minimum discretization was 0.2 m along the surface. For SA II, maximum vertical discretization was 7 m near the bottom boundary and minimum discretization was 0.4 m near the surface. Three dimensionality was modeled with axisymmetric flow. Soil types incorporated in both analyses were limited to the three textures that appeared predominant in the crater region (Figure 11). The playa was represented by a 10 m wide by 3 m thick region of silt loam, underlain by a 10 m wide by 7 m thick region of loam. The remainder of the subsurface was loamy sand. Hydraulic properties for the three soil types (Table 4) were consistent with Hokett and Gillespie (1998) who obtained these values from the HYDRUS-2D catalog for soil texture, based on Carsel and Parrish (1988).

Because of the non-linear nature of the finite difference equation that HYDRUS-2D solves, an iterative process must be used to obtain solutions of linearized algebraic equations. To ensure a satisfactory degree of agreement was obtained, the maximum number of iterations was set at 20 (upper ideal iteration = 7, lower ideal iteration = 3). Water content and pressure head tolerance were both set at 1.e-003 for ponding events, and 5.e-004 and 0.1, respectively, for drainage events.

Time discretization was sufficient to allow a given volume of water to infiltrate. Atmospheric conditions during the drainage event were time dependent. Evaporation was constant ( $0.008 \text{ md}^{-1}$ ) and consistent with average summertime values for Area 5 (Shott et al., 1997). Precipitation values were taken from the daily totals at Well 5b. For ease of input, monthly totals were divided by 30 and assigned as daily totals, admittedly losing some storm characteristics (duration, intensity).

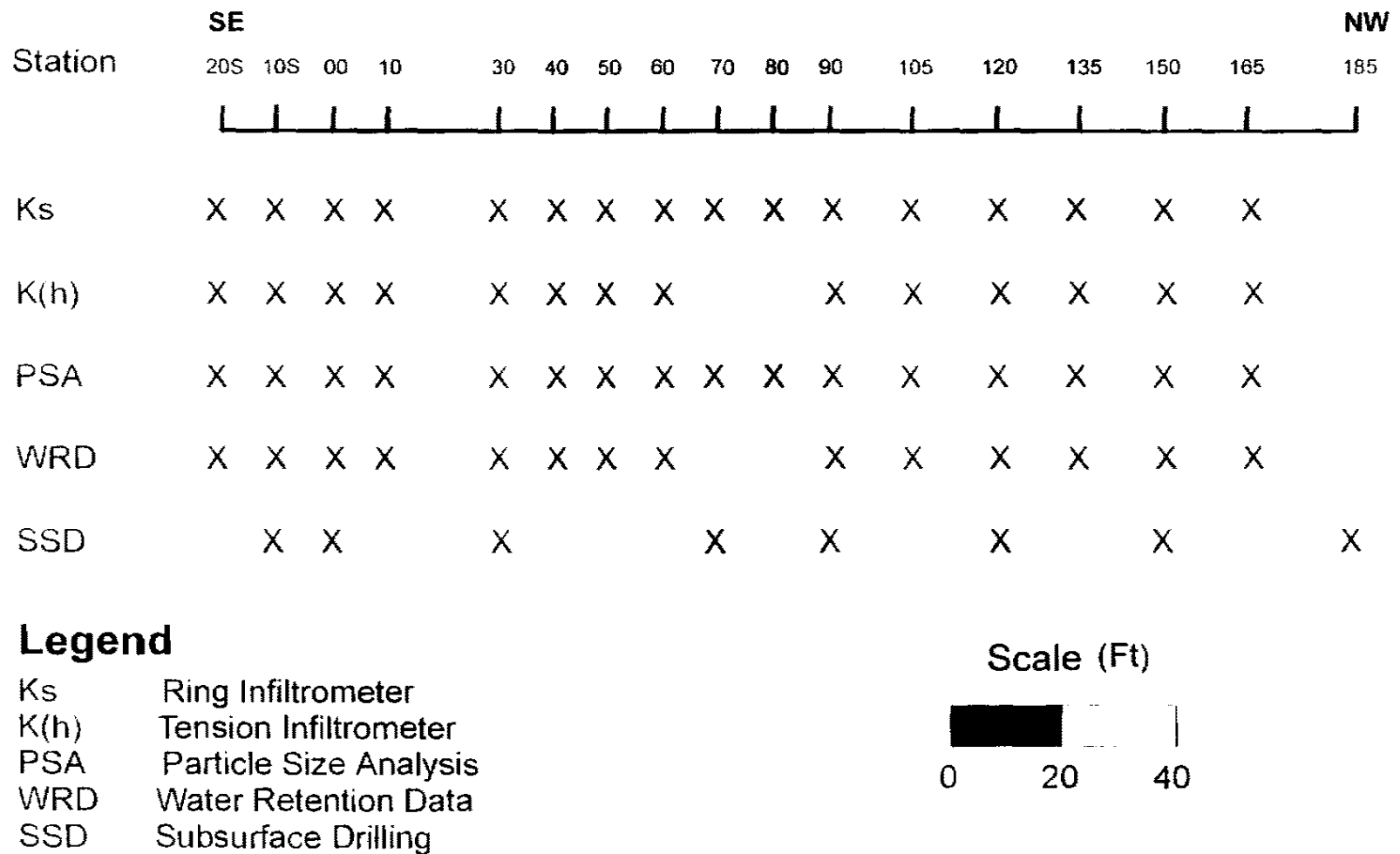


**Figure 8.** Summary of field and laboratory procedures for sampling sites along transect of crater U5a.

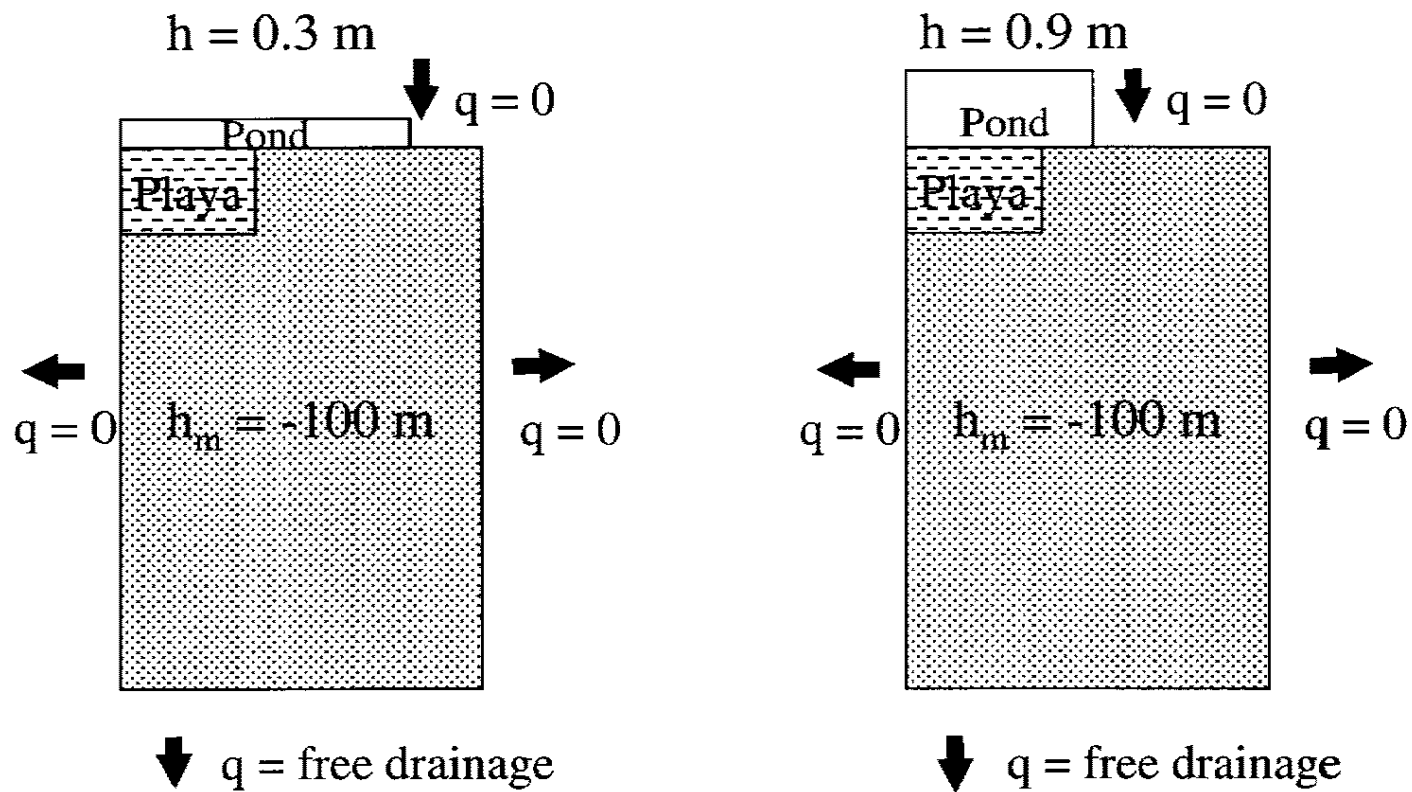


**Figure 9.** Diagram of the boundary conditions for Sensitivity Analysis I illustrating the pond depth and lateral extent variation.

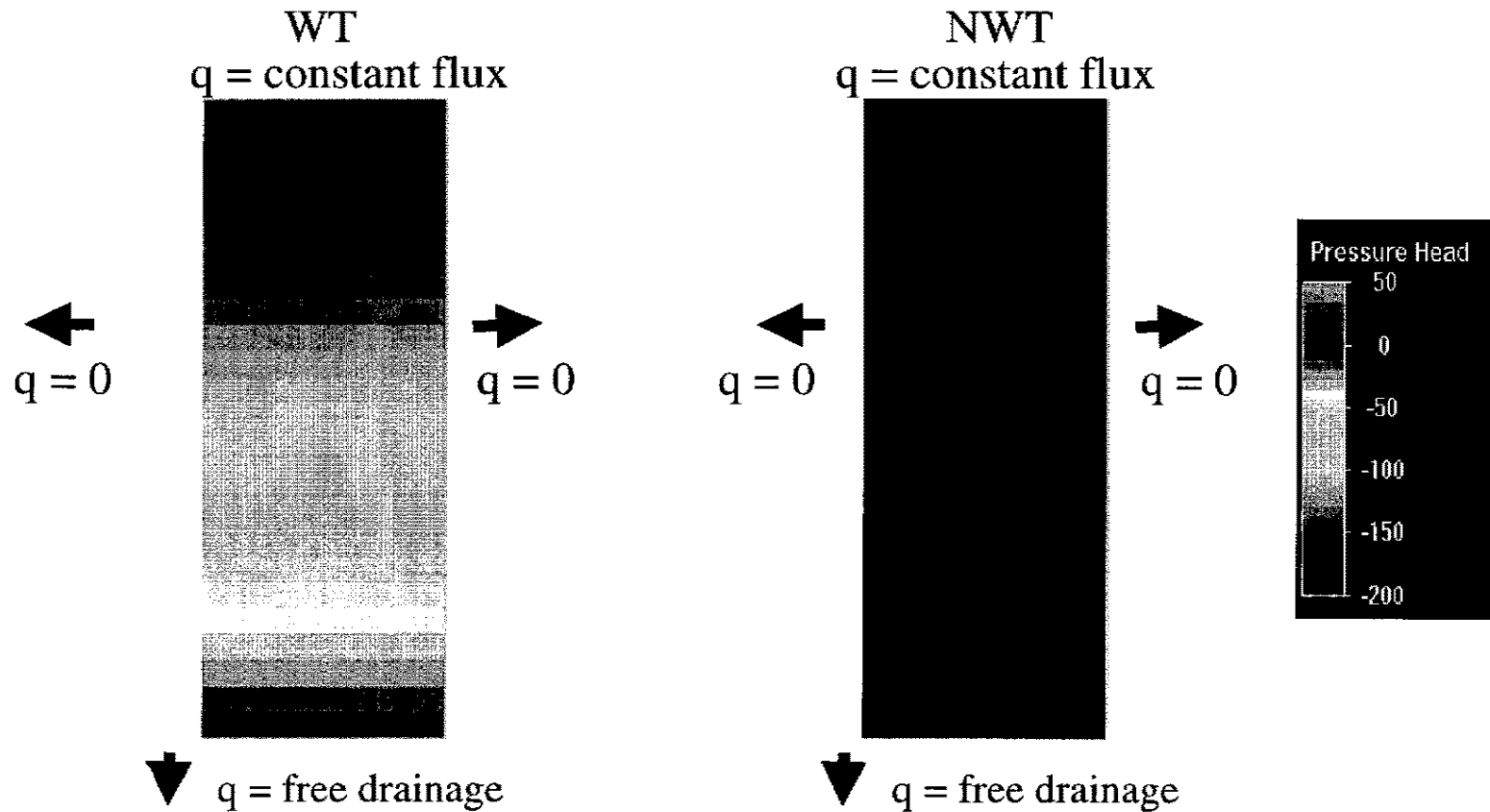


**Figure 10.** Diagram illustrating the initial conditions for Sensitivity Analysis II in which the pressure head was in equilibrium with the bottom water table (WT) or set to a constant head of -200 m (NWT).

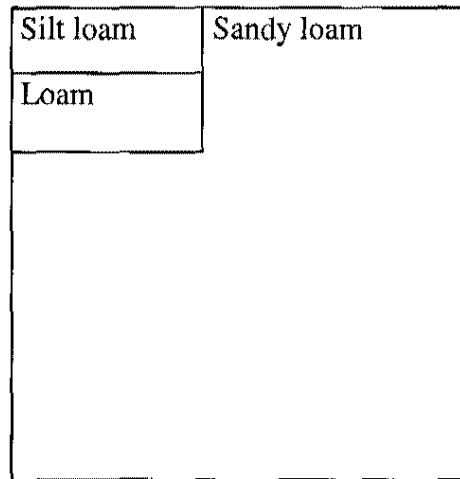


**Figure 11.** Schematic of three soil types used in Sensitivity Analysis I and II.

**Table 3.** Ponding event characteristics (Hokett and French, 1998).

Pond event	Year	Month	Volume (m <sup>3</sup> )
1	1	2	876
2	1	10	382
3	8	3	333
4	11	3	271
5	14	1	419
6	16	1	1369
7	18	1	530
8	20	1	358
9	20	4	284
10	24	1	210
11	26	2	530
12	28	1	333
13	28	11	333
14	29	2	555

**Table 4.** Hydrus-2D soil properties used for SA I and II.

Soil	Qr	Qs	Qa	Qm	alpha	n	Ks (md <sup>-1</sup> )	Kk (md <sup>-1</sup> )	Qk
Loamy sand	0.57	0.41	0.57	0.41	12.4	2.28	3.502	3.502	0.41
Silt loam	0.034	0.46	0.034	0.46	1.6	1.37	0.06	0.06	0.46
Loam	0.078	0.43	0.078	0.43	3.6	1.56	0.2496	0.2496	0.43

## CHAPTER 3

### RESULTS AND DISCUSSION

#### **Introduction**

The final estimation of recharge potential beneath a subsidence crater depends upon many hydrologic parameters, boundary and initial conditions. To accurately assess the effect of uncertainty in these variables, the study attempted to isolate different variables and analyze the sensitivity of the model to each. The volume of surface runoff that enters crater U5a can be predicted from the precipitation record and some understanding of the hydraulics involved. While this input may be the single most important determinant of recharge and the most uncertain in estimation, the uncertainty in runoff was not addressed in this study.

The behavior of the surface runoff upon entering the crater was the focus. Soil conditions within the crater prior to arrival of the pond may be moist because most predicted ponding events occur in the winter months when storms are of longer duration and lower intensity, however the largest ponding events may occur during high intensity summer storms when the soil can be extremely dry. Thus, the sensitivity to the initial condition needs to be evaluated. If the surface runoff flows to the crater low

point (playa), then the low permeability playa could act as a barrier to flow.

Alternately, substantial infiltration could occur in the coarse soil immediately upon entering the crater, resulting in a much diminished pond. Hokett and French (1998) proposed that a pond restricted in lateral extent to the playa and a small peripheral area surrounding the playa will preferentially focus recharge through this annular region. They assumed a 2 m lateral extent beyond the playa and a 30 cm depth. However, if surface area of the pond is substantially increased, infiltration will occur over the larger area and maximum depth of water movement for a given volume of water may be far shallower. The floor of the crater exhibits little relief and an intensive survey of the present day topography would yield a sufficiently accurate stage-volume relationship. Such data does not exist for most craters, including U5a, so an estimation of pond depth and lateral extent must be made for given runoff volumes. Thus, the sensitivity of recharge estimates to the boundary conditions representing the pond's lateral extent and depth needs to be evaluated.

### **Sensitivity Analysis I**

Sensitivity Analysis I examined ponding depths of 30 and 90 cm spread laterally along the surface for 5 m, 12 m, 15 m, and 20 m to determine how sensitive infiltration and subsurface water movement were to these boundary conditions. The affectability of water movement to the depth of a pond was tested by placing a constant head flux boundary of 30 cm and 90 cm at the four prescribed lateral extents. For this analysis, two ponds of 271 m<sup>3</sup> and 419 m<sup>3</sup> were separated by a 990 day drainage event. Initial conditions were set at -100 m, which represents a dry antecedent condition. The model

was run until the predetermined volume of water had infiltrated the surface and the results compared. The method of infiltrating a set volume of water most closely represents reality yet strongly influences the maximum depth of water movement. The head prescribed to the pond will control the time to fully infiltrate the pond.

The greater pressure head at the surface did affect the rate of infiltration and thus the time required to infiltrate the prescribed pond volume (Table 5). For the same volume of pond, the deeper pond infiltrated an average of 33% faster, directly proportional to the difference in pond depths. In each case, varying pond depth from 30 to 90 cm proved to have a negligible effect on the final depth of water movement (Table 6). Water content profiles appeared nearly identical for pond depths of 30 cm and 90 cm (Figure 12). A larger head (deeper pond depth) for one lateral extent would mean a greater volume of water, therefore resulting in a deeper wetting front. In this study, a relatively small range of heads was examined but the fact that a set volume of water was infiltrated limited the effect. If the infiltration simulation was run for a set time or if it simulated a falling head for an initial pressure head, the effect would be far more pronounced.

In the case of the 5 m lateral extent, the simulation was stopped after 30 days although the entire volume of water had not infiltrated. The confining layers of silt loam and loam limited water movement beneath the playa. Flat topography of the playa region in crater U5a would preclude the possibility of a 30 cm deep pond being confined to so small a lateral extent. It did successfully demonstrate the “capping” ability of the playa material. Final water contents of all scenarios where the pond extended beyond the playa demonstrate the preferential movement of water outside of

the fine-grained material. Infiltration is focused through the peripheral region of the playa.

If deeper water movement is taken to be a “worst case” scenario for purposes of risk assessment, then lateral extent of the pond is a controlling factor of potential recharge. The surface area covered by the pond is a function of many factors, including volume of pond and crater topography. The surface runoff volume depends upon storm intensity, antecedent moisture condition of the soil, and soil hydraulic conductivity. Considering only surficial soil texture, as in the case of SA I, the pond extending 2 m beyond the playa, as assumed by Hokett and French (1998), had the deepest water movement and the pond extending 10 m beyond the playa resulted in the shallowest (excluding the 5 m case, for reasons listed above), as seen in Figure 13. The difference between wetting front depths was clearly evident after only 2 ponding events. Following only 2 of the modeled 14 ponding events, water movement in the 12 m pond penetrated 60% deeper than the 20 m pond.

### **Sensitivity Analysis II**

Sensitivity Analysis II (SA II) examined the effects of initial condition on recharge estimates. Crater U5a is located in an extremely arid environment where potential evapotranspiration greatly exceeds precipitation. These factors produce dry soils overlying a very deep water table. Knowing that unsaturated hydraulic conductivity decreases as water content decreases, an attempt to quantify potential recharge due to initial conditions beneath crater U5a was undertaken.

Three separate initial matric heads of -10 m, -200 m, and matric head set in equilibrium with the water table were modeled for a series of 14 ponds and drainage events. The playa region was represented by silt loam over silt, with the remainder of the domain as sandy loam, as assumed by Hokett and French (1998). Pond depth and lateral extent were set at 60 cm and 12 m, respectively. The deep water table at 200 m below land surface results in a matric head changing linearly with depth for a value of 0 at the water table to -200 m at the surface.

The first scenario represented relatively moist conditions, as the entire domain was set at  $h = -10$  m. The higher matric head did not depict actual field observations, but rather was meant as an upper limit. While this initial condition is by no means close to the soil field capacity ( $h = -3.5$  m) or saturation ( $h = 0$  m), water movement reached a depth of 130.0 m.

The second initial condition observed was -200 m throughout the domain (Figure 14). This matric condition was chosen to equal the depth of the water table and to represent an extremely dry lower limit, even in close proximity to the water table. Maximum depth of water movement was 129.8 m, nearly equal to that of the -10 m condition (Figure 15).

The third initial condition modeled was a matric head set in equilibrium with the water table (Figure 14). This approach more closely approximates actual field conditions. Near the water table, the soil will be saturated in the capillary fringe but under negative heads. The unsaturated soil will become increasingly drier as the land surface is approached. For this condition, water infiltration and redistribution reached a

depth of 129.5 m, once again nearly mirroring the results of the first two scenarios (Figure 15).

The similar depths for all three initial conditions can be explained by an examination of the hydraulic conductivity function,  $K(h)$  and water retention function,  $\theta(h)$  as shown in Figure 16 and Figure 17, respectively. Although the matric heads for the first two scenarios span an order of magnitude (-200 m to -10 m), the entire range is very dry with minimal difference in water storage capacity. Water retention data for sandy loam showed residual water content was reached by  $h = -10$  m. Water content decreased minimally below this point. As unsaturated hydraulic conductivity is a function of head or water content,  $K(h)$  will be relatively the same low value for each of these initial conditions. In the third scenario, matric head was linearly proportional to depth, therefore matric heads ranged from -200 m to -130 m over this infiltration depth range. Once again, such dry conditions would dictate a similar  $K(h)$  and available water storage throughout the simulation. However, for this initial condition, the rate of water movement would be expected to increase as the wetting front approached the water table. The simulation ended when the wetting front was still nearly 70 m from the saturated zone. Within 10 m of the water table ( $h = -10$  m), water content would begin to be great enough to strongly influence the hydraulic conductivity and storage capacity, thereby accelerating the rate of downward redistribution. The graph of hydraulic conductivity versus head (Figure 16) shows a break in the relatively flat gradient above  $h = -1000$  m for the coarse material. This matric head, representing close proximity to the water table, would dominate the rate of unsaturated flow. A simple least-squares regression for depth of water movement from time predicts the wetting front will reach

a depth of 190 m at 49.5 years. Results of SA II appear to show a negligible effect of initial conditions on depth of water movement to the tested depth.

### **Particle Size Analysis along Surface Transect**

Hydrometer and dry sieve results from soil samples taken along the surface transect showed a spatial relation for particle size analysis (Figure 18). Moving south away from the large erosional gullies, soil textures became increasingly fine-grained (Table 7). The playa region was distinguishable by a high clay content and the absence of vegetation (Figure 19). The northernmost sampling stations (90 through 165) are loamy sand to sandy loam. A sharp change in texture occurs between stations 70 and 80, the surficial beginning of the playa region. Within the playa, the soil texture continues to become finer towards the south, grading from silt loam to clay. This occurrence is not surprising, as the predominant direction of overland flow is from the gullies in the north towards the south. Upon entering the crater (and leaving the more confining channels), flow velocity decreases and the heavier, coarser material is preferentially deposited near the gully entrance. The two southernmost sampling locations, 10S and 20S, are sandy loam, representing more recent erosion from the steep crater walls. Sampling stations outside of the crater (A, B, and C) were loamy sand to sandy loam.

### **Particle Size Analysis with Depth**

Depth disturbed soil samples were collected in the field with the Gidding's probe and analyzed in the laboratory by the hydrometer and dry sieve methods. If intermittent ponding occurred since crater formation as predicted by the surface runoff

modeling, then subsurface examination would find a pattern of layering with depth of the sedimentation events. It is unlikely that the playa would extend down to the original crater surface (14.6 m below present-day land surface). Instead there would exist alternating layers of fine playa material and coarse material, representing deposition from individual pond events. Neither of these two possibilities was found. Results showed two modes of deposition occurred within crater U5a. The soil texture of the upper 6 m at the crater center, stations 30 and 70, exhibited gradual coarsening of soil texture with depth (Figure 20). Not only was the total sand content found to continuously increase with depth, but this size fraction was found to get coarser, with a gradual shift from very fine sand to very coarse sand (Table 8). Additionally, the deepest samples, at 5.9 m, contained gravel size particles. Soil texture determination was also completed in the field by Dr. G. V. Wilson (Appendix A). These results matched closely those determined in the laboratory and provide further evidence of coarsening with depth at other transect locations. The heavier, coarser sediment would be deposited first in the crater. The lighter, finer sediment would remain suspended until the flowing water stagnated and velocity decreased in the vicinity of the playa. Since there was no alternating coarse to fine layering in this zone of deposition, it is clear this is a single ponding event. This trend has the appearance of a crater-sized sedimentation cylinder. The particle size distribution at the crater center strongly suggests a single large ponding event deposited the upper 6 m of sediment, given the contact with gravel at 6 m. Additionally, deep drilling conducted by Hokett and Gillespie showed gravelly loamy sand below this suggesting that the entire 14.6 m was

deposited in one event. A simplified cross section of the crater is presented in Figure 21.

A surface of fine-grained silts and sands form a near continuous layer around the northern half of the crater sideslope and appears in places along the steeper southern slopes. This surface expression has the appearance of pond deposition, the top of which appears to constitute a high water mark (Figure 7). Field observations and measurements using an estimated slope and measured distance from the rim of the crater to the top of this surface coating show a uniform height of 5 m below the rim, again suggesting water deposition. A stage-volume relationship can be calculated from the topographic survey of crater U5a and this apparent high water mark. Assuming the large ponding event occurred on the original crater dimensions, it would have had a volume of approximately 63,000 m<sup>3</sup>. This large pond is further supported by the large erosional gullies which are evidence of a high energy event.

The surface of the crater bottom outside the playa region was high in gravel and sand down to 2.5 m. While the surface does increase in elevation away from the playa, it rises only 100 cm at station 120. Thus, this coarse surface material of gravel and sand north of the playa is not from the same deposition event as that seen at the crater center which supports an initial single large deposition event. Below the 2.5 m depth, the particle size distribution does mimic the distribution at the crater center. The coarse upper 2.5 m to the north side of the playa suggests that subsequent deposition events of considerably lower magnitude occurred. However, it appeared to be of sufficient energy to cut into and mix with the upper portion of the previous deposition near the

entrance into the crater. The sediment would fall out in accordance with Stokes' Law, leaving a gradation from coarse to fine particle with distance from the gully entrance.

### **Saturated and Unsaturated Hydraulic Conductivity**

Infiltration into the soil is the flux of water vertically downward through the surface. Once steady state is reached, the hydraulic gradient approaches unit so that the infiltration rate can be considered the saturated hydraulic conductivity for the ring infiltrometer measurements and  $K(h = 15 \text{ cm})$  for the tension infiltrometer measurements. Results of the ring infiltrometer and tension infiltrometer measurements conducted for saturated and unsaturated hydraulic conductivities appeared to be related to soil texture. The same spatial trend for particle sizes held true for  $K_{SAT}$  and  $K(h)$  as well, with values decreasing from north to south and then increasing at the toe slope position south of the playa (Table 9). Results of the field infiltration procedures are presented in Appendix B.

Steady-state infiltration for the ring infiltrometer was reached relatively quickly for the coarse soils, less than an hour in most cases. Within the playa, measurements were taken for a 24-hour period to ensure accuracy of the steady-state measurement. Some lateral flow may have occurred but the results seem reasonable.

Along the transect of crater U5a, distinct zones of hydraulic conductivity were identified. More than two orders of magnitude difference existed for  $K_{SAT}$  between the playa region of silty clay to clay and the coarse loamy sands. The  $K_{SAT}$  for sandy loam and loamy sand soils within the crater was 4.0 m/d (coefficient of variation = 52 %). Mean values for stations 20S and 10S were 25% lower due to the greater percent of

silts. The fine-grained playa material had  $K_{SAT}$  values spanning 2 orders of magnitude, with a mean  $K_{SAT}$  of 0.05 m/d and a coefficient of variation of 60 %. Thus the  $K_{SAT}$  of the playa region is nearly 2 orders of magnitude lower than the coarse material outside.

Measurements for  $K(h)$  at -15 cm head were begun immediately following the ring infiltrometer procedure for  $K_{SAT}$ , meaning the soil was saturated at the initiation of all tension infiltrometer measurements. As infiltration continued, the rate decreased to a steady-state value as the soil desaturated into equilibrium with the prescribed tension. The flux into the soil under the prescribed tension under steady-state flow was taken to be  $K(h)$ . For the loamy sand to sandy loam textures, unsaturated conductivities were decreased by approximately 50% over  $K_{SAT}$ . Average value of  $K(h = -15 \text{ cm})$  for these soils was 2.2 m/d (coefficient of variation = 91 %). Within the playa, rates decreased by only 20% over the associated  $K_{SAT}$  values. Average value of  $K(h = -15 \text{ cm})$  for these fine-grained soils was 0.03 m/d (coefficient of variation = 133 %). Thus, there is nearly a 2 order decrease in  $K$  (both  $K_{SAT}$  and  $K(h = -15 \text{ cm})$ ) between the playa and coarse material. Tension infiltrometer malfunction prevented measurements from stations 50 and 80. Measurements of  $K(h = -15 \text{ cm})$  for the fine grained material may need further evaluation to be reliability qualified. Stations 30 and 40 actually demonstrated a slight increase in infiltration rates from the saturation to -15 cm head, whereas stations 60 and 70 produced decreases in rates of 1 to 2 orders of magnitude. Expected rates at this tension for this texture would be a negligible difference from saturated conductivity rates. Once again, field techniques and equipment may have produced unreliable results at stations 60 and 70.

## Water Retention Characteristics

Hanging water columns and pressure chamber analysis for water retention characteristics were completed for each sampling station, with the exception of 50, 70, and 80 (Appendix C). For these three stations, only high tension measurements for loose soil were accomplished and lower tension values were taken from similarly textured samples. Data were graphed for volumetric water content,  $\theta$ , versus matric head (Figure 17). For purposes of the log function along the x-axis, 0 cm was graphed as -1 cm. A matric head of -15 cm was also chosen as the lowest applied tension to match the head used for the tension infiltrometer. The air entry pressure,  $h_a$ , is the point along the water retention curve where air begins to displace water within the pores such that water content has measurably decreased. This value would be less negative for coarser grained soils and more negative for finer grained soils due to the differences in soil structure and porosity. The saturated water content was directly measured as the water content upon removal of the core from the tub of water with the water level at the top of the core. Saturated water content was taken to equal porosity and calculated as a function of bulk density, the mass of the saturated core and the mass of the dry core. Another method of porosity, and therefore saturated water content, calculation follows the formula  $\theta_s = [1 - (\text{bulk density}/\text{particle density})]$ , where particle density is generally taken to be 2.65 g/cm<sup>3</sup>. In this study, these two methods of  $\theta_s$  determination do not yield the same result. The discrepancy could be caused by (1) the core not being fully saturated, (2) air entrapped within the core sample during saturation, or (3) the actual particle density does not equal 2.65 g/cm<sup>3</sup>. A sharp decrease in water content occurred

for all samples between -500 cm and -1000 cm head, which coincides with the change from intact core sample to loose soil in the ring.

Water content decreased rapidly in the coarse-grained soil at high (less negative) matric heads and approached residual water content at -100 cm for the loamy sand and sandy loam soils. Average bulk density  $\rho_B$  for the loamy sand was  $1.42 \text{ g/cm}^3$  and  $1.39 \text{ g/cm}^3$  for the sandy loam. Average saturated water contents for the loamy sand and sandy loam were  $0.42 \text{ cm}^3/\text{cm}^3$  and  $0.41 \text{ cm}^3/\text{cm}^3$ , respectively.

Water content decreased gradually in the fine-grained soils until -1000 cm, but still did not approach the anticipated residual water content at -3000 cm. Average bulk density for all the fine-grained soils was  $1.14 \text{ g/cm}^3$  and average saturated water content was  $0.51 \text{ cm}^3/\text{cm}^3$ .

### van Genuchten Parameters

The RETC code, developed by van Genuchten (1980), was used to model the water retention data by estimation of alpha, m and n. The residual water content was set to equal the measured value at  $h = -3000 \text{ cm}$  and the Mualem model [ $m = 1 - (1/n)$ ] was assumed in order to fit for the alpha and n parameters. Results are listed in Table 10.

Both alpha and n are shape parameters used to describe the water retention curve and are dependent upon the soil texture and structure. Alpha is related to the air entry value by  $\alpha \cong 1/h_a$ . For simplicity of notation,  $\alpha$  is considered positive as  $h_a$  is expressed as tension. Coarsely textured soils, such as sandy loam and loamy sand, will begin to lose water at lower tensions and thus will have a higher alpha value than fine-grained

soils. The  $n$  parameter describes the slope of the water retention curve and is a function of the pore size distribution (soil structure). A higher  $n$  value produces sharper decreases in  $\theta$  with  $h$  while lower  $n$  values produce gentler slopes. A coarse soil generally exhibits a sharp decrease in water content over a relatively small decrease in head so the value of  $n$  is greater than that of a fine-grained soil.

As in past sections, the coarse-grained loamy sand and sandy loam will be discussed separately from the fine-grained loam to clay materials. Alpha values for the coarse material were higher than those found in other studies (Shott et al., 1997; Bechtel Nevada, 1998d). This observation signifies a less negative air entry value than those found in similar studies. For this procedure, the sandy loam was found to have a slightly higher average value of  $0.044 \text{ cm}^{-1}$ , as opposed to  $0.038 \text{ cm}^{-1}$  for the loamy sand. Both values still indicate a large decrease in water content at a relatively high matric pressure (-23 cm to -26 cm). Shott et al. (1997) and Bechtel Nevada (1998d) fit alpha values of  $0.018 \text{ cm}^{-1}$  ( $h_a = -55 \text{ cm}$ ) and  $0.012 \text{ cm}^{-1}$  ( $h_a = -83 \text{ cm}$ ), respectively, but the first head applied to their core samples was -40 cm. The lower initial matric head (-40 cm vs. -15 cm) could account for their lower alpha parameters. The soil property menu furnished in HYDRUS-2D contains values based upon the work of Carsel and Parrish (1988) and more closely match the alpha values in this study. HYDRUS-2D provides an alpha value of  $0.075 \text{ cm}^{-1}$  ( $h_a = -13 \text{ cm}$ ) for sandy loam and  $0.124 \text{ cm}^{-1}$  ( $h_a = -8 \text{ cm}$ ) for loamy sand. The van Genuchten  $n$  parameter showed good agreement between the two coarser soil textures, loamy sand had  $n$  equal to 1.75 and sandy loam equaled to 1.74, and the Bechtel Nevada (1998d) value of 1.75. Shott et al. (1997) and HYDRUS-2D determined steeper slopes of the water retention curve. The  $n$  parameter

in Shott et al. (1997) was 1.9 and HYDRUS-2D has  $n$  equaling 1.89 for sandy loam and 2.28 for loamy sand. Given that  $n$  has a range of 1 to around 4, these values are fairly consistent and seem reasonable for these textures.

Alpha and  $n$  parameters for the fine-grained sediments matched expected results even more closely. Alpha values ranged from  $0.018 \text{ cm}^{-1}$  to  $0.023 \text{ cm}^{-1}$  ( $h_a = -43 \text{ cm}$  to  $-54 \text{ cm}$ ). HYDRUS-2D provides values  $0.019 \text{ cm}^{-1}$  to  $0.027 \text{ cm}^{-1}$  for the  $\alpha$  parameter of these textures. The shape of the water retention curve proved, as expected, to be far more gentle in the silts and clays than the sands, with average  $n$  values equaling 1.28. This result matches closely the HYDRUS-2D range of 1.23 to 1.31. Bechtel Nevada (1998d) and Shott et al. (1997) did not test for hydraulic properties of fine-grained soils, therefore no comparison can be made.

### **Final Modeling Scenario**

Physical characteristics of crater U5a support the conclusion that an extremely large ponding event occurred since crater formation. Three pieces of evidence exist:

(1) A ring of depositional material is clearly evident at a height of 20 m above the current crater floor. Stage-volume relationships of the initial crater dimensions place such a pond's volume at approximately  $63,000 \text{ m}^3$ .

(2) Large erosional gullies suggest intense high energy surface water events.

Distinct channels tracked for 8 km back toward the mountain ridges suggest extremely large events are possible, much greater than the  $0.65 \text{ km}^2$  used in runoff prediction.

- (3) Particle size analysis of the upper 6 m provides additional evidence of a large scale, one-time deposit of sediment. Soil texture becomes coarser with depth, with a clayey playa at the surface grading to sands and gravels. More recent surface flow into the crater has deposited a layer of coarse material along the crater surface but the visible sands and gravel do not represent the entire rubble chimney.

### Method of Final Modeling Scenarios

A more precise estimation of recharge potential at crater U5a was undertaken by incorporating data determined in the field and laboratory into a final modeling scenario. This process was divided into two separate procedures, an initial large pond event of 63,000 m<sup>3</sup> followed by a series of 14 smaller ponding and drainage events.

The large pond event indicated by depositional high water marks and laboratory particle size analysis was assumed to occur in the crater represented by the topography immediately following detonation. Neither playa surface nor depositional sequence would have existed and no spatial trend of hydraulic properties were assumed with depth. There is no question that heterogeneity exists in the subsurface, however a homogeneous media was selected for the modeling process. Subtle layering as examined by Bechtel Nevada (1998d) was not used. The preferred pathways for vertical flow that may exist due to the bulking of the rock or instrumentation of the shot hole were also not considered. Soil properties for the undisturbed alluvium were selected from the Area 5 PA (Shott et al., 1997) and discussed earlier in Table 2. Initial conditions were set in equilibrium with a water table along the bottom boundary.

Matric heads were a function of depth and ranged from 0 at the water table to  $-200$  m at the top boundary. As in Sensitivity Analysis I, no-flow boundaries were assigned along the vertical sides and free drainage along the bottom boundary. During infiltration of the pond, a constant pressure head along the crater surface to a height of 20 m above the crater floor was used. The remainder of the top boundary was a no flow condition. Following infiltration of  $63,000 \text{ m}^3$  of water, the entire top boundary was changed to an atmospheric condition. Evapotranspiration rates for the 30 years of drainage following infiltration were taken from the Area 5 PA (Shott et al., 1997) (Figure 22). The monthly average ET was divided by 30 days and applied uniformly throughout the month. The dimensions of the domain for this modeling scenario are shown in Figure 23. Depth to the water table was 200 m but a wider domain in the x direction (110 m) was chosen to avoid the influence of the right side no-flow boundary condition.

MESHGEN-2D generated a mesh of 3729 nodes, 7217 triangles, and 10,945 line segments for the domain. Finer discretizations were once again used near the soil surface to handle the region of distinct differences in fluxes and pressure gradients. The maximum vertical discretization was 6 m near the bottom boundary and minimum discretization was 0.5 m along the surface.

Infiltration of the pond was accomplished incrementally to capture some of the change in head that would occur as the water level initially rises. The time for the model to complete infiltration, therefore, does not accurately represent the actual time required. Head was increased with each successive day, with the greatest increase along the crater bottom. The first two head conditions ran for 1 day each, the second two head conditions ran for 5 days each, and the fifth head condition ran for 1.2 days. At

this location, the constant head went from 1 m to 20 m. After 13.2 days, simulated infiltration of 63,000 m<sup>3</sup> was completed and the top boundary was changed to an atmospheric condition. Redistribution for a period of 30 years was then simulated.

The second procedure consisted of modeling the 14 (relatively) small ponding/drainage cycles. A smaller, more detailed model domain was constructed to closely examine the effects of layered soil types on vadose-water flow. Also taken into consideration was actual surface topography that currently exists in crater U5a. Dimensions are shown in Figure 23 and 24. Sediment deposition since crater formation has been surveyed as a thickness of 14.6 m. The model extends approximately 5 m below that region. The actual crater surface is almost completely level throughout the playa region and then rises gradually to the steep walls. This gradient is captured in the model with a flat surface for the first 16 m, a slope of 0.03 over the next 29 m, and finally a slope of 0.87 over the next 15 m. Initial conditions were set throughout the domain at -10 m. This value represents the relatively wetter conditions that would have existed following the large ponding event previously discussed. This matric head is certainly higher than the initial conditions found in the undisturbed region adjacent to the crater in 1996 but considerably lower than the saturated ( $h = 0$ ) condition that would have existed following large pond deposition.

The same method and pond/drain characteristics were used as discussed in Sensitivity Analysis II. ET rates were identical to those discussed in Shott et al. (1997). Initial conditions, soil types, and model domain were quite different from any previously discussed and most closely represented actual conditions observed in the field.

Six soil textures in seven layers were modeled to represent the subsurface. Hydraulic properties and sources for the values are summarized in Table 11. A simplified cross section is shown in Figure 21. The top layers of silty clay and loamy sand are more recent depositions from the smaller series of ponding events. The remainder of the underlying sediments is most likely from the large ponding event that eroded the bulk of the erosional gullies found at the north end of the crater. The sediment suspended within the 63,000 m<sup>3</sup> pond was deposited based on the soil texture, represented by the coarsening with depth.

MESHGEN-2D generated a mesh of 2610 nodes, 4969 triangles, and 7578 line segments for the domain. As in all previous modeling scenarios, finer discretizations were used near the soil surface to manage the region of distinct differences in fluxes and pressure gradients. In this scenario, though, it was even more critical in order to handle the sharp contrast in soil types in the multi-layered system. The maximum vertical discretization was 2.5 m near the bottom boundary and minimum discretization was 0.12 m along the surface.

The final modeling scenario incorporated all field and laboratory data, as well as the information learned from the two sensitivity analyses, to predict potential recharge beneath crater U5a. The conceptual model for this simulation represents the most appropriate boundary conditions, initial conditions and soil properties and ponding event. Data and field observations point to a large ponding event measuring 63,000 m<sup>3</sup> in volume. Although this was possibly not the first runoff event to reach the crater, it was definitely the most significant in terms of size and recharge. Therefore, no ponding events were considered prior to the ultimate pond. A pond of this magnitude would

have saturated the initially dry crater which consisted of the collapsed original surface material. Evapotranspiration of this infiltrated water would prove to be negligible because (1) the sediment from this large pond would have covered the infiltrated water and (2) no salt cedar or other vegetation would have existed to transpire the infiltrated water. The entire volume of the pond could be considered available for infiltration and potential recharge. After the pond drained into the rubble chimney, the hydraulic gradient would redistribute the wetting front predominantly downward while subsequent smaller series of ponding/drainage events would continue. One complication with modeling the large pond event is the inability of HYDRUS-2D (and other numerical models of Richards' equation) to handle a change in the flow domain geometry midway through the simulation. Thus, the deposition of 14.6 m of sediment following infiltration of this large event cannot be modeled as a continuous infiltration-redistribution process. To adequately capture this process, the final modeling effort was separated into two parts: (1) infiltration of the large pond followed by 30 years of drainage using the original crater surface and (2) infiltration and drainage of 14 smaller ponds over a period of 30 years using the current surface features and the water content profile at the time the pond volume had infiltrated.

#### Results of Final Modeling Scenarios

Infiltration of the large pond was simulated by progressively decreasing heads along the crater bottom and the sloped crater walls and allowing the model to run for set periods of time that approximated the falling head. The elapsed time that the model predicted for the pond to fully infiltrate is not accurate but the behavior of the wetting

front as it redistributed through the homogeneous media over the subsequent 30 years is a fair representation. Results are summarized in Table 12.

The modeling of the large pond examined five different steps for a simulated 13.2 days. Over this time 63,400 m<sup>3</sup> of surface water was infiltrated. The downward movement of the wetting front reached a depth of 38 m in this 13.2 days (Figure 25). The water content at this depth was 0.35 m<sup>3</sup>/m<sup>3</sup>, which is greatly elevated over the undisturbed condition of 0.075 m<sup>3</sup>/m<sup>3</sup>. The pond fully saturated the soil prior to and during the deposition of the 14.6 m of sediment.

The end of the infiltration of the large pond was considered Time = 0 for the beginning of the 30 year redistribution. The domain remained constant, ignoring the presence of the sediment occurring from deposition. The upper boundary condition was switched from a constant head to an atmospheric condition, where ET was allowed, and the wetting front allowed to drain. The movement of that wetting front reached a depth of 140 m below the original crater bottom in just 10 years (Figure 26). According to this simulation, surface water from the original ponding event reached the water table at 200 m below land surface within 30 years (Figure 26). The rate of movement of the wetting front towards the end of the simulations was 2.5 m/year. Net rate of water loss from the bottom boundary (water table) during the final time step was 21.3 m<sup>3</sup>/yr. Loss due to evapotranspiration over this same time period equaled 2400 m<sup>3</sup>, 3.8% of the originally infiltrated water, with some of this total loss coming from the undisturbed region adjacent to the crater. A more likely scenario is that the ET loss would be lower than this due to the surface sealing for the sediment and lack of vegetation. Thus, the time to reach the water table may actually be sooner than predicted.

Volumetric water contents of borehole U5a-N1 determined from neutron moisture meters showed an increase from the undisturbed values of borehole U5a-N2 (Hokett and Gillespie, 1996) (Figure 27). A dramatic shift in water contents occurs 8 to 10 m deep at the crater playa region, being highly water stressed above 8 meters. Previous modeling attempts by Hokett and French (1998) have been unable to duplicate these results. The modeling of periodic, small ponding events in the range of 300 m<sup>3</sup> to 500 m<sup>3</sup> never penetrated below the fine-grained playa region, leaving predicted matric potentials extremely low in the area of the borehole measurements. Hokett and French (1998) predicted focused recharge with high  $\theta$  along the peripheral region of the playa but the area directly beneath the playa remained similar to the undisturbed, pre-test initial conditions. However, simulation of the large pond on coarse-grained soil reproduced these wetter conditions and closely reflected the observed measurements. Throughout the modeled depth profile, volumetric water contents were in the range of 0.10 to 0.15 m<sup>3</sup>/m<sup>3</sup>. The exact time elapsed since the proposed large ponding event is unknown so the time step that best represents current conditions and the maximum depth of the wetting front cannot be determined. The modeling performed in this study, however, most closely reflects the increased matric head found with depth beneath the playa.

A basic understanding of a large pond on the original crater surface was achieved by modeling 30 years of subsequent drainage. This exercise provided no insight into the hydraulic behavior of the crater surface following the deposition of 14.6 m of sediment from the large pond as it now exists. The crater surface, immediately following detonation of the “Wishbone” event, consisted of coarse sandy loam and

loamy sand, providing a transmissivity for rapid infiltration. Sediment suspended in the large pond settled out in the manner of a sedimentation cylinder with progressively coarser material with depth. Knowledge of the ability of the crater's "natural cap" to retard or allow water movement was required to properly quantify current and future recharge potential. This study attempted to discern this ability by examining six smaller ponding events on the sediment infill.

A smaller modeling domain was created to investigate the hydraulic properties of the depositional material. This approach permitted the layering required to adequately capture the heterogeneous nature of the shallow surface sediments, including the hydraulic parameters of the fine-grained playa material. The ability of these soils to transmit or prevent flow would lend much understanding to the recharge potential of a subsidence crater after a natural capping had occurred.

Six separate ponding events were placed on the crater bottom and allowed to infiltrate their respective volume of water, using the previously discussed method. Each was then followed by an associated drainage period. The initial condition of the entire domain was set at  $-10$  m to reflect the sufficient period for drying before the next. Pond infiltration occurred extremely rapidly, owing to the lateral spread of the pond extending across the coarse soil. During drainage periods, much of the moisture loss occurred in the area adjacent to the crater, an undisturbed region set at a matric head equal to  $-10$  m for model simplicity. The total net inflow of water to the subsurface showed a generally cyclic pattern (Table 13). Immediately following ponding events, the upper layers of the model increased in water content, as expected. Over the drainage period, however, most of that moisture was evapotranspired to the atmosphere.

The domain was separated into four observation areas to examine net inflow/outflow (Figure 28) and the results summarized in Table 14. The uppermost portion of the crater (region 1) had a net loss of water and the deepest portion (region 4) remained unchanged, indicating no water movement reached a depth of 18 m. Region 2 had an increase in total water volume. Region 3 included the entire undisturbed area of the crater, so the significant loss of water directly reflects this fact. HYDRUS-2D output (Figure 29) shows graphically the penetration of the wetting front into regions 2 and 3. These results show that although a large portion of the precipitation does not become available for recharge, a small percent can.

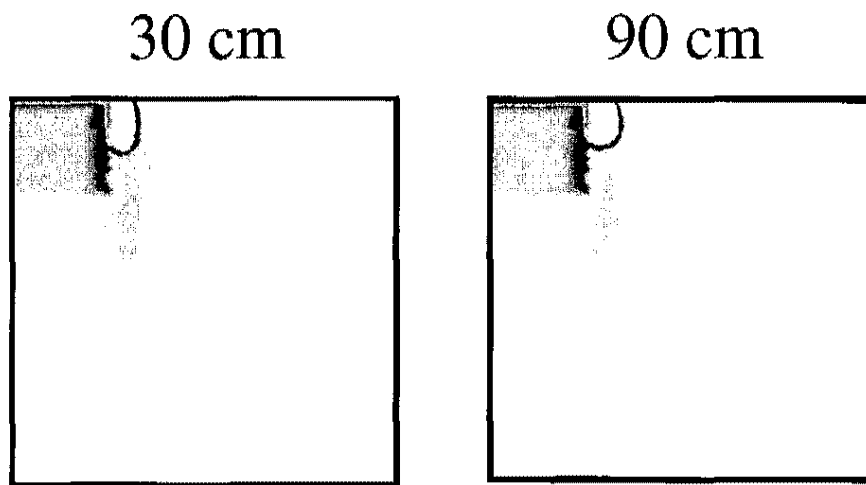
Modeling results show that the closure of a subsidence crater by the deposition of fine-grained sediments can act to prevent infiltration. This hydraulic barrier is provided by the sufficient layering of heterogeneous soils and associated increased storativity of the fine-grained surface material. The size and frequency of the modeled ponds may greatly exceed the actual occurrence, yet the simulated crater with layered sediments performed adequately in prohibiting deep percolation. The presence of the wetting front beneath the uppermost layers outside the playa region does exist and should not be ignored, however the relatively small volume places it into perspective. The playa can restrict percolation. The coarse material edges can serve as a preferred flow region, as predicted by Hokett and French (1998) if the pond is extended beyond its border. If these conditions are met, the whole of the pond's volume is focused in a small peripheral area and deeper movement of the wetting front will occur. The larger, deeper ponds modeled along the gentle grade of the crater bottom spreads the infiltration across a large surface area, resulting in muted recharge potential. The flow

of water through the clay layers or flow from the loamy sands into the silts and loams limit the amount of water available for deeper percolation.

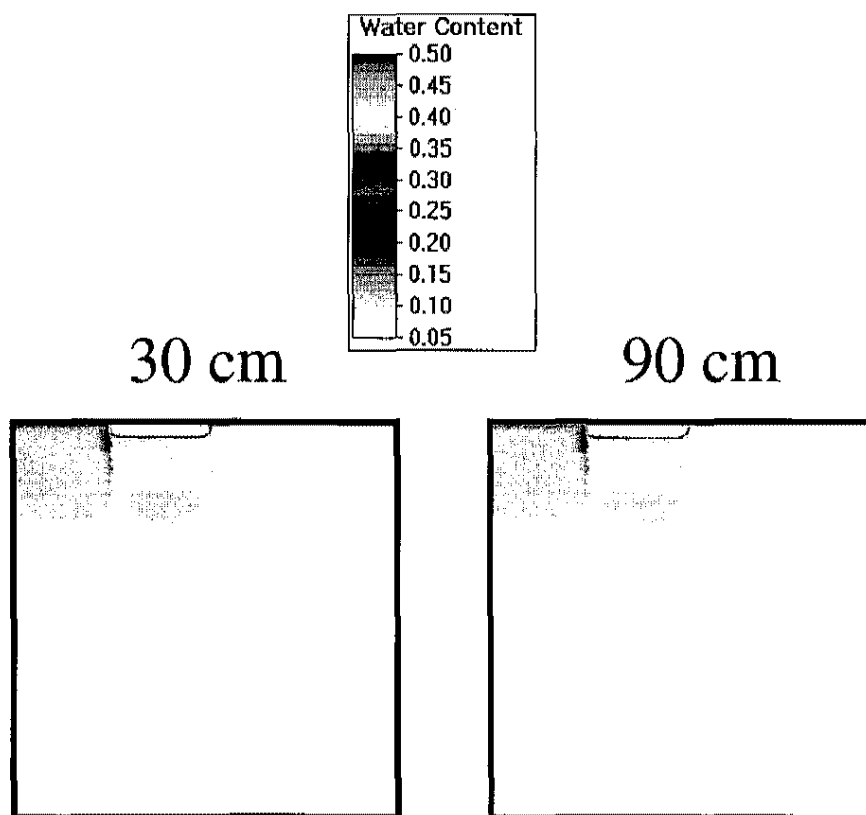
### Conclusion of the Final Modeling Scenario

Three pieces of evidence were discussed previously to support the conclusion that an extremely large ponding event occurred since crater formation. Verification of this conclusion comes from modeling results. The simulated water contents matched closely those determined in the field and laboratory. The instrumented borehole admittedly reaches only 30 m, so validation of modeling results is impossible beyond this depth. The most credible explanation for the wet conditions directly beneath the playa point to a large ponding event occurring before the layered sediment that constitutes the current crater morphology was deposited.

Future recharge, above and beyond the water that already resides in the system, is controlled by the current hydraulic parameters. The large pond did flow onto the coarse sands and gravel and readily infiltrated the surface. Given time to redistribute, the model predictions had the wetting front reaching the deep water table in 30 years. Nearly 15 m of layered soils, including a sequence of clay, silt and sandy loam layers with depth, effectively prohibit significantly more recharge. Assuming infrequent ponding events two orders of magnitude less volume than the large pond, the deposited sediment will recycle much of the precipitation and ponded surface water. A natural crater closure is therefore provided.



Lateral extent of pond = 12 m



Lateral extent of pond = 20 m

**Figure 12.** HYDRUS-2D modeling results for SA I showing depth of infiltration after 2 ponding events for 30 and 90 cm head at two lateral extents. The flow domain was 40 m deep.

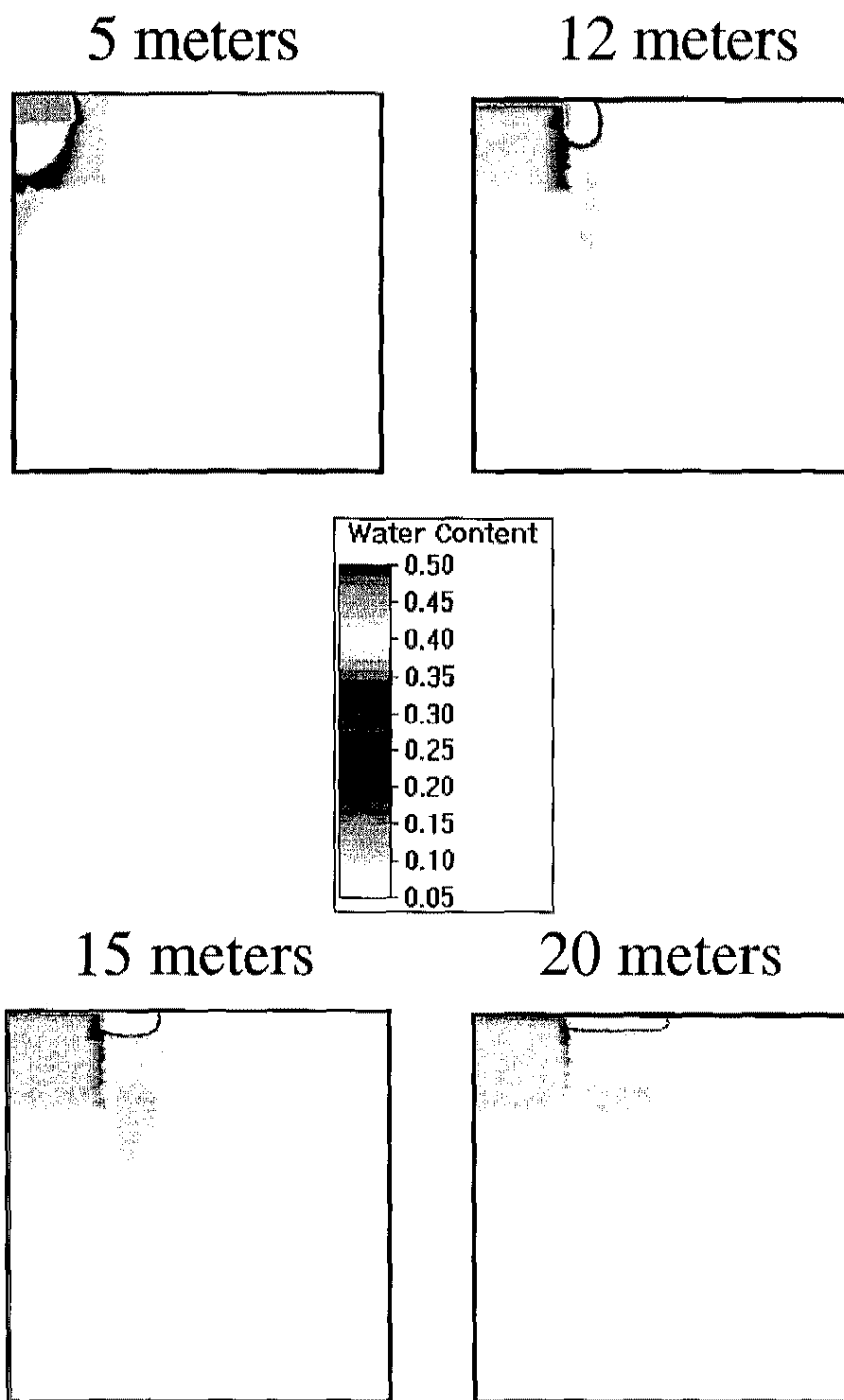


**Figure 13.** Modeling results for SA I showing the depth of water movement into the 40 m deep domain after 2 ponding events for 5, 12, 15, and 20 m lateral extent of ponds.

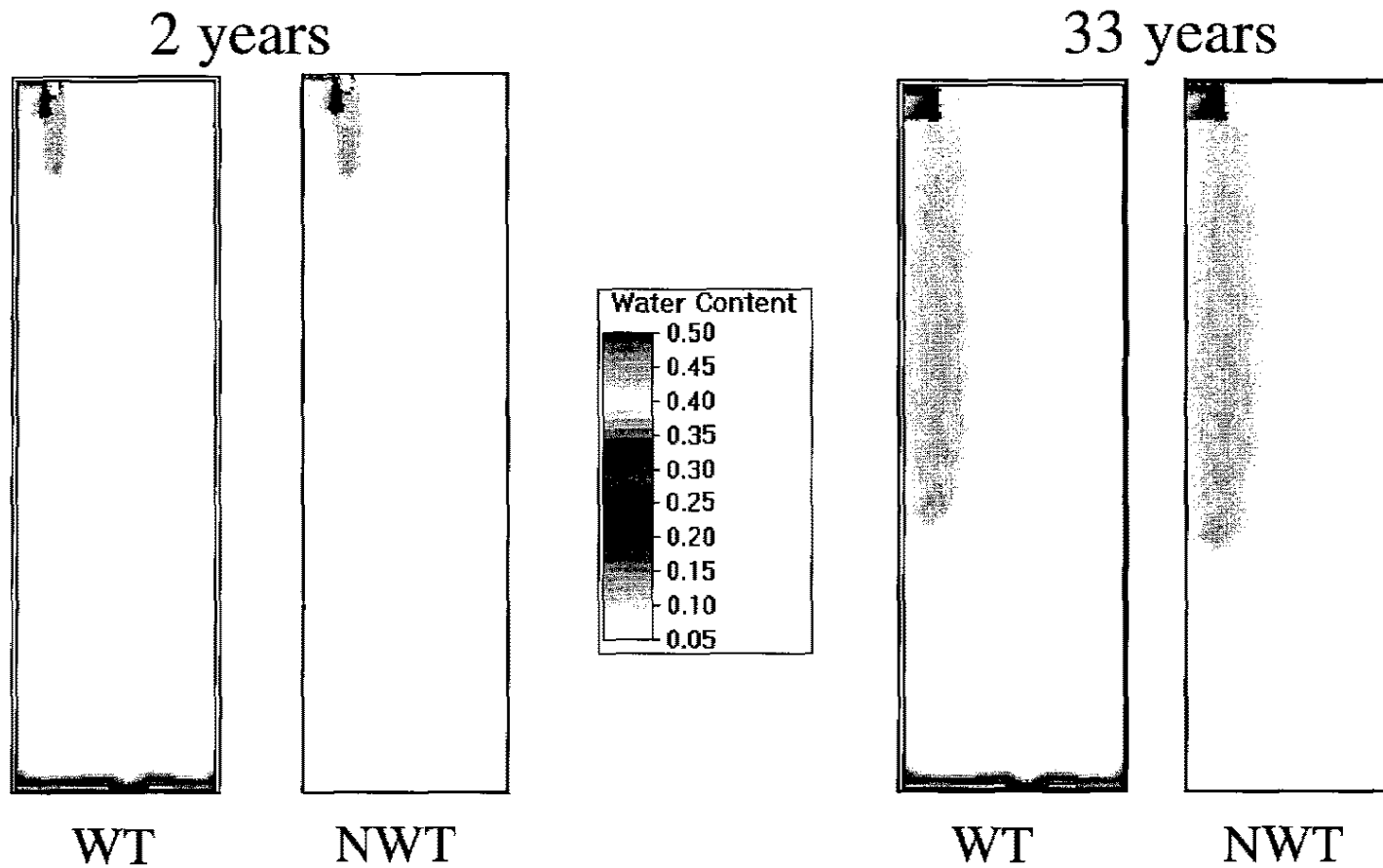


**Figure 14.** HYDRUS-2D modeling results of SA II indicating the initial conditions tested (WT = equilibrium with the water table; NWT = -200 m matric head throughout domain) at two selected time periods.

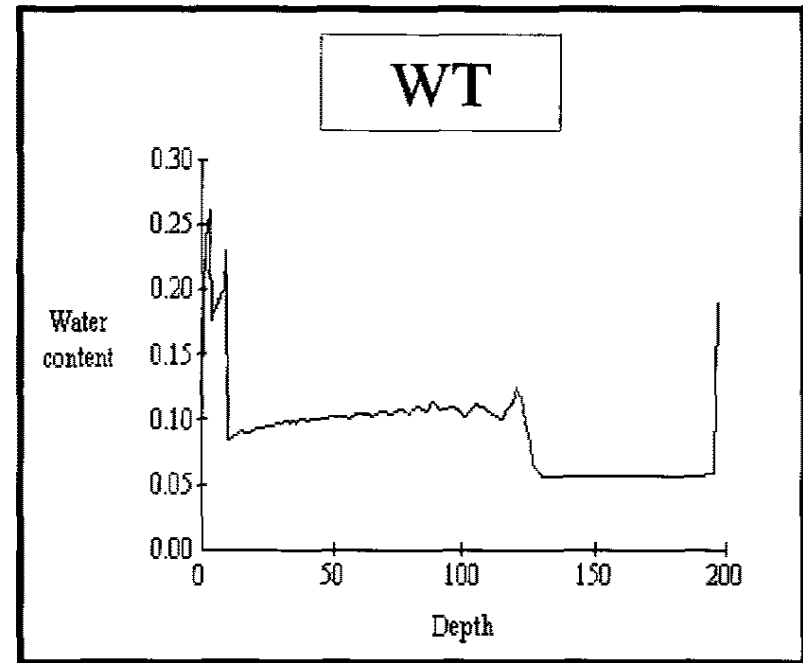
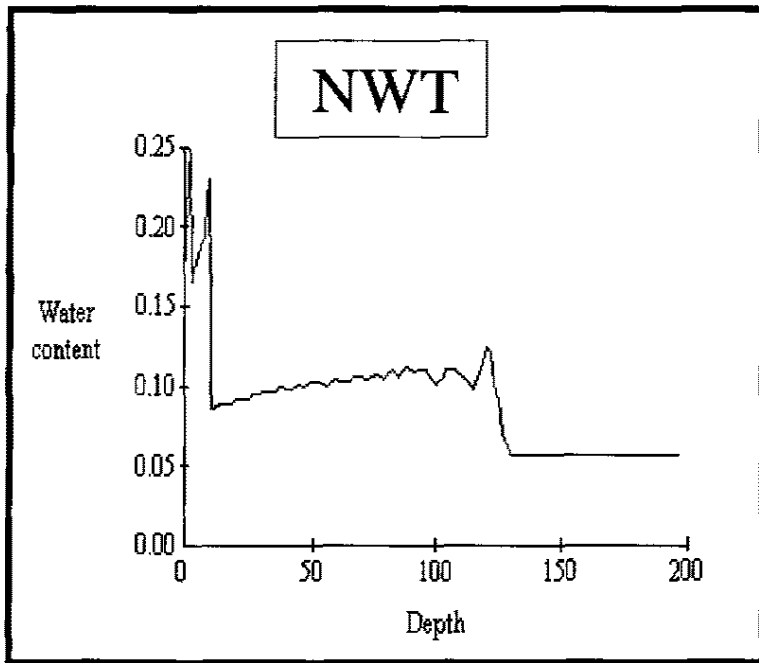


**Figure 15.** Maximum depth of water movement for 33 years of simulations for (a) initial conditions of -200 m throughout the domain (NWT) and (b) initial conditions set in equilibrium with water table at the bottom boundary (WT).

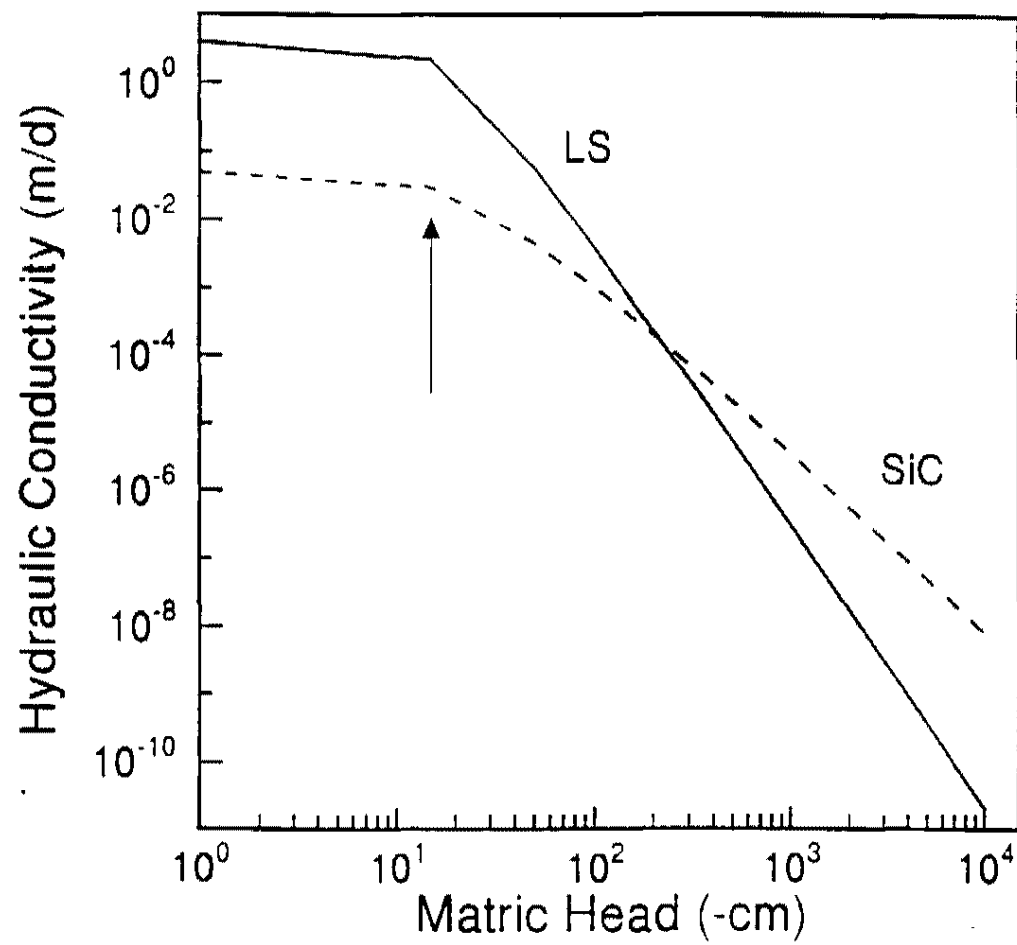


**Figure 16.** Unsaturated hydraulic conductivity for loamy sand and silty clay. Arrow indicates field measurement at matric head = -15 cm.

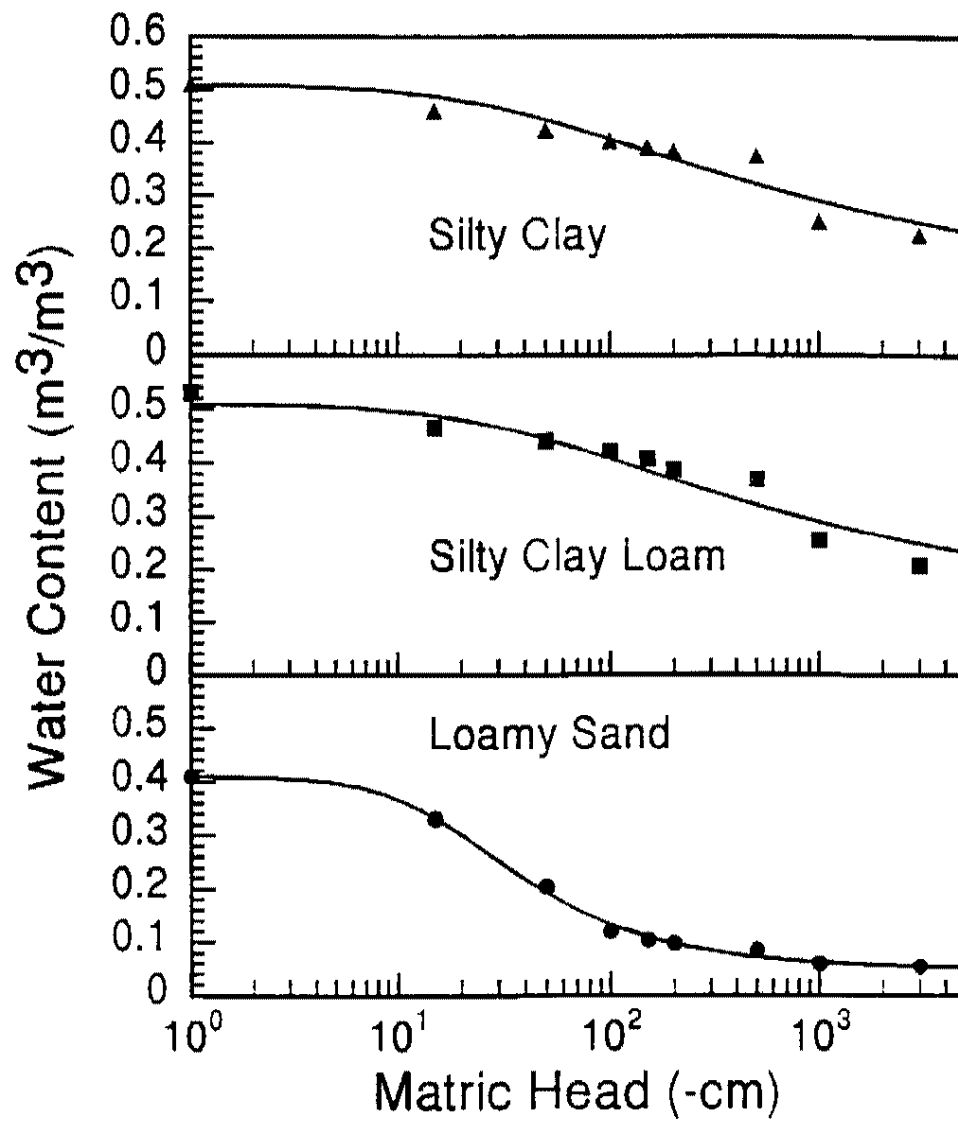


**Figure 17.** Water retention measurements (symbols) and van Genuchten model (line) for three representative soil types.

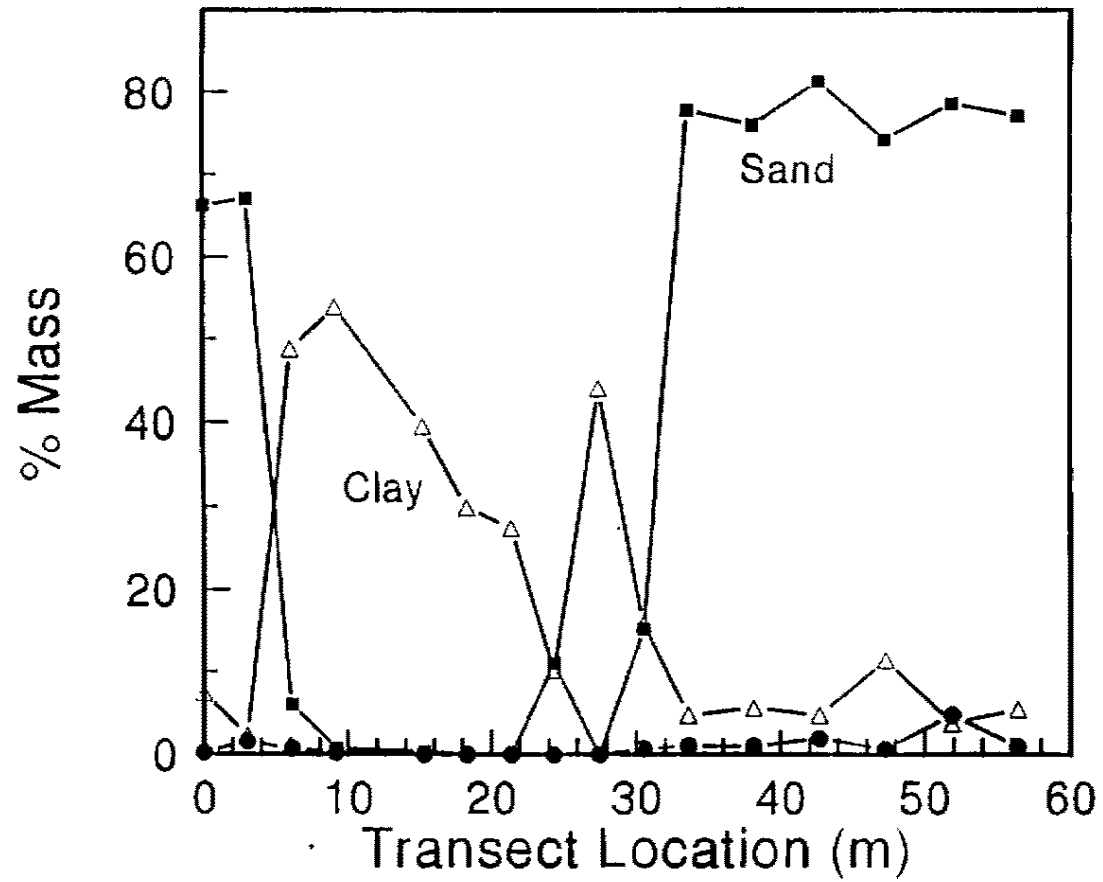
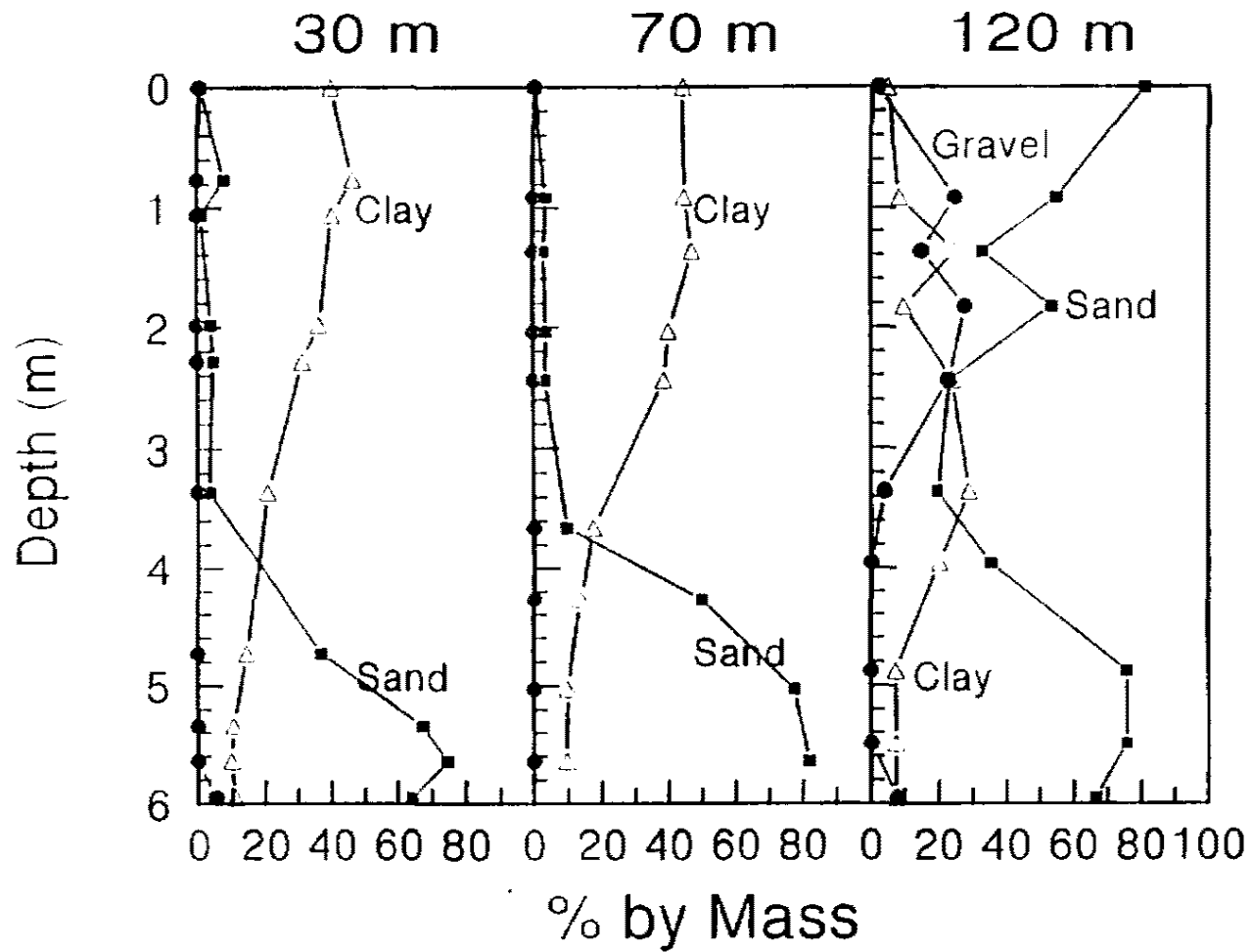


Figure 18. Particle size analysis profiles at transect locations along crater bottom with clay, sand, and gravel indicated by open triangle, solid square, and solid circle symbols, respectively.



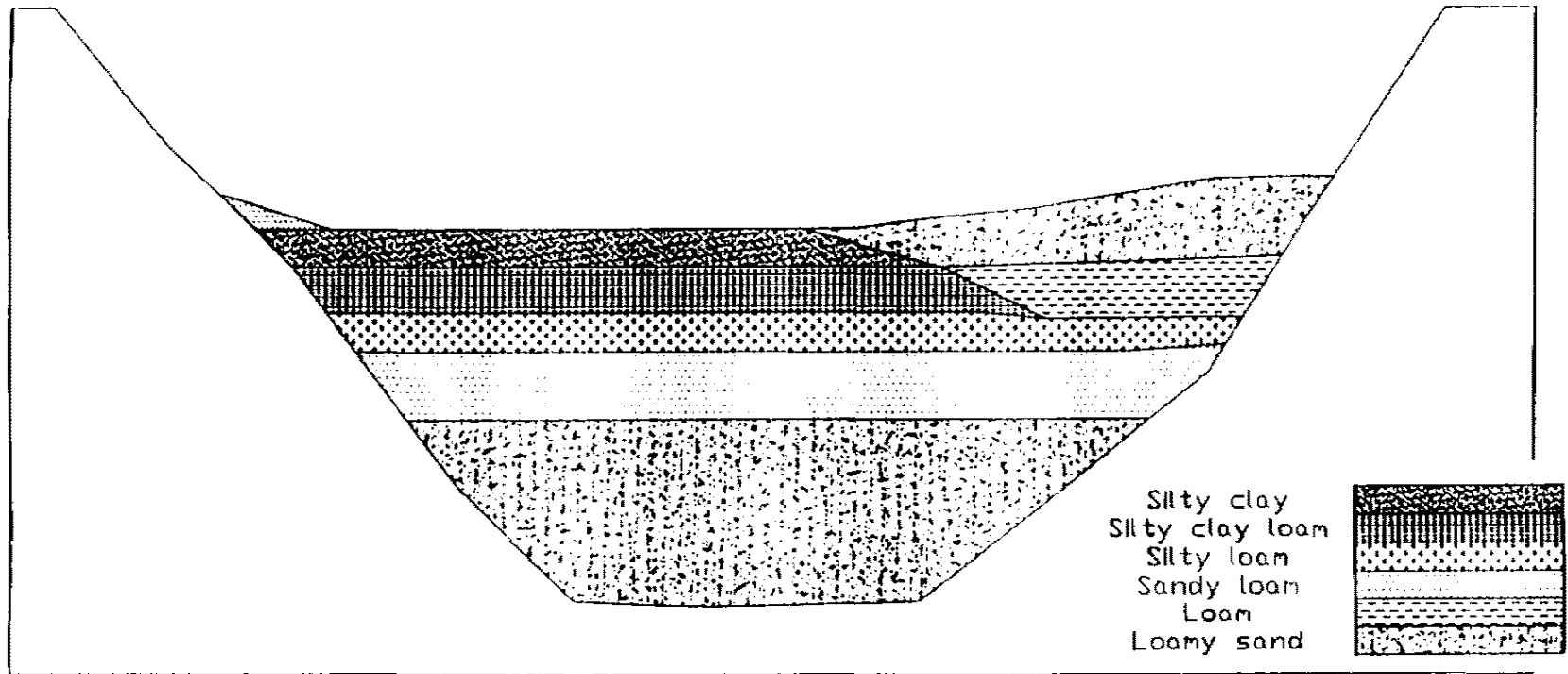
**Figure 19.** Picture of surface playa in crater U5a.



**Figure 20.** Particle size analysis profiles at transect locations 30, 70, and 120 m with clay, sand, and gravel indicated by open triangle, solid square, and solid circle symbols, respectively.

SE

NW



Silty clay  
Silty clay loam  
Silty loam  
Sandy loam  
Loam  
Loamy sand

Vertical Scale (m)  
0 5 10

Horizontal Scale (m)  
0 10 20

Figure 21. Simplified cross-section of crater U5a based upon analysis of the drilling samples.

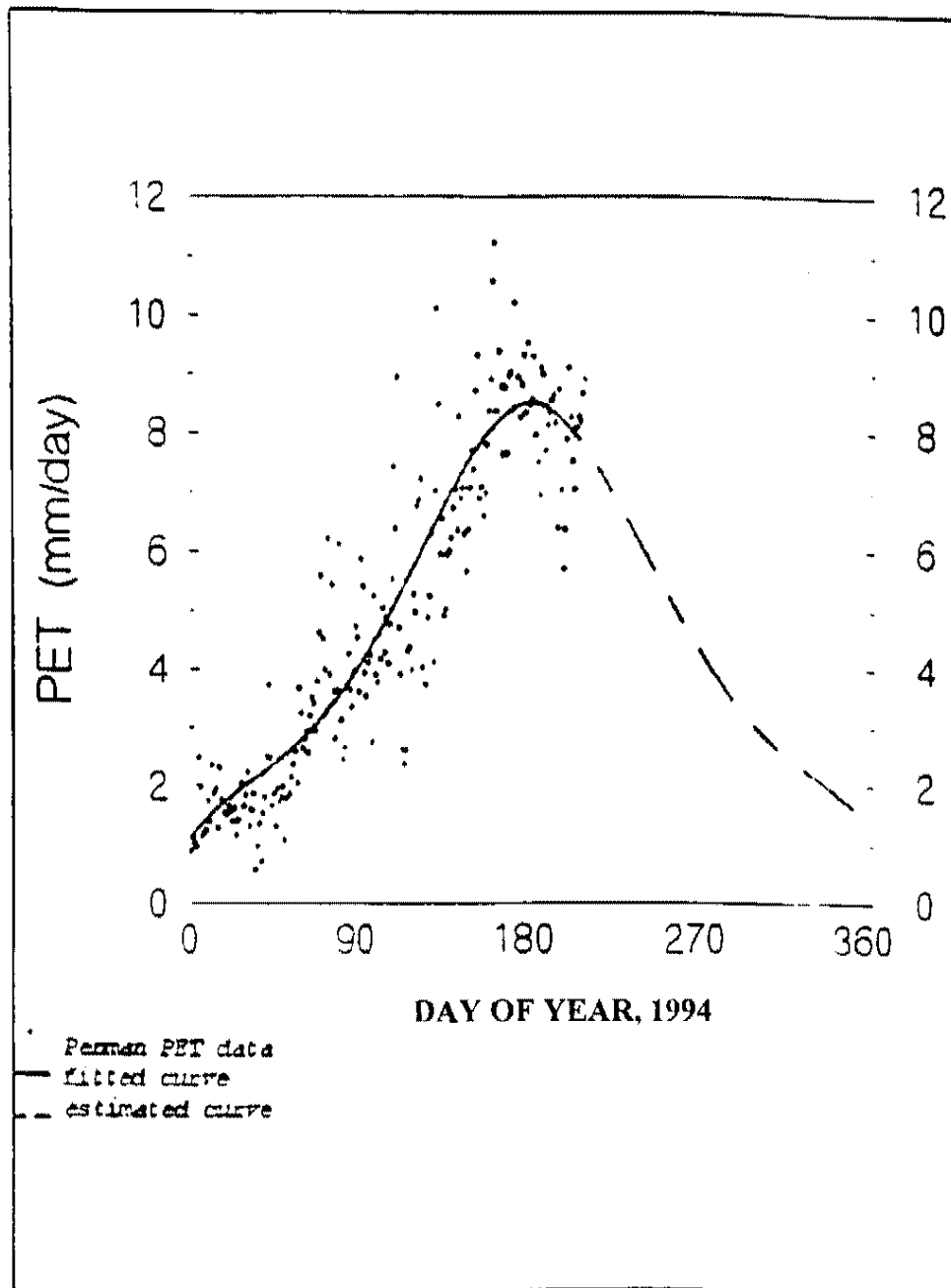


**Figure 22.** Potential evapotranspiration calculated with the Penman combination equation from micro-meteorological data for Area 5 (From Shott et al., 1997).

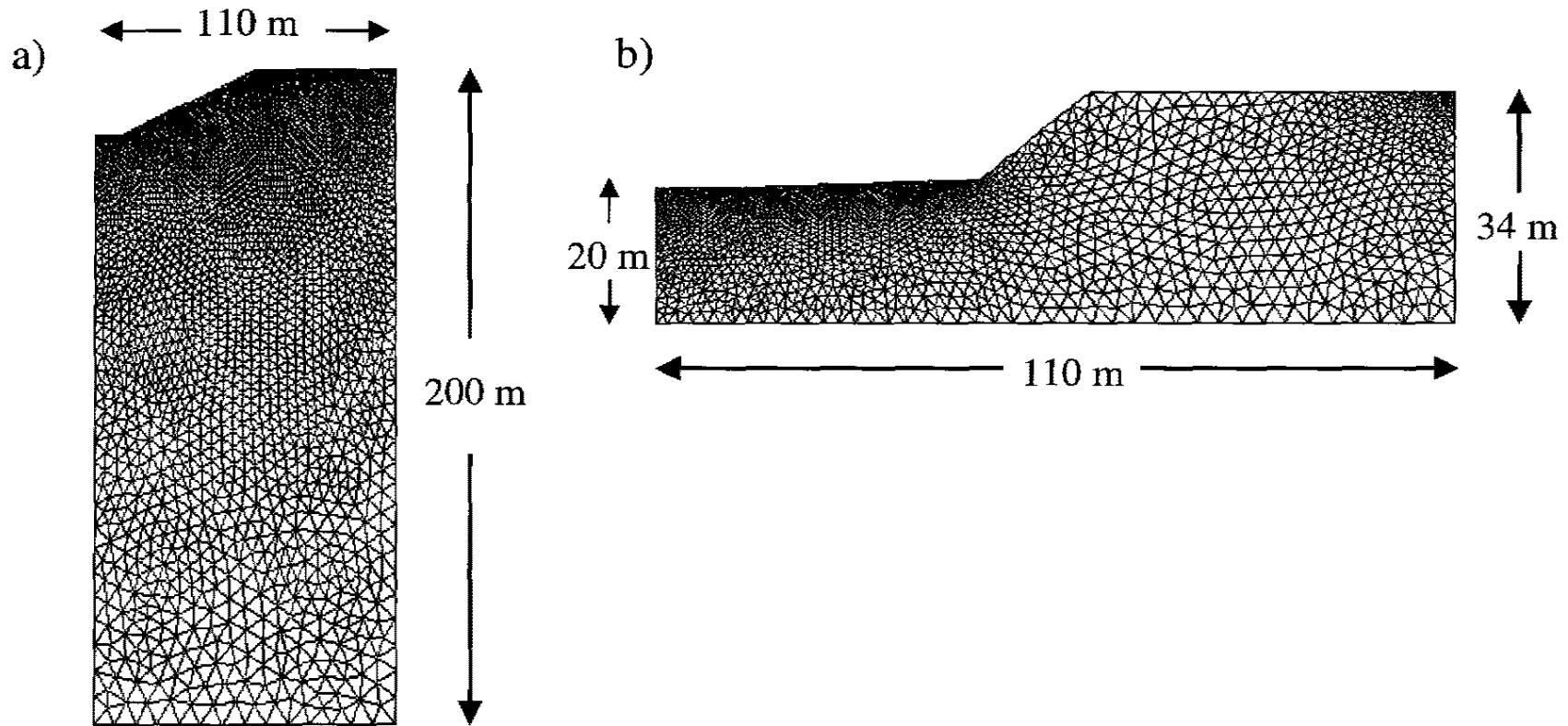
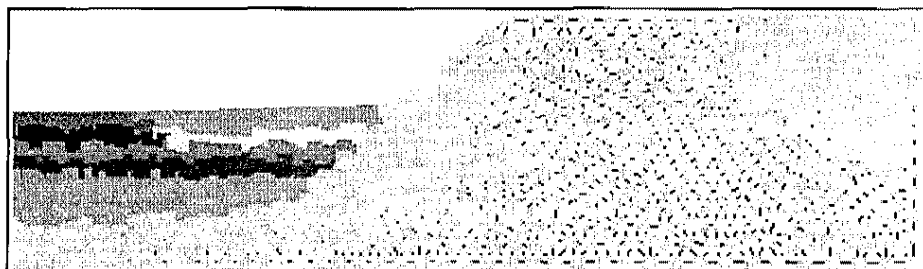


**Figure 23.** Diagrams showing the mesh and domain for the final modeling scenarios: (a) original crater surface to the water table and (b) present crater with sediment infill.

a)



b)

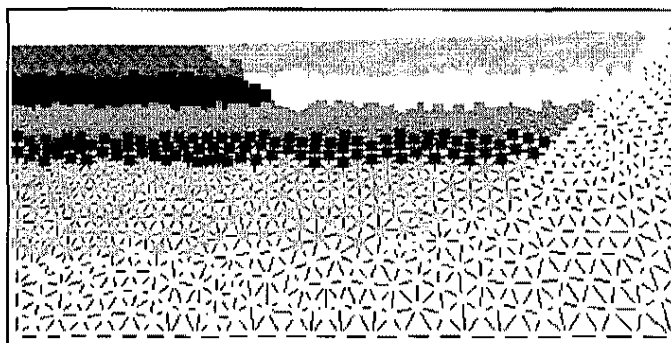
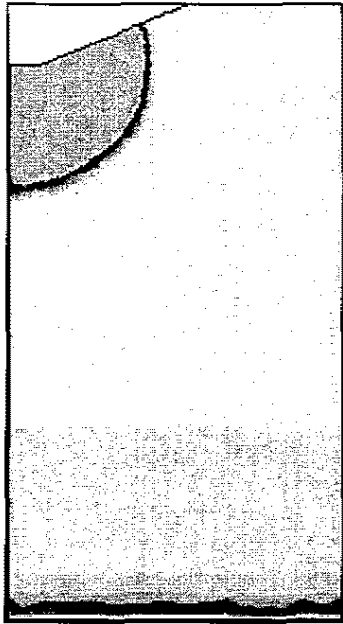
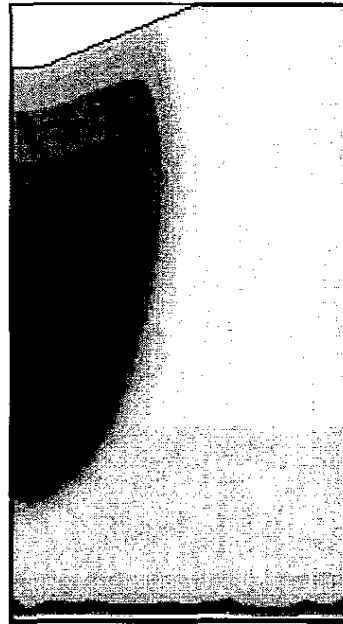


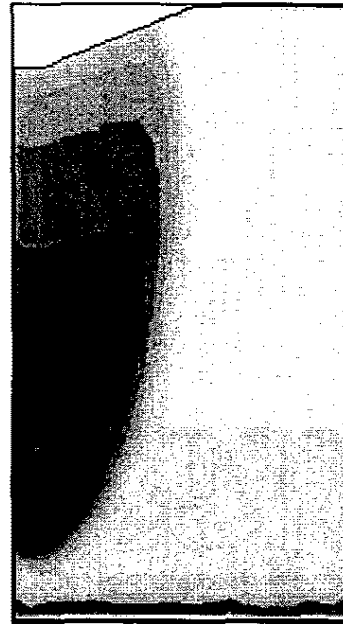
**Figure 24.** Domain and geometry depicting sediment layering for a) entire domain and b) crater infill region.



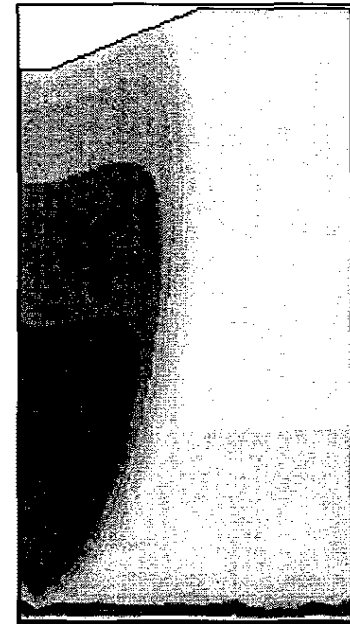
T= 0



T = 10 years



T = 20 years



T = 30 years

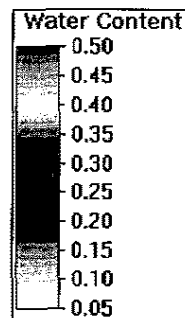


**Figure 25.** Modeling results showing water movement to the bottom of the 200 m deep domain following infiltration of 63, 000 m<sup>3</sup> ponding event.

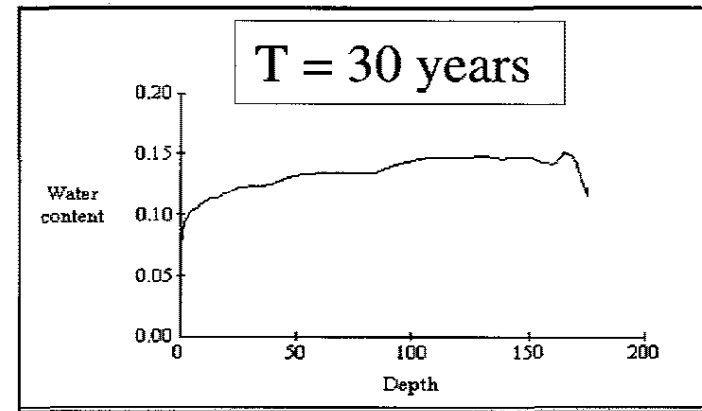
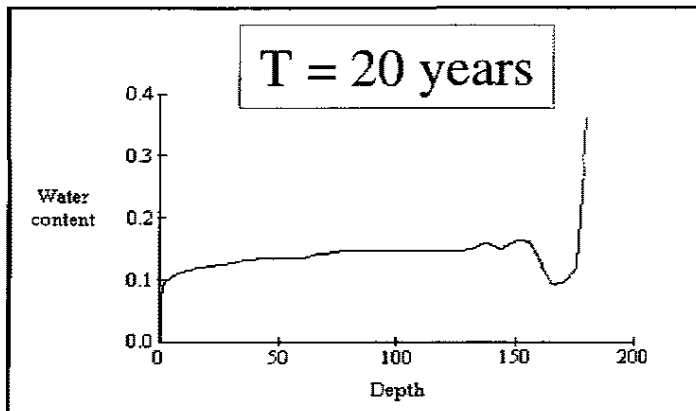
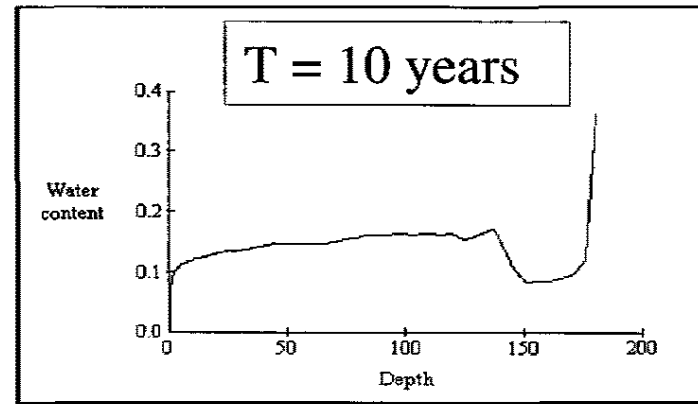
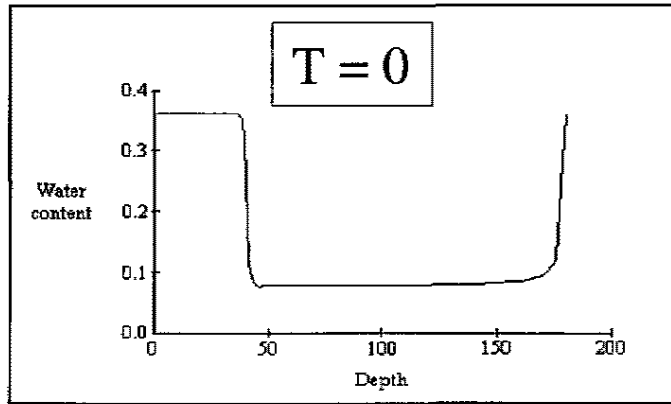


**Figure 26.** Modeling results of water content ( $\text{m}^3/\text{m}^3$ ) versus depth (m) from the center of the playa region following infiltration of  $63,000 \text{ m}^3$  ponding event.

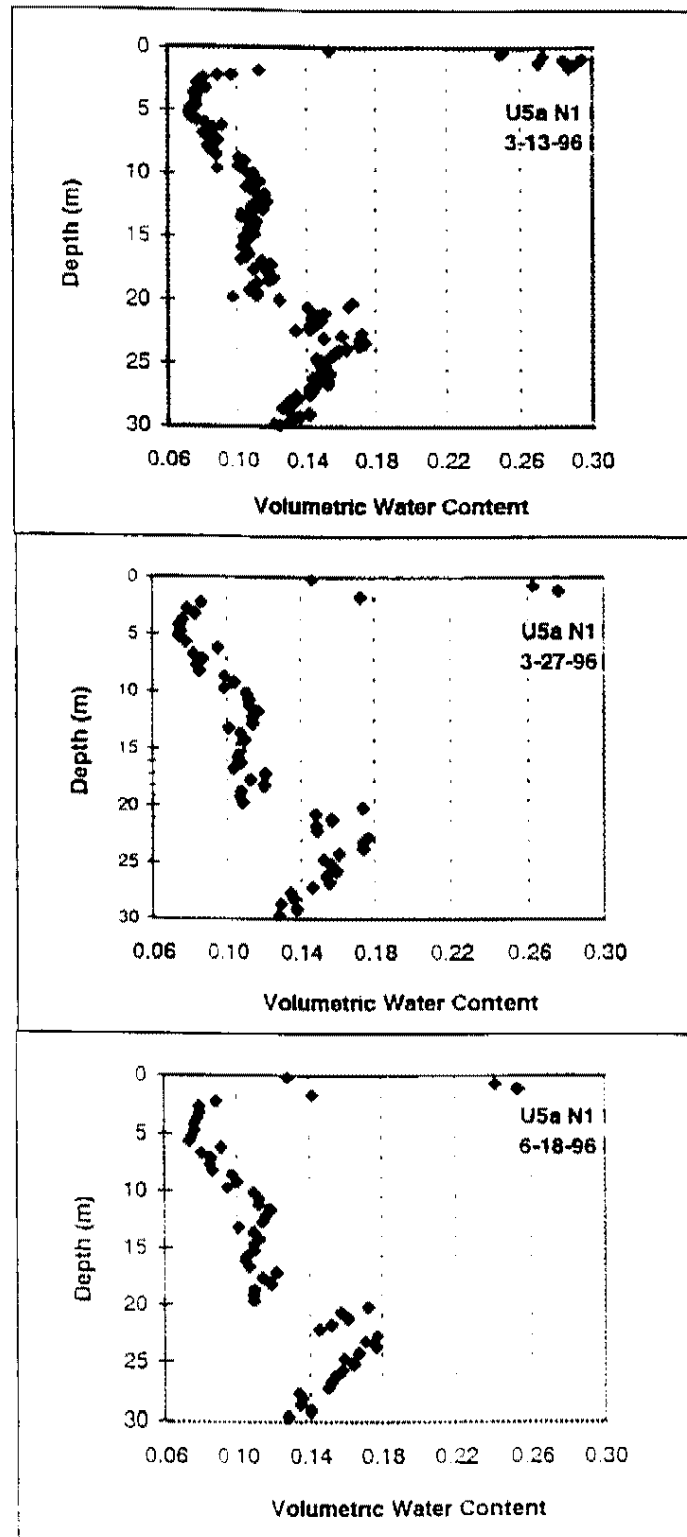


**Figure 27.** Water contents measured with a neutron moisture meter during the spring and summer of 1996 for U5a-N1 (From Hokett and Gillespie, 1996).

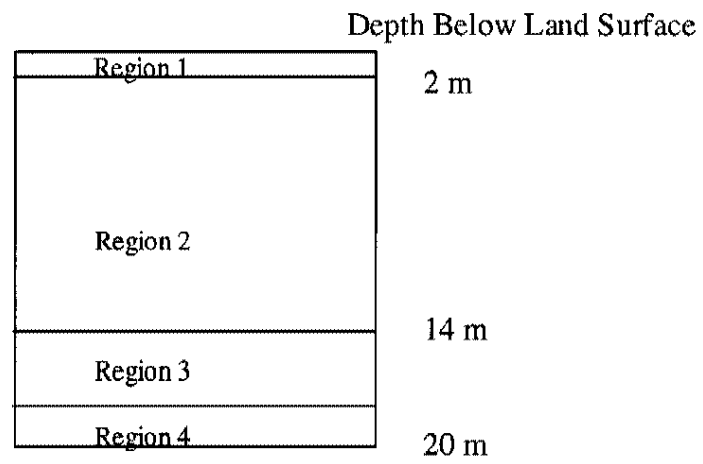


**Figure 28.** Multi-layered sediment observation regions for examination of inflow/outflow.

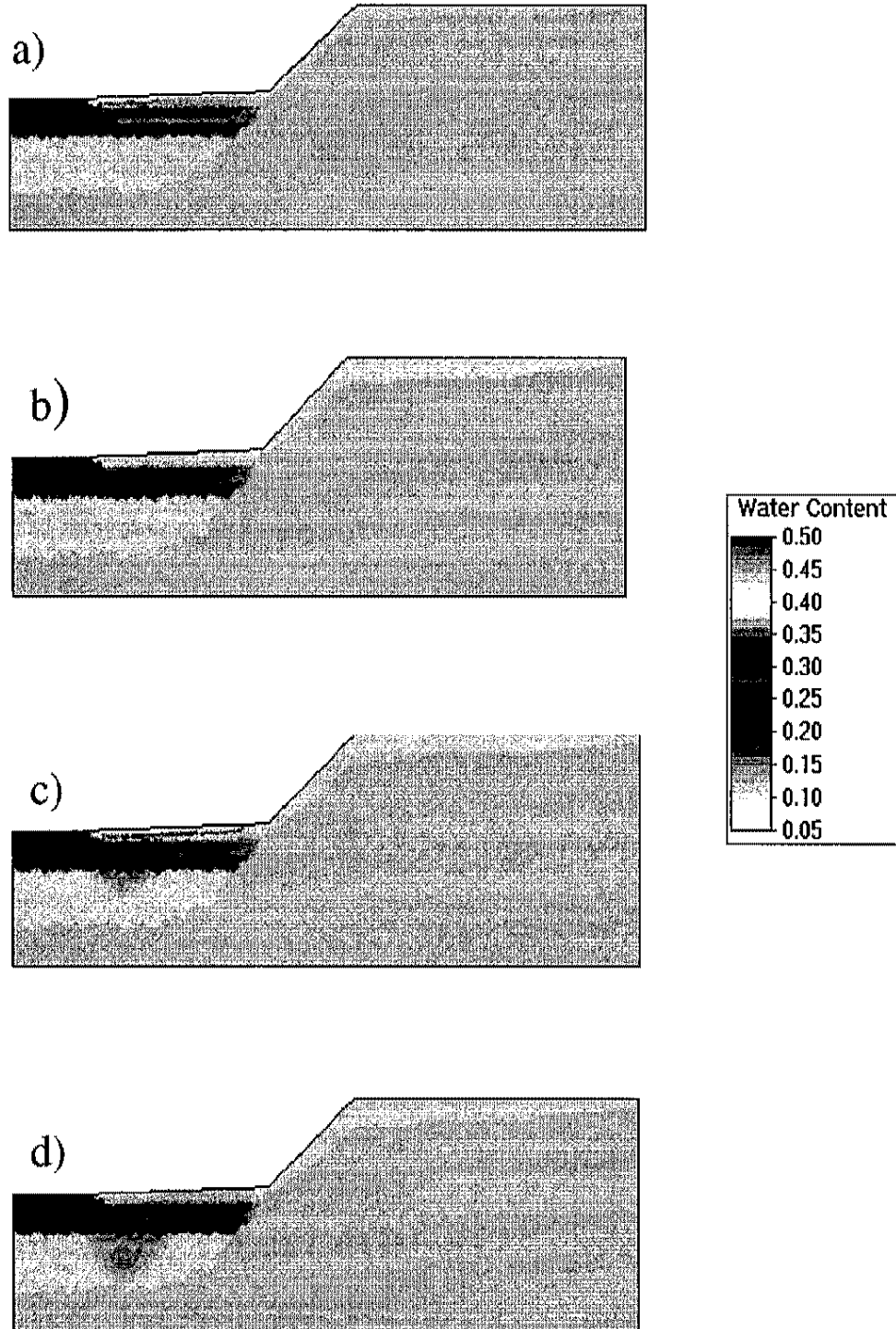


**Figure 29.** HYDRUS-2D modeling results showing water content distribution in the multi-layered sediment in the crater at the end of (a) infiltration of the 2nd pond, (b) redistribution of the 2nd pond, (c) infiltration of the 6th pond, and (d) redistribution of the 6th pond.

**Table 5.** Combined time (in days) for infiltration of 2 pond events.

Depth	5m	12 m	15 m	20 m
30 cm	60	0.9	0.3	0.1
90 cm	60	0.6	0.2	0.08

**Table 6.** Maximum depth (in meters) of water movement.

Depth	5m	12 m	15 m	20 m
30 cm	11.4	18.6	16.9	11.2
90 cm	10.9	18.7	16.9	11.6

**Table 7.** Particle size analysis along crater transect.

STA	Texture	Gravel %	Sand %	Silt %	Clay %
20S	SL	0.2	66.2	26.2	7.4
10S	SL	1.5	68.0	28.2	2.3
00	SiC	0.7	6.5	44.0	48.8
10	SiC	0.2	3.2	42.8	53.9
30	SiCL	0	1.7	58.8	39.5
40	SiCL	0	0.7	69.5	29.8
50	SiCL to SiL	0	0.3	72.3	27.4
60	SiL	0	0.5	89.3	10.2
70	SiC	0	1.0	54.9	44.1
80	SiL	0.7	15.4	68.2	15.8
90	LS	1.0	77.8	16.3	4.9
105	LS	1.0	76.1	17.3	5.6
120	LS	1.9	81.3	12.0	4.8
135	SL	0.7	74.2	13.7	11.4
150	LS	4.8	78.5	12.8	3.9
165	LS to SL	0.9	77.1	16.4	5.5
A	LS	3.5	75.1	17.2	4.2
B	SL	4.1	65.8	21.5	8.6
C	LS to SL	2.6	74.5	16.4	6.5

**Table 8.** Particle size analysis for depth (m) at transect locations 30, 70, 120, and 150 for very fine sand (VFS), fine sand (FS), medium sand (MS), coarse sand (CS), and very coarse sand (VCS).

Sta 30	VFS	FS	MS	CS	VCS
0.76	0.2	0.2	0	0	0
1.07	0.1	0.1	0	0	0
1.98	0	0	0	0	0
2.29	0	0	0	0	0
3.35	1.0	1.0	0	0	0
4.72	12.6	18.8	5.8	0	0
5.33	26.9	42.5	3.9	0.3	0
5.64	30.0	50.8	4.3	0.2	0.1
5.94	16.6	31.4	10.2	4.9	4.9
Sta 70	VFS	FS	MS	CS	VCS
0.91	0.3	0.4	0	0	0
1.37	0.2	0.3	0.1	0	0
2.04	0.3	0.3	0	0	0
2.44	0.1	0.1	0	0	0
3.66	0.2	0.2	0	0	0
4.27	12.0	16.7	1.1	0.1	0
5.03	27.7	47.7	5.8	0.4	0
5.64	22.5	48.1	14.1	2.6	0.6
5.94	14.7	29.5	11.8	6.4	6.8
Sta 120	VFS	FS	MS	CS	VCS
0.91	16.1	34.0	16.6	7.3	3.0
1.37	7.8	17.1	8.5	4.0	3.1
1.83	17.0	34.6	13.7	7.0	7.0
2.44	6.3	13.3	6.2	3.1	3.0
3.35	4.0	8.4	3.8	1.9	1.7
3.96	10.3	15.4	1.3	0.4	0.2
4.88	22.9	35.6	3.1	0.2	0.1
5.49	25.0	44.7	8.5	1.4	0.2
5.94	18.0	35.3	12.4	5.1	3.5
Sta 150	VFS	FS	MS	CS	VCS
2.43	6.9	16.9	10.0	4.8	4.1
3.81	1.1	2.7	1.5	0.6	0.5
5.34	23.6	38.4	4.3	0.4	0

**Table 9.** Hydraulic conductivities for sampling stations.

STA	Texture	Ksat (m/day)	K(h = -15 cm) (m/day)
20S	SL	1.3	0.5
10S	SL	1.7	0.04
00	SiC	0.1	0.01
10	SiC	0.05	0.003
30	SiCL	0.05	0.09
40	SiCL	0.02	0.08
50	SiCL to SiL	0.02	
60	SiL	0.04	0.0005
70	SiC	0.05	0.008
80	SiL	0.06	
90	LS	3.6	2.2
105	LS	7.0	6.2
120	LS	5.0	2.0
135	SL	4.3	1.4
150	LS	6.7	4.1
165	LS to SL	2.5	1.4
	Avg coarse-grain	4	0.05
	Coeff of variation	52%	60%
	Avg fine-grain	2.2	0.03
	Coeff of variation	91%	133%

**Table 10.** Laboratory and RETC results for soil properties.

Texture	Station	Bulk density	theta r	theta s	alpha (-1/cm)	n
SL	20S	1.41	0.065	0.42	0.051	1.67
	20S	1.42	0.065	0.43	0.033	1.9
	10S	1.45	0.065	0.43	0.041	1.62
	10S	1.35	0.065	0.44	0.059	1.48
	135	1.36	0.035	0.3	0.044	1.71
	135	1.37	0.035	0.38	0.034	2.06
Avg		1.39		0.41	0.04	1.74
SiC	00	1.1	0.12	0.48	0.035	1.34
	00	1.25	0.12	0.55	0.022	1.44
	10	1.2	0.12	0.51	0.018	1.3
	10	1.19	0.12	0.51	0.028	1.25
	70		0.1	0.53	0.019	1.32
	70		0.1	0.51	0.018	1.3
Avg		1.18		0.52	0.023	1.32
SiCL	30	1.13	0.12	0.5	0.013	1.38
	30	1.09	0.12	0.54	0.03	1.3
	40	1.15	0.12	0.53	0.022	1.29
	40	1.06	0.12	0.51	0.029	1.26
	50		0.095	0.53	0.021	1.28
	50		0.095	0.51	0.027	1.25
Avg		1.11		0.52	0.02	1.29
LS	90	1.36	0.05	0.46	0.021	1.53
	90	1.36	0.05	0.47	0.037	1.55
	105	1.47	0.05	0.37	0.037	1.76
	105	1.44	0.05	0.41	0.034	1.79
	120	1.47	0.05	0.41	0.054	1.86
	120	1.29	0.05	0.46	0.036	1.73
	150	1.64	0.035	0.37	0.047	1.96
	150	1.36	0.035	0.4	0.032	1.74
	165	1.33	0.057	0.43	0.038	1.8
	165	1.48	0.057	0.4	0.042	1.73
Avg		1.42		0.42	0.04	1.75
Si to SiL	60	1.14	0.12	0.51	0.045	1.21
	60	1.11	0.12	0.48	0.064	1.18
	80		0.095	0.54	0.04	1.26
	80		0.095	0.48	0.019	1.3
Avg		1.12		0.5	0.042	1.24

**Table 11.** Hydraulic properties for soil types used in the final modeling scenario.

Soil	Qr	Qs	Qa	Qm	alpha	n	Ks	Kk	Qk	Source
Loamy sand	0.05	0.41	0.05	0.41	8.5	1.45	4.8	4.8	0.41	field, lab
Loam	0.078	0.43	0.078	0.43	3.6	1.56	0.25	0.25	0.43	HYDRUS-2D
Sandy loam	0.075	0.36	0.075	0.361	1.83	1.9	0.64	0.64	0.36	Area 5 PA
Silt loam	0.034	0.46	0.034	0.46	1.6	1.37	0.06	0.06	0.46	HYDRUS-2D
Silty clay loam	0.12	0.52	0.12	0.52	2.0	1.29	0.02	0.02	0.52	field, lab
Silty clay	0.12	0.51	0.12	0.51	2.3	1.33	0.04	0.04	0.51	field, lab

**Table 12.** Summary of large pond infiltration/drainage simulation.

Time (days)	Volume of water (m <sup>3</sup> )	Inflow (m <sup>3</sup> )	Total inflow (m <sup>3</sup> )
0	632500	0	0
1	638600	6100	6100
2	644600	6000	12100
7	664900	20300	32400
12	690200	25300	57700
13.2	695900	5700	63400
11070	693500	-2400	61000

**Table 13.** Summary of layered profile infiltration/drainage simulation.

Event	Time (days)	Inflow (m <sup>3</sup> )	Cumulative inflow (m <sup>3</sup> )
P1		890	890
D1	210	-1359	-469
P2		390	-79
D2	2280	-924	-1003
P3		342	-661
D3	1050	-369	-1030
P4		276	-754
D4	990	-380	-1134
P5		418	-716
D5	690	-242	-958
P6		1374	416
D6	690	-609	-193

**Table 14.** Total inflow/outflow of water for six infiltration/  
drainage events.

Time	Region 1	Region 2	Region 3	Region 4
Initial	920 m <sup>3</sup>	6470 m <sup>3</sup>	97600 m <sup>3</sup>	8730 m <sup>3</sup>
Final	861m <sup>3</sup>	8390 m <sup>3</sup>	96000 m <sup>3</sup>	8730 m <sup>3</sup>

## CHAPTER 4

### SUMMARY

Not all surface flow resultant from intense summer convective storms or prolonged winter precipitation may pass along the gentle slopes of the alluvial fans to the low spots of the Flats, with unsubstantial infiltration along the way. Some of this flow is now funneled into subsidence craters creating artificial recharge basins. A relatively small amount of rainfall, formerly spread throughout a large area maybe focused into a depression. Potential for significant recharge exists.

The physical characteristics of crater U5a provide the evidence necessary to determine the possibility of anomalous recharge. Vegetation, deep erosional gullies, 14.6 m of sediment washed into the crater in 30 years, and a fine-grained playa are all associated with periodic surface water events captured by crater U5a. Hokett and Gillespie (1996) recognized this fact and began a more intense examination of the subsurface conditions and runoff mechanisms. They found that water content beneath the crater's low spot was 38% greater than in an adjacent, undisturbed location. Preliminary modeling for a simplified scenario demonstrated the ability of a given volume of water to infiltrate through the coarse material on the periphery of the playa region.

The first objective of this study was to evaluate the uncertainty in the crater recharge estimates of Hokett and French (1998) due to model assumptions (0.3 m deep and 12 m wide). To accomplish this task, different boundary and initial conditions were tested for sensitivity. Two ponding events separated by a drainage event were modeled using constant head upper boundary conditions of 0.3 and 0.9 m and extending 5 m, 12 m, 15 m, and 20 m. The 5 m pond was unable to infiltrate through the fine-grained material that extended 10 m laterally but the other three conditions demonstrated preferential flow through the periphery of the playa. Deepest water movement occurred in the pond extending only 2 m beyond the edge of the playa, where the set volume of water was focused through the smallest area of coarse material. Thus, the approach of Hokett and Gillespie (1998) provides a worst-case scenario. The effects of the depth of ponds tested were negligible. The greater head infiltrated faster, but the depth of the wetting front was nearly identical in both cases. This was reasoned to be due to an equal volume being infiltrated under each head. If these heads were infiltrated for equal amounts of time, the longer head would provide a larger volume and likely deeper infiltration.

The second sensitivity analysis examined the effects of varying initial conditions on the depth of water movement beneath the crater. Three scenarios were modeled: (1) initial matric head of  $-10$  m throughout the domain, (2) initial matric head of  $-200$  m throughout the domain, and (3) initial matric head set in equilibrium with the water table at the bottom boundary. This latter case (3) most closely approximates actual conditions at the NTS alluvial fans. After simulating 14 pond/drainage cycles over 32 years, depth of water movement in all three cases was approximately 130 m,



consistent with the results of Hokett and French (1998) who set the initial condition at -10 m. The similar depths for all three conditions can be explained by the dependence of unsaturated hydraulic conductivity and water storage on head or water content. The entire range of initial conditions is very dry and  $K(h)$  remains nearly the same low value. In the case of matric head being linearly distributed with depth, as the wetting front reaches a closer proximity to the saturated zone, hydraulic conductivity will nonlinearly increase and water storage capacity will decrease. It is expected that this would result in accelerating the flow rate as the wetting front approaches the water table.

The final objective of this study was to assess media properties of the crater and incorporate them into two final modeling scenarios to refine estimates of recharge potential beneath a subsidence crater. The work of Hokett and Gillespie (1998) focused recharge along the periphery of the playa. While this work reflects attributes of the current crater morphology, it failed to produce water contents beneath the playa that resembled the borehole measurements. Field observations of crater U5a offered three pieces of evidence to suggest an extremely large ponding event occurred on the initial crater surface creating the current crater morphology: (1) a ring of depositional material high on the crater walls, (2) deep, wide erosional gullies suggestive of high intensity surface water, and (3) soil textures that become coarser with depth, grading from clays at the surface to gravel at 6 m below land surface. A stage-volume relationship for the original crater surface estimated a volume of such a pond to be nearly  $64,000 \text{ m}^3$ . The first scenario modeled the infiltration and redistribution of this large pond through the coarse material that was present throughout the rubble chimney predicted the wetting

front reaching the water table in 30 years. A fourth evidence for this large event was the observation that the borehole measurements of Hokett and Gillespie (1996) closely matched the predicted water contents.

The modeling of this large pond utilized a homogeneous soil throughout the rubble chimney. It was not the intent of this study to suggest such a domain actually exists, but rather to incorporate field and laboratory observations as closely as possible. Modeling attempts discussed earlier used a domain with ten subtle, continuous layers that proved to be a barrier to flow. A similar approach was not taken in this study due to the lack of evidence to support such layering. Any layers that may have existed before the weapon detonation most likely would not remain after the collapse of the rock and soil. In fact, the preexisting layers may actually be slanted inwards, creating a funnel for water flow. The method used in this study could also not be considered a true “conservative approach” either. Preferential flowpaths due to the bulking of the geologic media and instrumentation of the shot hole were ignored. Subsurface characterization has failed to identify these features but the likelihood of locating a narrow vertical pathway with a single vertical borehole is slim. Admittedly, any of the above listed could exist, but it was felt that this study incorporated characteristics most closely resembling reality.

The second scenario modeled in this study was to qualify the potential for future recharge through the layered soil deposited by the large pond. A smaller model domain was created incorporating the hydraulic properties of six soil textures. Six ponding/drainage cycles were applied to the surface, with depths and lateral extents consistent with the predicted pond volume. At the conclusion of the simulation, water

movement through the layered domain was minimal, with most precipitation being recycled back to the atmosphere. From these results, it can be concluded that the deposited sediment acts as a barrier to future flow. The low hydraulic conductivity and high water storage capacity of the deposited material provided a favorable environment for deep rooting plants which further prevent future recharge by recycling water to the atmosphere.

This study does not suggest that all, or even most, craters exhibit similar hydraulic behavior. Crater U5a was originally chosen for study because it displayed evidence for a “worst-case” scenario of crater recharge. Another undisturbed crater, within a few kilometers of U5a, shows little evidence of surface water capture. Other craters have shown in preliminary investigations to capture numerous small ponding events but not large volumes. The location of the crater on the alluvial fan or its position relative to surface water flow channels is probably the most significant determinant of its ability to act as a recharge basin. In addition, crater U5a has been left undisturbed since its creation. Current engineering practices at the Area 3 and Area 5 RWMS may be able to prohibit flow into craters by the construction of berms, caps, or liners. Additionally, these findings suggest that craters, like U5a, that exhibit a high potential for surface water capture, thus recharge, can self-heal in a short time. The self-healing nature of craters has important implications to the impacts of subsidence at the RWMS low level waste trenches that warrant further study.

The threat of recharge through a nuclear subsidence crater cannot be easily dismissed. Surface water capture by each crater will differ, however, the landscape position, fan infiltration properties, as well as the physical characteristics of the crater

can provide predictive capability for the potential to capture runoff. The soil morphology of the shallow subsurface and surface biology can provide evidence of the potential for recharge. Only after a flux of water toward the water table can be confidently estimated, can the possibility of radionuclide migration by the wetting front be legitimately studied. This single crater type of analysis can then be extended to a regional scale assessment of the potential for focused recharge in craters to impact groundwater flow pathways and contaminant migration.

## REFERENCES

- Allison, G.B., Gee, G.W., and Tyler, S.W., 1994, Vadose-zone techniques for estimating ground-water recharge in arid and semiarid regions: *Soil Science Society of America Journal*, v. 58, p. 6-14.
- Anderson, T.W., 1995, Summary of the Southwest Alluvial Basins, regional aquifer-system analysis, south-central Arizona and parts of adjacent states: U.S. Geological Survey Professional Paper 1406-A.
- Bechtel Nevada, 1997, Interim geology report, Area 3 Radioactive Waste Management Site, DOE/Nevada Test Site, Nye County, Nevada, U.S. Department of Energy, Nevada Operations Office.
- Bechtel Nevada, 1998a, Hydrogeologic characterization of U-3at collapse zone: Data Report, U.S. Department of Energy, Nevada Operations Office.
- Bechtel Nevada, 1998b, Hydrogeologic characterization of U-3bh collapse zone: Data Report, U.S. Department of Energy, Nevada Operations Office.
- Bechtel Nevada, 1998c, Hydrogeologic characterization of U-3bl collapse zone: Data Report, U.S. Department of Energy, Nevada Operations Office.
- Bechtel Nevada, 1998d, Hydrogeologic characterization of the unsaturated zone at the Area 3 Radioactive Waste Management Site: Data Report, U.S. Department of Energy, Nevada Operations Office.
- Boardman, C.R., 1970, Engineering effects of underground nuclear explosives, *in* Proceedings, Symposium on Engineering with Nuclear Explosives, CONF-700101: Las Vegas, Nevada, p. 43-67.
- Bolt, G.H., 1956, Physico-chemical analysis of the compressibility of pure clays: *Geotechnique*, v. 8, p. 86-90.
- Broadhurst, W.L., 1942, Recharge and discharge of the ground-water reservoirs on the High Plains in Texas: *Eos Trans, American Geophysical Union*, v. 1, p. 9-15.
- Brooks, R.H. and Corey, A.T., 1964, Hydraulic properties of porous media. Hydrology Paper No. 3: Civil Engineering Department, Colorado State University, Fort Collins, Colorado, 27 p.

- Brotherson, J.D. and Winkle, V., 1986, Habitat relationships of saltcedar (*Tamarix ramosissima*) in central Utah: Great Basin Naturalist, v. 46, p. 535-541.
- Burbey, T.J. and Prudic, D.E., 1991, Conceptual evaluation of regional ground water flow in the carbonate-rock Province of the Great Basin, Nevada, Utah, and adjacent states: U.S. Geological Survey Professional Paper 1409-D.
- Burdine, N.T., 1953, Relative permeability calculations from pore-size distribution data: Petrology Transactions: American Institute Mining Metallurgic Engineering, v.198, p. 71-77.
- Busch, D.E., Ingraham, N.L., and Smith, S.D., 1992b, Water uptake in woody riparian phreatophytes of the southwestern United States: a stable isotope study: Ecological Applications 2, p. 450-459.
- Carroll, R.D., 1981, Seismic velocities and postshot properties in and near chimneys, *in* Proceedings, Monterey Containment Symposium, LA-9211-C: Monterey, California, Los Alamos National Laboratory, p. 379-396.
- Carsel, R. F. and Parrish, R.S., 1988, Developing joint probability distributions of soil Water retention characteristics: Water Resources Research, v. 24(5), p. 755-769.
- Cherry, J.T., Larson, D.B., and Rapp, E.G., 1968, Computer calculations of the Gasbuggy event: Lawrence Radiation Laboratory Report, UCRL-50419, 11 p.
- Claborn, B.J., Urban, L.V., and Opper, S.E., 1985, Frequency of significant recharge to the Ogallala aquifer from playa lakes: Final Rep., Project G-935-03: Texas Tech University: Water Resource Center, Lubbock, 24 p.
- Crowe, B., Hansen, W., and Sully, M., 1998, The consequences of disposal of low-level radioactive waste from the Fernald Environmental Management Project: Report of the DOE/Nevada Independent Panel, Los Alamos National Lab, LA-13453-MS, UC-840.
- Darcy, H., 1856, Les fontaines publique de la ville de Dijon. Dalmont, Paris.
- Delort, F. and Supiot, F., 1970, Nuclear stimulation of oil reservoirs, *in* Proceedings, Symposium on Engineering with Nuclear Explosives, CONF-700101: Las Vegas, Nevada, p. 649-661.
- Dettinger, M.D., 1989, Distribution of carbonate-rock aquifers in southern Nevada and the potential for their development-Summary of findings, 1985-1988: Carson City, Nevada, Program for the Study and Testing of Carbonate-Rock Aquifers in Eastern and Southern Nevada, Summary Report No. 1, 37 p.

- Domenico, P.A., Stephenson, D.A., and Maxey, G.B., 1964, Groundwater in Las Vegas Valley: University of Nevada, Desert Research Institute, Technical Report No. 7.
- El-Swaify, S.A. and Henderson, D.W., 1967, Water retention by osmotic swelling of certain colloidal clays with varying ionic composition: *Journal of Soil Science*, v. 18, p. 223-232.
- Fischer, J.M., 1992, Sediment properties and water movement through shallow unsaturated alluvium at an arid site for disposal of low-level radioactive waste near Beatty, Nye County, Nevada: U.S. Geological Survey Water Resources Investigations Report 92-4032, 48 p.
- Fouty, S., 1989, Chloride mass-balance as a method for determining long-term groundwater recharge rates and geomorphic surface stability in arid and semi-arid regions – Whiskey Flat and Beatty, Nevada [M.S. thesis]: Tucson, University of Arizona, 130 p.
- French, R.H., 1986, Daily, seasonal, and annual precipitation at the Nevada Test Site, Nevada: Water Resources Center, Desert Research Institute, Las Vegas, Nevada, Publication 45042, DOE/NV/10384-01, 57 p.
- French, R.H. and S.L. Hokett, 1998, Arid region water harvest, *in* Proceedings, Ground Water Management Symposium, American Society of Civil Engineers.
- Gee, G.W. and Bauder, J.W., 1986, Particle size analysis, *in* Methods of Soil Analysis, part I: American Society of Agronomy, Madison, Wisconsin, v. 9, p. 383-409.
- Gee, G.W. and Hillel, D., 1988, Groundwater recharge in arid regions: Review and critique of estimation methods: *Journal of Hydrology, Process*, 2, p. 255-266.
- Gee, G.W., Fayer, M.J., Rockhold, M.L., and Campbell, M.D., 1992, Variations in recharge at the Hanford Site: *Northwest Science*, v. 66, p. 237-250.
- Gee, G.W., Wierenga, P.J., Andraski, B.J., Young, M.H., Fayer, M.J., and Rockhold, M.L., 1993, Variations in water balance and recharge potential at three western desert sites: *Soil Science Society of America Journal*, v. 58, p. 63-72.
- Germain, L.S. and Kahn, J.S., 1968, Phenomenology and containment of underground nuclear explosions: Lawrence Livermore National Laboratory, Livermore, CA, UCRL-50482.
- Haines, W.B., 1930, The hysteresis effect in capillary properties and the modes of moisture distribution associated therewith: *Journal of Agricultural Science*, v. 20, p. 96-105.

- Healy, R.W., 1990, Simulation of solute transport in variably saturated porous media with supplemental information on modifications to the U.S. Geological Survey's computer program VS2D: U.S. Geological Survey Water Resources Investigations Report 90-4025.
- Higgins, G.H., 1970, Underground nuclear explosions, *in* Proceedings, Symposium on Engineering with Nuclear Explosives, CONF-700101: Las Vegas, Nevada, p. 29-42.
- Hokett, S. L. and Gillespie, D. R., 1996, Preliminary evaluation of recharge potential at subsidence crater U5A in Frenchman Flat, Nevada Test Site: Water Resources Center, Desert Research Institute, Las Vegas, Nevada, DOE/NV/11508-15, 40 p.
- Hokett, S.L. and French, R.F., 1998, Evaluation of recharge potential at subsidence crater U5a in Frenchman Flat, Nevada Test Site: Water Resources Center, Desert Research Institute, Las Vegas, Nevada, DOE/NV/11508-32DRI.
- Holzer, A., 1970, Gasbuggy in perspective, *in* Proceedings, Symposium on Engineering with Nuclear Explosives, CONF-700101, Volume 1: Las Vegas, Nevada, p. 29-42.
- Jeppson, R.W., 1974, Axisymmetric infiltration in soils, I. Numerical techniques for solution: *Journal Hydrology*, v. 23, p. 111-130.
- Klute, A., 1986, Water retention: Laboratory methods, *in* Methods of Soil Analysis, Part I: American Society of Agronomy, Madison, Wisconsin, v. 9, p. 635-662.
- Kunkle, T. and Hawkins, W., 1997, An introduction to underground nuclear phenomenology or what happens when the bomb goes off: Short course on radionuclide migration: DOE/NV: Los Alamos National Laboratory.
- Laczniaik, R. J., Cole, J. C., Sawyer, D. A., and Trudeau, D. A., 1996, Summary of hydrogeologic controls on ground-water flow at the Nevada Test Site, Nye County, Nevada: U.S. Geological Survey Water Resources Investigations Report 96-4109, 59 p.
- Lappala, E.G., Healy, R.W., and Weeks, E.P., 1983, Documentation of computer program VS2D to solve the equations of fluid flow in variably saturated porous media: U.S. Geological Survey Water Resources Investigations Report 83-4099.
- Lehman, O., 1972, Playa water quality for ground water recharge and use of playas for impoundment of feedyard runoff, *in* Proceedings, Playa Lake Symposium, Publ.4: International Center for Arid and Semi-Arid Land Studies and Department of Geoscience: Texas Tech University, p. 25-30.
- Lindstrom, F.T., Cawfield, D.E., Daffern, D.D., and Emer, D.F., 1991, A simple one-dimensional isothermal and vertical vadose zone steady-state infiltration/evaporation model: REECO, DOE/NV/10630-17.

- Lombard, D.B., Bray, B.G., and Sohns, H.W., 1970, Technical considerations for plowshare applications to oil shale, *in* Proceedings, Symposium on Engineering with Nuclear Explosives, CONF-700101: Las Vegas, Nevada, p. 1343-1363.
- Luxmoore, R.J., Jardine, P.M., Wilson, G.V., Jones, J.R., and Zelanzy, L.W., 1990, Physical and chemical controls of preferred path flow through a forested hill slope: *Geoderma*, v. 46, p. 139-154.
- Millington, R.J., and Quirk, J.P., 1961, Permeability of porous solids: *Transactions, Faraday Soc.*, v. 57, p. 1200-1206.
- Mohanty, B.P., Bowman, R.S., Hendrickx, M.H., and van Genuchten, M.T., 1997, New piecewise-continuous hydraulic functions for modeling preferential flow in an intermittent-flood-irrigated field: *Water Resources Research*, v.33(9), p. 2049-2063.
- Mualem, Y., 1976, A new model for predicting the hydraulic conductivity of Unsaturated porous media: *Water Resources Research*, v. 12(3), p. 513-522.
- Office of Technology Assessment, 1989, The containment of underground nuclear explosions: U.S. Congress Report OTA-ISC-414, 80 p.
- Olsen, C.W., 1993, Site Selection and Containment Evaluation for LLNL Nuclear Events, *in* Proceedings, Seventh Symposium on Containment of Underground Nuclear Explosions, Volume 1: Kent, Washington, p. 85-119.
- Osterkamp, W.R. and Wood, W.W., 1987, Playa-lake basins on the southern high plains of Texas and New Mexico: Part I – Hydrologic, geomorphic and geologic evidence for their development: *Geological Society of America Bulletin*, v. 99, p. 215-223.
- Pavlikis, G. and Barden, L., 1972, Hysteresis in the moisture characteristics of clay soil: *Journal of Soil Science*, v. 23, p. 350-361.
- Piper, A.M. and Stead, F.W., 1965, Potential applications of nuclear explosives in development and management of water resources- Principles: U.S. Geological Survey Open-File Report TEI-857, 128 p.
- Pohll, G.M., Warwick, J.J., and Tyler, S.W., 1996, Coupled surface-subsurface hydrologic model of a nuclear subsidence crater at the Nevada test site: *Journal of Hydrology*, v. 186, p. 43-62.
- Reeve, M.J., Smith, P.D., and Thomasson, A.J., 1973, The effect of density on water retention properties of field soils: *Journal of Soil Science*, v. 24, p. 355-367.
- Richards, L.A., 1931, Capillary conduction of liquids in porous mediums: *Physics*, v. 1, p. 318-333.

- Rogers, L.A., 1970, Determining the effects on the Gasbuggy reservoir from computer simulation of the postshot gas production history, *in* Proceedings, Symposium on Engineering with Nuclear Explosives, CONF700101: Las Vegas, Nevada, p. 698-721.
- Sala, A., Smith, S.D., and Devitt, D.A., 1996, Water use by *Tamarix ramosissima* and associated phreatophytes in a Mojave Desert floodplain: Ecological Applications, v. 6(3), p. 888-898.
- Salter, P.J. and Williams, J.B., 1965, The influence of texture on the moisture characteristics of soils. Part I: A critical comparison of techniques for determining the available water capacity and moisture characteristic curve of a soil: Journal of Soil Science, v. 16, p. 1-15.
- Scanlon, B. R. and Goldsmith, R. S., 1997, Field study of spatial variability in unsaturated flow beneath and adjacent to playas: Water Resources Research, v. 33(10), p. 2239-2252.
- Schmeltzer, J. S., Miller, J.J., and Gustafson, D.L., 1993, Flood assessment at the Area 5 Radioactive Waste Management Site and the proposed hazardous waste storage unit DOE/Nevada Test Site, Nye County, Nevada: Raytheon Services Nevada, Las Vegas, Nevada.
- Schmeltzer, J. S., Barker, L. E., and Blout, D. O., 1996, Site characterization data from the U3ax/bl exploratory boreholes at the Nevada Test Site: U.S. Department of Energy, Nevada Operations Office DOE/NV/11718-003.
- Shafroth, P.B., Friedman, J.M., and Ischinger, L.S., 1995, Effects of salinity on establishment of *Populus fremontii* (cottonwood) and *Tamarix ramosissima* (saltcedar) in the southwestern U.S.: Great Basin Naturalist, v. 55, p. 58-65.
- Sharma, M.L. and Uehara, G., 1968, Influence of soil structure on water relations in low humic latosols: I. Water Retention: Soil Science Society of America Proc., v. 32, p. 765-770.
- Shott, G.J., Barker, L.E., Rawlinson, S.E., and Sully, M.J., 1997, Performance assessment for the Area 5 RWMS at the Nevada Test Site, Nye County, Nevada. Revision 2.1: U.S. Department of Energy Report DOE/NV/11432-196.
- Shouse, P., Jury, W.A., and Stolzy, L.H., 1982, Field measurement and modeling of cowpea water use and yield under stress and well-watered growth conditions: Hilgardia, 50, p. 1-25
- Simunek, J., Sejna M., and van Genuchten, M.Th., 1996, Simulating water flow and solute transport in two-dimensional variably saturated media: International Ground Water Modeling Center, IGWMC-TPS 53, 167 p.

- Smettem, K.R.J., Chittleborough, D.J., Richards, B.G., and Leaney, F.W., 1991, The influence of macropores on runoff generation from a hillslope soil with a contrasting textural class: *Journal of Hydrology (Amsterdam)*, v. 122, p. 235-252.
- Smettem, K.R.J. and Kirkby, C., 1990, Measuring the hydraulic properties of a stable aggregated soil: *Journal of Hydrology*, v. 117, p. 1-13.
- Smith, D. K., 1995, Characterization of nuclear explosive melt debris: *Radiochimica Acta* 69, p. 157-167.
- Sophocleous, M. and Perry, C.A., 1985, Experimental studies in natural groundwater recharge dynamics: The analysis of observed recharge events: *Journal of Hydrology: Amsterdam*, v. 81, p. 297-332.
- Stephens, D.B. and Knowlton, R., 1986, Soil water movement and recharge through Sand at a semi-arid site in New Mexico: *Water Resources Research*, v. 22, p. 881-889.
- Teller, E., Talley, W., Higgins, C. and Johnson, C., 1968, *The Constructive Uses of Nuclear Explosives*: McGraw-Hill, New York, 320 p.
- Terhune, R.W., 1973, Prediction of nuclear explosion effects for Rio Blanco: Lawrence Livermore Laboratory Report UCRL-51377, 35 p.
- Thomas, G.W. and Moodie, J.E., 1962, Chemical relationships affecting the water-holding capacities of clays: *Soil Science Society of America Proc.*, v. 26, p. 153-155.
- Topp, G.C., 1969, Soil water hysteresis measured in a sandy loam compared with the hysteretic domain model: *Soil Science Society of America Proc.*, v. 33, p. 645-651.
- Tyler, S.W., Chapman, J.B., Conrad, S.H., Hammermeister, D.P., Blout, D.O., Miller, J.J., Sully, M.J., and Ginanni, J.M., 1996, Soil-water flux in the southern Great Basin, United States: Temporal and spatial variations over the last 120,000 years: *Water Resources Research*, v. 32(6), p. 1481-1499.
- Tyler, S., McKay, A., Hess, A., Jacobson, J. and Taylor, K., 1986, Effects of surface collapse structures on infiltration and moisture redistribution: University of Nevada, Desert Research Institute, Publication 45045, 48 p.
- Tyler, S.W., McKay, W.A., and Mihevc, T.M., 1992, Assessment of soil moisture movement in nuclear subsidence craters: *Journal of Hydrology*, v. 139, p. 159-181.
- van Genuchten, M.Th., 1980, A closed-form solution for predicting the hydraulic conductivity of unsaturated soils: *Soil Science Society of America Journal*, v. 44, p. 892-898.

- van Genuchten, M.Th., 1978, Calculating the unsaturated hydraulic conductivity with a new closed-form analytical model, Water Resources Program: Department of Civil Engineering, Princeton University, 63 p.
- Warren, D.K. and Turner, R.M., 1975, Saltcedar (*Tamarix ramosissima*) seed production, seedling establishment, and response to inundation: Journal of the Arizona Academy of Science, v. 10, p. 135-144.
- White, W.N., Broadhurst, W.L., and Lang, J.W., 1946, Ground water in the high plains of Texas: U.S. Geological Survey Water Supply Paper, v. 889-F, p. 381-420.
- Wilson, G.V. and Luxmoore, R.J., 1988, Infiltration, macroporosity, and mesoporosity distributions on two forested watersheds: Soil Science Society of America Journal, v. 52, p. 329-335.
- Wilson, G.V., Jardine, P.M., and Gwo, J.P., 1992, Modeling the hydraulic properties of a multiregion soil: Soil Science Society of America Journal, v. 56, p. 1731-1737.
- Winograd, I.J. and Doty, G.C., 1980, Paleohydrology of the southern Great Basin with special reference to water table fluctuations beneath the Nevada Test Site during the late (?) Pleistocene: U.S. Geological Survey Open-File Report 80-569, 91 p.
- Winograd, I.J. and Thordarson, William, 1975, Hydrogeologic and hydrochemical framework, southcentral Great Basin, Nevada-California, with special reference to the Nevada Test Site: U.S. Geological Survey Professional Paper 712-C, 126 p.
- Wood, W.W. and Osterkamp, W.R., 1987, Playa-like basins on the Southern High Plains of Texas and New Mexico, II, A hydrologic model and mass-balance arguments for their development: Geological Society of America Bulletin, v. 99, p. 224-230.
- Wood, W.W. and Sandford, W.E., 1995, Chemical and isotopic methods for quantifying ground-water recharge in a regional, semiarid environment: Ground Water, v. 33, p. 458-468.

APPENDIX A  
PARTICLE SIZE ANALYSIS

Results of field "feel" test by G.V. Wilson.  
 Depths (ft) are mid-interval at sampling stations

10S	
6'-8"	SiCL
28"-30"	SiCL-SiL
30"-55"	SiL
60"-66"	SiL
67"-72"	Si-L
8	L (S,G)
10	GL
10.5	GL

10	
1	SiCL
2	SiCL
4	SiCL (<C)
6	SiCL
7	SiCL
9	SiCL
12	SiL
14	SiL
16	SiL
17	SiL-L

30	
1	SiCL
3	SiCL
4	SiCL (<C)
6	SiCL
7	SiCL
8	SiCL
12	SiL
14	SiL
16	SiL
18	SiL- L (fs)
19	L (>fs)
20	L (ms,cs)

70	
1	SiCL
4	SiCL
5	SiCL (<C)
6	SiCL (<C)
7	SiCL
9	SiCL
13	SiL
15	SiL
17	SiL-L (fs)
19	L (fs,ms)
20	GL

90	
1	L-LS
2	SiL-SiCL
2.5	SiL-SiCL
5	SiCL
6	SiCL (<C)
10	SiCL (<<C)
13	SiL
14	SiL-L
17	L (fs,ms)
19	GL
20	LS

120	
0	GLS
4	GLS
5	SiL-SiCL
7	SiL
9	SiCL (G)
12	SiL
14	SiL
17	SiL-L (fs)
19	L
20	LS

150	
4	GLS
5	GLS
6	GL
10	GSiL
15	SiCL
19	SiL (fs)
20	SiCL-SiL

185	
1	GLS
4	GLS
6	GLS
8	GSiL
10	GSiL-L
12	GSiL-L
14	GSiL-L
16	GSiL
18	GSiL

APPENDIX B  
SATURATED AND UNSATURATED  
HYDRAULIC CONDUCTIVITY

STA 20S	avg head = 4.75				
Ksat					
Time (min)	Vol (L)		Infiltration (cm)	Rate (cm/min)	Rate (m/d)
0	0		0	0	0
12	1.25		2.608712536	0.217392711	3.130455
27	2.5		2.608712536	0.173914169	2.504364
54	3.75		2.608712536	0.096618983	1.3913134
82	5		2.608712536	0.093168305	1.3416236
	with insert 1 cm = 3.36 cm <sup>3</sup>				
K(h)			infil (cm)	Rate (cm/min)	Rate (m/d)
Time (sec)			18.5		
0	18.5		0	0	0
15	19.6		1.1	0.000768861	0.6642963
30	20.2		0.6	0.000419379	0.3623434
45	21.3		1.1	0.000768861	0.6642963
60	22.3		1	0.000698965	0.6039057
75	23.3		1	0.000698965	0.6039057
90	24.3		1	0.000698965	0.6039057
105	25.3		1	0.000698965	0.6039057
120	26.2		0.9	0.000629068	0.5435151
135	27.2		1	0.000698965	0.6039057
150	28.1		0.9	0.000629068	0.5435151
165	29		0.9	0.000629068	0.5435151
180	29.9		0.9	0.000629068	0.5435151
195	30.8		0.9	0.000629068	0.5435151
210	31.7		0.9	0.000629068	0.5435151
225	32.6		0.9	0.000629068	0.5435151
240	33.5		0.9	0.000629068	0.5435151

STA 10S						
Ksat						
Time (min)	Vol (L)		Infiltration (cm)	Rate (cm/min)	Rate (m/d)	
0	0		0		0	
7.5	1.25		2.608712536	0.347828338	5.00872807	
12.25	2.5		2.608712536	0.549202639	7.908518	
70	5		5.217425071	0.090345023	1.30096833	
95	6.25		2.608712536	0.104348501	1.50261842	
120	7.5		2.608712536	0.104348501	1.50261842	
141	8.75		2.608712536	0.124224406	1.78883145	
163	10		2.608712536	0.118577843	1.70752093	
with insert 1 cm = 3.36 cm <sup>3</sup>						
K(h)	reservoir		infil (cm)	Rate (cm/min)	Rate (m/d)	
Time (min)	reading (cm)					
0	19		19	0	0	
1	19.5		0.5	0.005242237	0.075488215	
2	19.7		0.2	0.002096895	0.030195286	
3	20		0.3	0.003145342	0.045292929	
4	20.2		0.2	0.002096895	0.030195286	
5	20.5		0.3	0.003145342	0.045292929	
6	20.8		0.3	0.003145342	0.045292929	

STA 00						
Ksat						
Time (min)	Vol (L)		Infiltration (cm)	Rate (cm/min)	Rate (m/d)	
0	0		0	0	0	
12	0.3		0.626091009	0.05217425	0.751309	
32	0.55		0.521742507	0.02608713	0.375655	
282	2.05		3.130455043	0.01252182	0.180314	
735	3.65		3.339152046	0.0073712	0.106145	
1350	5.8		4.486985561	0.00729591	0.105061	
	with insert 1 cm = 3.36 cm <sup>3</sup>					
K(h)	reservoir		infil (cm)	Rate (cm/min)	Rate (m/d)	
Time (min)	cm			Rate (cm/min)	Rate (m/d)	
0	0		0	0	0	
2	0.1		0.1	0.00052423	0.00754891	
8	0.3		0.2	0.000349487	0.00503261	
12	0.5		0.2	0.00052423	0.00754891	
14	0.7		0.2	0.00104846	0.01509783	
16	0.9		0.2	0.00104846	0.01509783	
18	1.2		0.3	0.00157269	0.02264674	
20	1.4		0.2	0.00104846	0.01509783	

STA 10							
Ksat							
Time (min)	Vol (L)		Infiltration (cm)	Rate (cm/min)	Rate (m/d)		
0	0		0	0	0		
5	0.4		0.834788011	0.1669576	2.404189		
294	1.25		1.773924524	0.00613815	0.088389		
622	1.8		1.147833516	0.00349949	0.050393		
1362	3		2.504364034	0.00338428	0.048734		
	with insert 1 cm = 3.36 cm <sup>3</sup>						
K(h)	reservoir		infil (cm)	Rate (cm/min)	Rate (m/d)		
Time (min)	cm			Rate (cm/min)	Rate (m/d)		
0	0		0	0	0		
5	0.1		0.1	0.000209692	0.00301957		
10	0.2		0.1	0.000209692	0.00301957		
15	0.3		0.1	0.000209692	0.00301957		
20	0.4		0.1	0.000209692	0.00301957		

Time (min)	Vol (L)	Infiltration (cm)	Rate (cm/min)	Rate (m/d)
0	0	0	0	0
235	1.15	2.40001553	0.01021283	0.14706
355	1.65	1.04348501	0.00869571	0.12522
1045	2.8	2.40001553	0.00347828	0.05009
with insert 1 cm = 3.36 cm <sup>3</sup>				
K(h)	reservoir	infil (cm)	Rate (cm/min)	Rate (m/d)
Time (min)	cm		Rate (cm/min)	Rate (m/d)
0	0	0	0	0
1	0.5	0.5	0.0052423	0.07548913
2	1.1	0.6	0.00629076	0.09058695
3	1.7	0.6	0.00629076	0.09058695
4	2.3	0.6	0.00629076	0.09058695

STA 40							
Ksat							
Time (min)	Vol (L)		Infiltration (cm)	Rate (cm/min)	Rate (m/d)		
0	0		0	0	0		
267	0.5		1.04348501	0.0039082	0.05628		
492	1		1.04348501	0.0046377	0.06678		
612	1		1.04348501	0.0030246	0.04355		
1302	1.55		1.14783352	0.0016635	0.02395		
	with insert 1 cm = 3.36 cm <sup>3</sup>						
K(h)	reservoir		infil (cm)	Rate (cm/min)	Rate (m/d)		
Time (min)	cm						
0	0		0	0	0		
2	1.1		1.1	0.00576653	0.083038		
4	2.1		1	0.0052423	0.0754891		
6	3.2		1.1	0.00576653	0.083038		
8	4.2		1	0.0052423	0.0754891		

STA 50							
Ksat							
Time (min)	Vol (L)			Infiltration (cm)	Rate (cm/m)	Rate (m/d)	
0	0			0	0	0	
128	1.25			2.60871254	0.0203806	0.29348	
370	1.875			1.30435627	0.0053899	0.07761	
1060	2.375			1.04348501	0.0015123	0.02178	

STA 60							
Ksat							
Time (min)	Vol (L)		Infiltration (cm)	Rate (cm/min)	Rate (m/d)		
0	0		0	0	0		
19	0.2		0.41739401	0.0219681	0.31634		
29	0.05		0.1043485	0.0104349	0.15026		
209	0.25		0.52174251	0.0028986	0.04174		
469	0.3		0.62609101	0.002408	0.03468		
	with insert 1 cm = 3.36 cm <sup>3</sup>						
K(h)			infil (cm)	Rate (cm/min)	Rate (m/d)		
Time (min)							
0			0	0	0		
32			0.1	3.2764E-05	0.0004718		
84			0.1	2.0163E-05	0.0002903		
140			0.1	1.8723E-05	0.0002696		

Time (min)	Vol (L)	Infiltration (cm)	Rate (cm/min)	Rate (m/d)
0	0	0	0	0
80	0.2	0.41739401	0.00521743	0.07513
275	0.85	1.35653052	0.00695657	0.10017
525	1.65	1.66957602	0.0066783	0.09617
1293	2.85	2.50436403	0.00326089	0.04696
with insert 1 cm = 3.36 cm <sup>3</sup>				
K(h)	reservoir	infil (cm)	Rate (cm/min)	Rate (m/d)
Time (min)	cm			
0	2.2	0	0	0
1	2.3	0.1	0.00104846	0.01509783
2	2.35	0.05	0.00052423	0.00754891
3	2.4	0.05	0.00052423	0.00754891

STA 80						
Ksat						
Time (min)	Vol (L)			Infiltration (cm)	Rate (cm/m)	Rate (m/d)
0	0			0	0	0
10	0.5			1.043485014	0.1043485	1.50262
89	1			1.043485014	0.0132087	0.1902
284	1.9			1.878273026	0.0096322	0.1387
534	2.5			1.252182017	0.0050087	0.07213
1301	4.1			3.339152046	0.0043535	0.06269

STA 90						
Ksat						
Time (min)	Vol (L)		Infiltration (cm)	Rate (cm/m)	Rate (m/d)	
0	0		0	0	0	
3.75	1.25		2.60871254	0.6956567	10.0175	
12.25	2.5		2.60871254	0.3069074	4.41947	
21.25	3.75		2.60871254	0.2898569	4.17394	
30.25	5		2.60871254	0.2898569	4.17394	
39.75	6.25		2.60871254	0.2746013	3.95426	
52	7.5		2.60871254	0.2129561	3.06657	
62.5	8.75		2.60871254	0.2484488	3.57766	
73	10		2.60871254	0.2484488	3.57766	
	1 cm = 15.34 cm <sup>3</sup>					
K(h)	reservoir		infil (cm)	Rate (cm/min)	Rate (m/d)	
Time (min)	cm			Rate (cm/min)	Rate (m/d)	
0	7.8		7.8			
0.25	8.4		0.6	0.11488127	1.6542903	
0.5	8.5		0.1	0.01914688	0.275715	
0.75	9.4		0.9	0.1723219	2.4814354	
1	10.2		0.8	0.15317502	2.2057203	
1.25	11		0.8	0.15317502	2.2057203	
1.5	11.8		0.8	0.15317502	2.2057203	
1.75	12.5		0.7	0.13402815	1.9300053	
2	13.4		0.9	0.1723219	2.4814354	
2.25	14.3		0.9	0.1723219	2.4814354	
2.5	15.1		0.8	0.15317502	2.2057203	
2.75	16		0.9	0.1723219	2.4814354	
3	16.8		0.8	0.15317502	2.2057203	
3.25	17.8		1	0.19146878	2.7571504	
3.5	18.7		0.9	0.1723219	2.4814354	
3.75	19.5		0.8	0.15317502	2.2057203	
4	20.2		0.7	0.13402815	1.9300053	
4.25	21.2		1	0.19146878	2.7571504	
4.5	22.1		0.9	0.1723219	2.4814354	
4.75	23.1		1	0.19146878	2.7571504	
5	23.9		0.8	0.15317502	2.2057203	
5.25	24.8		0.9	0.1723219	2.4814354	
5.5	25.6		0.8	0.15317502	2.2057203	

Time (min)	Vol (L)	Infiltration (cm)	Rate (cm/min)	Rate (m/d)
0	0	0	0	0
3.75	2.5	5.21742507	1.3913134	20.0349
10.5	5	5.21742507	0.7729519	11.1305
19.75	7.5	5.21742507	0.564046	8.12226
29.25	10	5.21742507	0.5492026	7.90852
39.25	12.5	5.21742507	0.5217425	7.51309
49.75	15	5.21742507	0.4968976	7.15533
60.5	17.5	5.21742507	0.4853419	6.98892
71.25	20	5.21742507	0.4853419	6.98892
1 cm = 15.34 cm <sup>3</sup>				
K(h)	reservoir	infil (cm)	Rate (cm/min)	Rate (m/d)
Time (min)	cm		Rate (cm/min)	Rate (m/d)
0	16	0	0	0
0.25	20	4	0.76587512	11.028602
0.5	21	1	0.19146878	2.7571504
0.75	23.5	2.5	0.47867195	6.8928761
1	25.75	2.25	0.43080476	6.2035885
1.25	28	2.25	0.43080476	6.2035885
1.5	30	2	0.38293756	5.5143009
1.75	32.5	2.5	0.47867195	6.8928761
2	34.5	2	0.38293756	5.5143009
2.25	36.5	2	0.38293756	5.5143009
2.5	38.5	2	0.38293756	5.5143009
2.75	40.75	2.25	0.43080476	6.2035885
3	43	2.25	0.43080476	6.2035885
3.5	47	4	0.38293756	5.5143009
3.75	49.5	2.5	0.47867195	6.8928761
4	51.25	1.75	0.33507037	4.8250133
4.25	53.5	2.25	0.43080476	6.2035885



STA 135							
Ksat	head = 0 to 4cm						
Time (min)	Vol (L)			Infiltration (cm)	Rate (cm/m)	Rate (m/d)	
0	0			0	0	0	
6.5	1.25			2.608712536	0.4013404	5.7793	
11.5	2.5			2.608712536	0.5217425	7.51309	
20	4			3.130455043	0.3682888	5.30336	
24.5	4.5			1.043485014	0.2318856	3.33915	
31	6.75			4.695682564	0.7224127	10.4027	
37.75	8			2.608712536	0.3864759	5.56525	
44.75	9			2.086970029	0.2981386	4.2932	
51.75	10			2.086970029	0.2981386	4.2932	
	1 cm = 15.34 cm <sup>3</sup>						
K(h)	reservoir		infil (cm)	Rate (cm/min)	Rate (m/d)		
Time (min)	cm			Rate (cm/min)	Rate (m/d)		
0	24.4		0	0	0		
0.25	25		0.6	0.114881268	1.6542903		
0.75	26		1	0.09573439	1.3785752		
1.5	27.7		1.7	0.108498975	1.5623852		
2	28.8		1.1	0.105307829	1.5164327		
2.5	29.9		1.1	0.105307829	1.5164327		
3	31		1.1	0.105307829	1.5164327		
3.5	32		1	0.09573439	1.3785752		
4	33		1	0.09573439	1.3785752		
4.5	34.1		1.1	0.105307829	1.5164327		
5	35.2		1.1	0.105307829	1.5164327		
5.5	36.1		0.9	0.086160951	1.2407177		
6	37.4		1.3	0.124454707	1.7921478		
6.5	38.4		1	0.09573439	1.3785752		
7	39.5		1.1	0.105307829	1.5164327		
7.5	40.5		1	0.09573439	1.3785752		
8	41.5		1	0.09573439	1.3785752		



STA 165						
Ksat						
Time (min)	Vol (L)		Infiltration (cm)	Rate (cm/m)	Rate (m/d)	
0	0		0	0	0	
1.5	0.5		1.04348501	0.6956567	10.0175	
6	1.75		2.60871254	0.5797139	8.34788	
15.75	3		2.60871254	0.2675603	3.85287	
26.25	4.25		2.60871254	0.2484488	3.57766	
40.5	5.5		2.60871254	0.1830675	2.63617	
56	6.75		2.60871254	0.168304	2.42358	
1 cm = 15.34 cm <sup>3</sup>						
K(h)	reservoir		infil (cm)	Rate (cm/min)	Rate (m/d)	
Time (min)	cm			Rate (cm/min)	Rate (m/d)	
0	6.7		0	0	0	
0.25	7.1		0.4	0.07658751	1.1028602	
0.5	7.2		0.1	0.01914688	0.275715	
0.75	7.5		0.3	0.05744063	0.8271451	
1	7.7		0.2	0.03829376	0.5514301	
1.25	8.1		0.4	0.07658751	1.1028602	
1.5	8.3		0.2	0.03829376	0.5514301	
1.75	8.5		0.2	0.03829376	0.5514301	
2	8.8		0.3	0.05744063	0.8271451	
2.25	9		0.2	0.03829376	0.5514301	
2.5	9.1		0.1	0.01914688	0.275715	
2.75	9.6		0.5	0.09573439	1.3785752	
3	10		0.4	0.07658751	1.1028602	
3.25	10.4		0.4	0.07658751	1.1028602	
3.5	10.9		0.5	0.09573439	1.3785752	
3.75	11.3		0.4	0.07658751	1.1028602	
4	11.9		0.6	0.11488127	1.6542903	
4.25	12.3		0.4	0.07658751	1.1028602	
4.5	12.7		0.4	0.07658751	1.1028602	
4.75	13.2		0.5	0.09573439	1.3785752	
5	13.7		0.5	0.09573439	1.3785752	

STA A						
Ksat						
Time (min)	Vol		Infiltration (cm)	Rate (cm/min)	Rate (m/d)	
0	0		0	0	0	
17	0.75		1.56522752	0.0920722	1.32584	
54	1		0.52174251	0.0141011	0.20306	
95	1.5		1.04348501	0.0254509	0.36649	
	1 cm = 15.34 cm <sup>3</sup>					
K(h)	reservoir		infil (cm)	Rate (cm/min)	Rate (m/d)	
Time (min)	cm			Rate (cm/min)	Rate (m/d)	
0	6.4		0	0	0	
3	6.5		0.1	0.00159557	0.0229763	
6	6.6		0.1	0.00159557	0.0229763	
9	6.8		0.2	0.00319115	0.0459525	
12.25	6.9		0.1	0.00147284	0.0212088	
16	7.1		0.2	0.00255292	0.036762	
19	7.2		0.1	0.00159557	0.0229763	
24	7.4		0.2	0.00191469	0.0275715	
29	7.6		0.2	0.00191469	0.0275715	

STA B						
Ksat						
Time (min)	Vol		Infiltration (cm)	Rate (cm/min)	Rate (m/d)	
0	0		0	0	0	
20	0.75		1.56522752	0.0782614	1.12696	
60	2		2.60871254	0.0652178	0.93914	
90	2.5		1.04348501	0.0347828	0.50087	
1 cm = 15.34 cm <sup>3</sup>						
K(h)	reservoir		infil (cm)	Rate (cm/min)	Rate (m/d)	
Time (min)	cm			Rate (cm/min)	Rate (m/d)	
0	7.6		0	0	0	
5	7.9		0.3	0.00287203	0.0413573	
10	8.2		0.3	0.00287203	0.0413573	
12	8.3		0.1	0.00239336	0.0344644	
15	8.5		0.2	0.00319115	0.0459525	
17	8.6		0.1	0.00239336	0.0344644	
20	8.8		0.2	0.00319115	0.0459525	
24	9.1		0.3	0.00359004	0.0516966	
30	9.5		0.4	0.00319115	0.0459525	



APPENDIX C  
WATER RETENTION DATA

Station	Cell	Initial	15 cm	50 cm	100 cm	150 cm	200 cm	500 cm	750 cm	1000 cm	Dry	
	mass (g)	mass (g)	mass (g)	mass (g)	mass (g)	mass (g)	mass (g)	mass (g)	mass (g)	mass (g)	mass (g)	mass (g)
20S	156.81	241.76	233.53	219.84	209.88	207.55	204.55	200.8	199.44	198.87	186.89	
10S	157.11	249.32	241.32	230.58	218.88	215.12	212.87	210.31	209.11	208.49	191.99	
OO	155.49	209.83	200.8	195.74	192.31	190.35	188.39	186.11	183.4	180.58	146.15	
10	156.99	226.43	220.5	216.69	214.15	212.25	209.53	206.88	203.8	200.57	158.98	
30	158.96	215.92	210.07	206.21	203.86	201.9	199.55	197.23	195.79	193.51	149.78	
40	158.78	222.27	213.24	209.8	207.38	205.54	202.77	200.48	197.8	194.61	151.68	
60	154.12	218.5	208.28	206.89	204.27	202.05	201.48	200.48	198.62	197.93	150.83	
90	156.7	239.6	235.38	228.97	216.3	213.36	211.7	210.08	208.52	207.51	179.42	
105	158.17	243.32	237.3	225.75	212.98	212.11	211.28	207.25	205.14	204.41	194.14	
120	157.17	247.8	237.81	220.99	209.96	207.71	206.91	205.31	204.24	203.79	194.11	
135	157.71	229.7	215.44	204.18	195.1	193.64	192.9	192.31	191.36	190.36	180.56	
150	157.4	266.35	260.08	237.25	230.2	228.55	227.7	227.33	226.06	225.4	216.89	
165	156.95	232.49	223.91	210.94	198.76	194.83	191.36	188.06	186.09	184.43	175.43	
A	156.79	256.27	243.43	240.7	230.05	229.28	228.55	226.36	225.36	224.97	212.02	
B	156.5	252.11	240.75	233.87	228.5	228.3	227.55	227.54	227.24	226.95	216.86	
C	158.24	231.79	221.52	215	203.01	201.09	199.65	198.5	197.63	197.25	188.41	
	Initial-Dry	Bulk Dens		Saturated	15 cm	50 cm	100 cm	150 cm	200 cm	500 cm	750 cm	1000 cm
Station	(g)	theta g	g/cm <sup>3</sup>	theta v	theta v	theta v	theta v	theta v	theta v	theta v	theta v	theta v
20S	54.87	0.2936	1.41156	0.41526	0.35297	0.24937	0.17399	0.15636	0.13365	0.10527	0.09498	0.09066
10S	57.33	0.29861	1.45008	0.43387	0.37333	0.29205	0.2035	0.17505	0.15802	0.13865	0.12956	0.12487
OO	63.68	0.43572	1.10385	0.48193	0.41359	0.3753	0.34934	0.33451	0.31967	0.30242	0.28191	0.26057
10	67.45	0.42427	1.20076	0.51046	0.46558	0.43675	0.41753	0.40315	0.38256	0.36251	0.3392	0.31475
30	66.14	0.44158	1.13127	0.50055	0.45628	0.42706	0.40928	0.39444	0.37666	0.3591	0.3482	0.33095
40	70.59	0.46539	1.14562	0.53423	0.46589	0.43985	0.42154	0.40761	0.38665	0.36932	0.34904	0.32489
60	67.67	0.44865	1.1392	0.51213	0.43478	0.42426	0.40443	0.38763	0.38332	0.37575	0.36168	0.35645
90	60.18	0.33541	1.35514	0.45544	0.42351	0.37499	0.27911	0.25686	0.2443	0.23204	0.22023	0.21259
105	49.18	0.25332	1.46631	0.37219	0.32664	0.23922	0.14258	0.136	0.12972	0.09922	0.08325	0.07772
120	53.69	0.2766	1.46609	0.40633	0.33072	0.20343	0.11995	0.10292	0.09687	0.08476	0.07666	0.07326
135	49.14	0.27215	1.36375	0.37189	0.26397	0.17876	0.11004	0.09899	0.09339	0.08892	0.08173	0.07417
150	49.46	0.22804	1.63814	0.37431	0.32686	0.15408	0.10073	0.08824	0.08181	0.07901	0.0694	0.0644
165	57.06	0.32526	1.325	0.43183	0.3669	0.26874	0.17656	0.14682	0.12056	0.09558	0.08067	0.06811
A	44.25	0.20871	1.60136	0.33488	0.23771	0.21705	0.13645	0.13062	0.1251	0.10853	0.10096	0.09801
B	35.25	0.16255	1.63792	0.26677	0.1808	0.12873	0.08809	0.08658	0.0809	0.08083	0.07856	0.07636
C	43.38	0.23024	1.42304	0.3283	0.25058	0.20123	0.11049	0.09596	0.08506	0.07636	0.06978	0.0669
$V_{CORE} \text{ cm}^3 =$	132.4											

Station	Cell	Initial	15 cm	50 cm	100 cm	150 cm	200 cm	500 cm	750 cm	1000 cm	Dry	
	mass (g)	mass (g)	mass (g)	mass (g)	mass (g)	mass (g)	mass (g)	mass (g)	mass (g)	mass (g)	mass (g)	mass (g)
20S	156.83	244.79	237.26	226.99	210.63	207	203.01	202.68	202.31	200.99	188.43	
10S	157.04	237.12	227.43	214.62	206.5	203.74	201.94	201.2	200.59	198.8	178.32	
OO	157.04	238.27	229.12	223.18	220.69	216.99	212.14	202.96	197.73	217	165.97	
10	157.73	228.33	218.6	213.83	210.86	209.17	208.27	207.03	206.2	205.39	157.66	
30	157.12	217.03	207.48	202.3	199.64	197.11	195.54	194.19	193.29	192.33	145.41	
40	158.45	212.79	202.44	196.35	193.63	191.61	190.66	189.4	188.21	187.17	141.1	
60	157.21	216.84	201.49	199.58	197.99	196.77	195.78	193.14	191.98	191.35	147.61	
90	157.46	241.98	234.74	224.91	209.7	207.53	204.3	203.45	202.84	202.22	180.37	
105	158.44	244.86	238.17	226.29	211.82	208.3	207.08	206.36	206.02	204.7	190.2	
120	156.84	231.67	221.67	211.21	195.69	190.7	188.46	187.72	187.09	186.48	170.19	
135	157.31	232.93	225.03	212.04	195.61	193.13	192.01	191.66	191.36	190.38	181.94	
150	157.48	233.11	228.77	215.66	200.94	197.5	196.82	196.19	195.73	194.37	179.77	
165	154.5	248.61	241.77	227.94	217.49	214.01	211.98	211.33	211.05	210.64	195.61	
	Initial-Dry		Bulk Dens	Saturated	15 cm	50 cm	100 cm	150 cm	200 cm	500 cm	750 cm	1000 cm
Station	(g)	theta g	g/cm <sup>3</sup>	theta v	theta v	theta v	theta v	theta v	theta v	theta v	theta v	theta v
20S	56.36	0.2991	1.42319	0.42653	0.36955	0.29182	0.16801	0.14054	0.11034	0.10784	0.10504	0.09505
10S	58.8	0.32974	1.34683	0.445	0.37166	0.27472	0.21327	0.19238	0.17876	0.17316	0.16854	0.15499
OO	72.3	0.43562	1.25355	0.54717	0.47792	0.43297	0.41412	0.38612	0.34941	0.27994	0.24036	0.3862
10	70.67	0.44824	1.19079	0.53483	0.46119	0.42509	0.40262	0.38983	0.38302	0.37363	0.36735	0.36122
30	71.62	0.49254	1.09826	0.54202	0.46975	0.43054	0.41041	0.39127	0.37938	0.36917	0.36236	0.35509
40	71.69	0.50808	1.06571	0.54255	0.46422	0.41813	0.39755	0.38226	0.37507	0.36553	0.35653	0.34866
60	69.23	0.46901	1.11488	0.52393	0.40776	0.39331	0.38128	0.37204	0.36455	0.34457	0.33579	0.33102
90	61.61	0.34158	1.36231	0.46626	0.41147	0.33708	0.22197	0.20555	0.1811	0.17467	0.17005	0.16536
105	54.66	0.28738	1.43656	0.41367	0.36304	0.27313	0.16362	0.13698	0.12775	0.1223	0.11973	0.10974
120	61.48	0.36124	1.28542	0.46528	0.3896	0.31044	0.19298	0.15522	0.13827	0.13267	0.1279	0.12328
135	50.99	0.28026	1.37417	0.38589	0.32611	0.2278	0.10345	0.08469	0.07621	0.07356	0.07129	0.06387
150	53.34	0.29671	1.35778	0.40368	0.37083	0.27162	0.16021	0.13418	0.12903	0.12427	0.12079	0.11049
165	53	0.27095	1.47742	0.4011	0.34934	0.24467	0.16559	0.13925	0.12389	0.11897	0.11685	0.11375
V <sub>CORE</sub> cm <sup>3</sup> =	132.4											

Station	Porosity	500 cm	1000 cm	3000 cm	Dry	Ring
		(g)	(g)	(g)	(g)	(g)
20S	1.42	29.51	29.8	29.21	26.18	3.95
10S	1.43	32.56	32.68	32.05	28.78	3.95
OO	1.51	35.81	35.48	34.16	27.38	3.95
10	1.54	30.23	30.52	29.42	22.95	3.95
30	1.5	33.2	32.82	31.1	24.8	3.95
40	1.53	36.21	35.98	34.08	26.69	3.95
50	1.53	31.45	30.96	29.56	23.5	3.95
60	1.54	34.22	34.38	33.28	25.44	3.95
70	1.53	36	34.94	34	26.86	3.95
80	1.53	32.51	31.91	30.72	25.1	3.95
90	1.46		28.75	28.37	26.25	3.95
105	1.37		31.95	31.6	29.49	3.95
120	1.41		35.18	34.85	32.48	3.95
135	1.3		29.71	28.86	27.25	3.95
150	1.37		33.66	32.92	31.23	3.95
165	1.43		33.08	32.63	30.23	3.95
A	1.33		29.02	28.42	26.68	3.95
B	1.27		23.52	23.09	21.58	3.95
C	1.33					

Station	Porosity	500 cm	1000 cm	3000 cm	Dry
		(g)	(g)	(g)	(g)
20S	1.42	27.06	27.35	26.76	22.23
10S	1.43	30.11	30.23	29.6	24.83
OO	1.51	33.36	33.03	31.71	23.43
10	1.54	27.78	28.07	26.97	19
30	1.5	30.75	30.37	28.65	20.85
40	1.53	33.76	33.53	31.63	22.74
50	1.53	29	28.51	27.11	19.55
60	1.54	31.77	31.93	30.83	21.49
70	1.53	33.55	32.49	31.55	22.91
80	1.53	30.06	29.46	28.27	21.15
90	1.46		26.3	25.92	22.3
105	1.37		29.5	29.15	25.54
120	1.41		32.73	32.4	28.53
135	1.3		27.26	26.41	23.3
150	1.37		31.21	30.47	27.28
165	1.43		30.63	30.18	26.28
A	1.33		26.57	25.97	22.73
B	1.27		21.07	20.64	17.63
C	1.33				

## VITA

Department of Geoscience  
University of Nevada, Las Vegas

David Matthew Ely

### Home Address:

1720 East John Street #1  
Seattle, WA 98112

### Degrees:

Bachelor of Science, Marine Science, 1990  
University of South Carolina

### Publications:

Ely, D. M., Wilson, G. V., Hokett, S. L., French, R. H., and Johnson, T. E.,  
1998, Uncertainty in recharge at subsidence craters in response to spatial  
patterns in hydraulic properties at Frenchman Flat, Nevada Test Site: American  
Geophysical Union Abstracts, v. 79, n. 17, p. 147.

Thesis Title: Uncertainty in recharge from subsidence craters at Frenchman Flat,  
Nevada Test Site: Impacts of initial and boundary conditions and media  
properties

### Thesis Examination Committee:

Chairperson, Dr. Glenn V. Wilson, Ph.D.  
Committee Member, Dr. Richard H. French, Ph.D.  
Committee Member, Dr. David L. Weide, Ph.D.  
Graduate Faculty Representative, Dr. Donald H. Baepler, Ph.D.